

NASA CR-135026

BBN Report No. 3176

SOFTWALL ACOUSTICAL CHARACTERISTICS AND MEASUREMENT CAPABILITIES OF THE NASA LEWIS 9 x 15 FOOT LOW SPEED WIND TUNNEL

(NASA-CR-135026) SOFTWALL ACOUSTICAL CHARACTERISTICS AND MEASUREMENT CAPABILITIES OF THE NASA LEWIS 9x15 FOOT LOW SPEED WIND TUNNEL (Bolt, Beranek, and Newman, Inc.)
103 p HC \$5.50.

N76-32202

Unclas

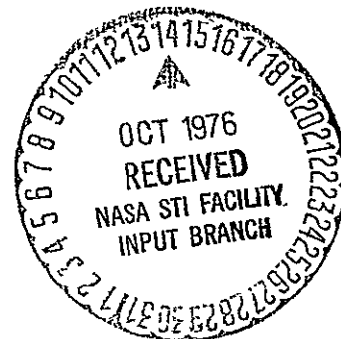
CSSL 14B G3/09

05270

by Peter E. Rentz

BOLT BERANEK AND NEWMAN INC.

prepared for



NATIONAL AERONAUTICS AND SPACE ADMINISTRATION

NASA Lewis Research Center

Contract NAS3-19410

1 Report No. NASA CR-135026		2 Government Accession No.		3 Recipient's Catalog No.	
4 Title and Subtitle Softwall Acoustical Characteristics and Measurement Capabilities of the NASA Lewis 9 x 15 Foot Low Speed Wind Tunnel				5 Report Date June 1976	
				6. Performing Organization Code	
7 Author(s) Peter E. Rentz				8. Performing Organization Report No. 3176	
9 Performing Organization Name and Address Bolt Beranek and Newman Inc. 21120 Vanowen Street Canoga Park, California 91303				10. Work Unit No.	
				11 Contract or Grant No. NAS3-19410	
12 Sponsoring Agency Name and Address National Aeronautics and Space Administration Washington, D. C. 20546				13 Type of Report and Period Covered Contractor Report	
				14 Sponsoring Agency Code	
15 Supplementary Notes Project Manager, James A. Diedrich NASA Lewis Research Center, Cleveland, Ohio					
16 Abstract Experimental evaluations of the acoustical characteristics and source directionality measurement capabilities of the NASA Lewis 9 x 15 foot low speed wind tunnel in the treated or softwall configuration were performed. The results show that the softwall treatment along with the use of aerodynamically clean microphone supports has significantly improved the directionality measurement capabilities. Specifically, the radius of measurement is limited by the size of the test section, instead of the 3.0 foot (1 m) limitation of the hardwall test section. In addition, the wind on noise level in the test section has been reduced 10 dB. Reflections from the microplane support boom, even after absorptive covering, were found to induce measurement errors in the lower frequency bands of interest. Static tests of inlets are recommended to evaluate the severity of the problem which depends on the nature of the source. Reflections off of the diffuser back wall were shown to be significant. Tunnel noise coming up the diffuser was postulated as being responsible, at least in part for the wind-on noise observed in the test section and settling chamber. Acoustic treatment for the back wall is recommended. Numerous procedural recommendations are set forth. The near field characteristics of finite sized sources and the theoretical response of a porous strip sensor in the presence of wind are presented as appendices.					
17. Key Words (Suggested by Author(s)) Acoustic Measurement Wind Tunnel			18. Distribution Statement Unclassified - Unlimited		
19. Security Classif. (of this report) Unclassified		20. Security Classif. (of this page) Unclassified		21. No. of Pages 95	22. Price*

* For sale by the National Technical Information Service, Springfield, Virginia 22161

TABLE OF CONTENTS

	<u>Page</u>
LIST OF TABLES	iii
LIST OF FIGURES	iv
1.0 SUMMARY	1
2.0 INTRODUCTION	2
2.1 Wind Tunnel Description	2
2.2 Hardwall Calibration	3
2.3 Relation to Preceding Work	4
3.0 SOFTWARE EVALUATION PROGRAM	5
3.1 Decay Rate Tests	6
3.2 Radial Traverse Tests	9
3.2.1 Radial Traverses, ILG Source	9
3.2.2 Radial Traverses, Speaker Source, Octave Band Noise	12
3.2.3 Radial Traverses, Wall and Boom Reflections, Speaker Source With Sine Wave Excitation, Omni-Directional Microphone	14
3.2.4 Radial Traverses, Boom Reflections, Speaker Source With Sine Wave Excitation, Omni-Directional Microphone	15
3.2.5 Radial Traverses, Boom Reflections, Speaker Source With Sine Wave Excitation, Directional Porous Strip Sensor	16
3.2.6 Use of Radial Traverses to Evaluate Boom Reflection Effects, Test Inlets	16
3.3 Directionality Measurement Demonstration Tests	17
3.3.1 Sweep Rate	17
3.3.2 Test Conditions and Centerline Levels	17
3.3.3 Comparison of Measured Directionality With Anechoic Room Measurements	18

TABLE OF CONTENTS (Cont'd)

	<u>Page</u>
3.4 Wind-On Tests	20
3.4.1 Inlet Directionality Measurement	21
3.4.2 Settling Chamber Wind-On Noise	23
3.4.3 Free Stream Microphone Test Section Wind-On Noise	24
3.4.4 Obstructed Microphone Test Section Wind-On Noise	26
3.4.5 Porous Strip Sensor Wind-On Noise	26
3.4.6 Diffuser Wind-On Noise	27
4.0 CONCLUSIONS AND RECOMMENDATIONS	28
5.0 SYMBOL DEFINITION	31
REFERENCES	33
APPENDIX A - Directivity Measurements of Finite Sized Sources	A-1
APPENDIX B - Theoretical Response of Continuous and Discrete Line Sensors in the Presence of Flow	B-1

LIST OF TABLES

<u>No.</u>		<u>Page</u>
I	Static Test Summary, Softwall Condition	5
II	Wind-On Test Summary, Softwall Condition.	6
III	Comparison of Residual Reverberation Decay Times (seconds) with Previous Hardwall Measurements	8
IV	Slopes of Sound Pressure Level Reduction with Distance, ILG Source, Radial Traverse Test.	11
V	Sound Pressure Levels at One Foot (0.305m), ILG Source, Radial Traverse Test, dB.	11
VI	Slopes of Sound Pressure Level Reduction with Distance Five Inch Speaker Source, Radial Traverse Test	13
VII	Sound Pressure Levels at One Foot (0.305m), Five Inch Speaker Source, Radial Traverse Test Speaker Current 0.25 Ampere	13
VIII	Summary of Measured Source Centerline Levels Corrected to One Foot Radius, Directionality Measurement Demonstration, Softwall Condition . .	19

LIST OF FIGURES

- No.
- 1 Overall Plan View of NASA Lewis 9 x 15 Foot Low Speed Test Section in the Return Leg of the 8 x 6 Foot Supersonic Wind Tunnel
 - 2 Wind Tunnel Test Section Plan View Showing Exhauster, 20" Inlet Stand (To Be Installed) Microphone Boom and Speaker Location
 - 3 Test Apparatus and Instrumentation Block Diagrams, Soft Wall Evaluation, 9 x 15 Foot Low Speed Wind Tunnel
 - 4 Octave Band Decays, Speaker Source at Inlet, Pointing Towards Settling Chamber, Microphone at 6' (1.8m) Position on Boom in Softwall Test Section
 - 5 Octave Band Decays, Speaker Source at Simulator Exit, Pointing Towards Diffuser, Microphone at 6' (1.8m) Position on Boom in Softwall Test Section
 - 6 ILG Source with Microphone Traversing Mechanism, Acoustically Treated (Softwall) 9 x 15 Foot Wind Tunnel Test Section
 - 7 Radial Traverse Along Centerline of ILG Source, Typical On-Line Plot, Softwall Test Section
 - 8 ILG Direct Field Calibration in Anechoic Room—
 - 9 Radial Traverse, Along Centerline of Speaker Source, Softwall Test Section
 - 10 Wall Reflection Radial Traverse, Softwall Test Section
 - 11 Bare Boom Reflection, Radial Traverse, Speaker Source, Softwall Test Section
 - 12 Boom with Foam Reflection, Radial Traverse, Speaker Source, Softwall Test Section
 - 13 Boom with Foam Reflection, Radial Traverse, Speaker Source, Porous Strip Sensor, Softwall Test Section
 - 14 Porous Strip Sensor, Weathervaning Microphone Sword, and Pitot Tube on Rotating Microphone Boom

LIST OF FIGURES (Cont'd)

- No.
- 15 Directionality Measurement of Horn Source with Omni-Directional Microphone, Typical On-Line Plot, Softwall Test Section
 - 16 Directionality Measurement of Horn Source at 4000 Hz with Omni-Directional Microphone, Typical On-Line Plot, Sweep Rate 2.5°/sec, Softwall Test Section
 - 17 Comparison of LE5-2 Speaker Directionality Measurements with Omni Microphone at Six Foot Radius in Softwall Test Section, Angled Towards Wall ($\alpha = 30$, $\psi = 40$), and in Anechoic Chamber
 - 18 Comparison of LE5-2 Speaker Directionality Measurements with Porous Strip Sensor in Softwall Test Section, Angled Towards Wall ($\alpha = 30$, $\psi = 48$), and with Omni Microphone in Anechoic Chamber
 - 19 Comparison of Horn Directivity Measurements with Omni Microphone in Softwall Test Section, Angled Towards Wall ($\alpha = 30$, $\psi = 40$), and in Anechoic Chamber
 - 20 Comparison of Horn Directionality Measurements with Porous Strip Sensor at Six Foot Radius in Softwall Test Section, Angled Towards Wall ($\alpha = 30$, $\psi = 45$), and with Omni Microphone in Anechoic Chamber
 - 21 B&K Microphone Output, $M = 0$, Inlet Directionality Test
 - 22 B&K Microphone Output, $M = 0.12$, Inlet Directionality Test
 - 23 B&K Microphone Output, $M = 0.15$, Inlet Directionality Test
 - 24 Porous Strip Sensor Output, $M = 0$, Inlet Directionality Test
 - 25 Porous Strip Sensor Output, $M = 0.12$, Inlet Directionality Test
 - 26 Porous Strip Sensor Output, $M = 0.15$, Inlet Directionality Test
 - 27 Settling Chamber Wind-On Sound Pressure Levels, Softwall Test Section
 - 28 Normalized, Settling Chamber, Wind-On Sound Pressure Levels, Softwall Test Section

LIST OF FIGURES (Cont'd)

- No.
- 29 Normalized, Settling Chamber, Wind-On Sound Pressure Levels, Softwall Test Section
 - 30 Normalized, Test Section, Free Stream, Sword Microphone, Wind-On Sound Pressure Levels, Softwall Test Section
 - 31 Normalized, Test Section, Obstructed Microphone, Wind-On Sound Pressure Levels, Softwall Test Section
 - 32 Normalized, Test Section, Lateral Microphone, Wind-On Sound Pressure Levels, Softwall Test Section
 - 33 Comparison of Free Stream, Obstructed, and Lateral Microphone, Wind-On Normalized Sound Pressure Levels, Softwall Test Section
 - 34 Normalized, Test Section, Porous Strip Sensor, Wind-On Sound Pressure Levels, Softwall Test Section
 - 35 Normalized, Diffuser, Wind-On Sound Pressure Levels, Softwall Test Section
 - 36 Calculated Sound Pressure Levels Versus Distance from Anular Incoherent Source
 - 37 Effect of Error in Acoustic Center Location
 - 38 Visualization of Waves in a Moving Medium
 - 39 Variation of the Theoretical Output of a 14 inch (36 cm) Porous Strip Sensor, in the Presence of Flow (Mach Number, $M = 0.15$)

1.0 SUMMARY

Experimental evaluations of the acoustical characteristics and source directionality measurement capabilities of the NASA Lewis 9 x 15 foot low speed wind tunnel in the treated or softwall configuration were performed.

The results show that the softwall treatment along with the use of aerodynamically clean microphone supports has significantly improved the directionality measurement capabilities. Specifically, the radius of measurement is limited by the size of the test section, instead of the 3.0 foot (1 m) limitation of the hardwall test section. In addition, the wind on noise level in the test section has been reduced 10 dB.

Reflections from the microphone support boom, even after absorptive covering, were found to induce measurement errors in the lower frequency bands of interest. Static tests of inlets are recommended to evaluate the severity of the problem which depends on the nature of the source.

Reflections off of the diffuser back wall were shown to be significant. Tunnel noise coming up the diffuser was postulated as being responsible, at least in part for the wind-on noise observed in the test section and settling chamber. Acoustic treatment for the back wall is recommended.

Numerous procedural recommendations are set forth. The near field characteristics of finite sized sources and the theoretical response of a porous strip sensor in the presence of wind are presented as appendices.

2.0 INTRODUCTION

The 9 x 15 foot low speed wind tunnel at the NASA Lewis Research Center (LeRC), Cleveland, Ohio, Figures 1,2(1)* is to be utilized for acoustic directivity measurements of normal and quieted inlets with simulated forward velocity. In order to accomplish these measurements in the adverse environment encountered in a wind tunnel, a special rotating-boom-microphone system was built and the tunnel test section was lined with screen protected fiberglass (2,3). The tunnel in this condition is referred to as being "softwall".

Subsequent to the installation of the microphone system and test section lining, static (no-wind) acoustical measurement tests were performed, the structural integrity of all acoustical hardware was verified, and a series of typical inlet noise measurements was conducted. Various acoustical measurement problems and structural deficiencies were defined, and corrective action was taken. The purpose of this report is to describe these efforts and to evaluate both the suitability and limitations of the softwall tunnel for directionality measurements.

2.1 Wind Tunnel Description

The 9 x 15 foot (2.72 x 4.58m) low speed wind tunnel at the NASA Lewis Research Center, Cleveland, Ohio, was built in the return leg of the 8 x 6 foot (2.44 x 1.83m) supersonic wind tunnel, Figure 1. Prior to construction of the subsonic 9 x 15 foot

*Numbers in parentheses indicate references listed.

test section, the 8 x 6 foot facility had received acoustic treatment downstream of the test section for the purpose of community noise abatement. The treatment consists of low frequency Helmholtz resonators, a lined duct muffler, wall treatment and acoustic baffles. Other aspects of the construction of the facility which relate to acoustic measurement are the presence of flow regulation doors upstream and downstream of the 9 x 15 foot test section, a cooler screen upstream of the settling chamber, and dryer beds between the diffuser leg and the drive fan, Figure 1.

The test section is constructed of steel covered with the removable fiberglass filled trays, Figure 2. The side walls also have four inch slots running the length of the test section, 27.7 ft (8.4m). The slots are backed with acoustically absorptive foam in the softwall condition.

The tunnel flow is induced by a seven stage axial flow compressor. Operation of the 9 x 15 foot low speed wind tunnel is usually conducted at a standard compressor rotational speed which ranges from 800 to 820 rpm. The desired flow in the 9 x 15 foot test section is achieved with the flow control doors.

2.2 Hardwall Calibration

Previous acoustic measurement evaluation of the untreated or hardwall 9 x 15 foot low speed wind tunnel consisted of calibrating tunnel chambers for sound power measurement, and defining the measurement limitations of omni-directional

microphones installed in the test section (4,5). These evaluations showed that direct field measurements would be seriously hampered by reverberation effects if made at a radius greater than 3.0 feet (1.0m) from the source. In addition, tunnel ambient noise and microphone wind noise limited the measurement amplitude range. The aforementioned test section wall treatment and the use of a directional porous strip sensor were recommended by BBN and adopted by LeRC to reduce the effects of reverberation and of tunnel generated noise.

The report on the hardwall acoustical measurement capabilities (5) also presents noise models for sound power measurement and for estimating tunnel wind-on noise generation. Comparison of wind-on noise measurements with the analytic models indicated the following:

1. Sound pressure levels measured by test section microphones are due to true acoustic levels, not turbulence induced pseudo-noise.
2. The most likely area of significant noise generation is the transition from the test section to the diffuser.

2.3 Relation to Preceding Work

Increasing interest in performing aero-acoustic measurements has resulted in a number of studies (6-17) similar to this one. Typically, the tunnel ambient noise and reverberant properties are described with the intended aim of making direct field measurements in an unmodified or a treated closed test section. Sound power measurement calibrations are also performed in open test section tunnels.

3.0 SOFTWALL EVALUATION PROGRAM

Acoustical measurement tests were conducted in the NASA Lewis 9 x 15 foot low speed wind tunnel in the softwall condition. The tunnel overall dimensions are shown in Figure 1, and the test section configuration is represented in Figure 2. Static tests included determination of the effect of reflections on direct field measurements using both omni-directional microphones and a porous strip sensor, and extensive demonstrations of directionality measurements. Wind-on test included ambient and microphone noise measurements and 395 plots of the directionality of a 12 inch (0.305m) inlet for various tunnel and inlet flow conditions.

The softwall static acoustic tests were performed jointly by BBN and LeRC in accordance with BBN-developed test plans. The specific types of tests and the dates performed are listed in Table I.

TABLE I
Static Test Summary, Softwall Condition

Type	Test Description	Performed By	Dates Performed
1.	Decay rate	BBN	26 July 1975
2.	Radial traverses to evaluate the change in sound pressure level with radius	BBN/LeRC LeRC	23,24,30 July 1975 August 1975
3.	Static directionality using calibrated sources	BBN/LeRC	25,28,29 July 1975

The test apparatus and instrumentation block diagrams for these tests are presented as Figures 3a, b and c, respectively.

Softwall wind-on tests were performed by LeRC with BBN requesting special tests and/or instrumentation. These tests and the dates performed are indicated in Table II.

TABLE II
Wind-On Test Summary, Softwall Condition

Type	Test Description	Performed By	Dates Performed
1.	Structural adequacy	LeRC	10,18 July 1975
2.	Microphone wind noise and tunnel flow noise	LeRC	10,18 July 1975 18 Dec. 1975 June 1976
3.	Inlet directionality	LeRC	15 Oct. to 22 Nov. 1975

3.1 Decay Rate Tests

Decay rate tests consisted of powering a five inch (13cm) speaker with octave band noise while monitoring the output of a one-half inch (1.3cm) microphone. The current to the speaker was interrupted, and the resultant decay recorded. Two conditions were so evaluated, first with the speaker at a typical inlet location pointing towards the settling chamber and the microphone at a four-foot (1.2m) position on the boom. Secondly, the speaker was positioned at the discharge of a simulator, pointing towards the diffuser, and the microphone again at a four-foot (1.2m) position, Figure 3a. The intent of these measurements was to identify the relationship between the direct field and reflected noise arriving at the microphone on the boom.

With the source directed toward the settling chamber, the level at the microphone dropped an average of 20 dB almost immediately upon disconnecting the speaker, Figure 4. This behavior was essentially independent of frequency, indicating an absence of significant reflections from the settling chamber upstream cooler screen. The 20 dB drop was, in all cases, followed by a gradual decay. The sixty dB reverberation times of these gradual decays were determined and compared with previously measured settling chamber decays, Table III. This comparison shows good numerical agreement. This agreement supports the expectation that settling chamber reverberation affects test section direct field measurements. However, the 20 dB drop in level shows that the effect of the settling chamber reverberant field on test section measurements is insignificant.

When the speaker was directed downstream, a different result was observed. The measured sound pressure level dropped only slightly when the speaker input was removed, Figure 5. Only after a period of time of 0.45 seconds, did the level drop significantly. This corresponds to the time for a sound wave to travel from the speaker to the diffuser "back" wall and return to the microphone.

This lack of discrimination between direct acoustic radiation from a source and the reflected energy off of the diffuser wall facing the test section would cause measurement error under certain circumstances. In the case of a simulator test with attenuated forward propagating noise, the error could be significant. In order to minimize this effect, the wall should be treated with at least two inches (5cm) of acoustic absorbing material equivalent to fiberglass of a density of four pounds per cubic foot (64kg/m^3).

The residual decay rates were also calculated and are compared with previous hardwall diffuser measurements, Table III. The close agreement shows that the residual decay is attributable to the diffuser decay, as expected from the geometry of the experiment. Unlike the situation with the settling chamber, the influence of this reverberant field on test section measurements could be significant. Extrapolation of the residual decay back up to the point in time when the speaker power was cut shows that the reverberant field is approximately equal to the measured level. However, acoustic treatment of the "back" wall will serve to reduce the reverberant field level as well as direct reflections. A repeat of the decay rate test following the wall treatment is recommended to quantify the improvement.

TABLE III

Comparison of Residual Reverberation Decay Times (seconds) with Previous Hardwall Measurements

Condition	Octave Band Center Frequency, Hz					
	250	500	1K	2K	4K	8K
Source Pointing Towards Settling Chamber	2.8	3.6	3.6	3.2	2.0	-
Hardwall, Settling Chamber (5)	3.6	3.5	3.0	2.5	1.65	0.95
Source Pointing Towards Diffuser	5.0	4.5	3.6	3.0	3.2	2.6
Hardwall, Diffuser (5)	5.0	4.9	4.1	3.3	1.9	1.0

3.2 Radial Traverse Tests

Radial traverses were performed with a LeRC designed and fabricated device which moves a microphone on a straight line path in a radial direction from an acoustic source. The apparatus is shown mounted in the test section with an ILG centrifugal fan noise source in Figure 6. The resultant sound pressure level was plotted directly in dB versus the logarithm of distance from the source. A minus 20 dB per decade slope would indicate error free measurement of the output of a point source. The test apparatus is shown in Figure 3b.

3.2.1 Radial Traverses, ILG Source

Forty-eight traverses were conducted using an ILG source (18) covering octave bands from 250 to 8000 Hz and eight orientations in the test section. Typical on-line plots are presented as Figure 7. The test conditions and slopes of the radial traverse plots are given in Table IV. The slopes average minus 16.4 dB, not the minus 20 dB expected for an ideal source in an anechoic space.

This non-ideal behavior could be attributed to the source, or acoustic reflections in the wind tunnel. Noting that the radial traverse plots, Figure 7, are essentially flat and free of standing wave patterns typical of reflections, the source was identified as the anomaly.

Subsequent measurements were made using the same ILG source in an anechoic room at BBN's Canoga Park facility. The results, Figure 8, are virtually identical with those observed in the

9 x 15 foot test section, indicating that the source is not ideal. A slope of minus 16.5 can occur if the acoustic source is offset from the assumed geometric center by 1.0 foot (0.305m), Appendix A. This is apparently the case with the ILG source which generates noise by turbulent interaction at the periphery of the rotor.

The indicated one-foot (0.305m) sound pressure levels for the ILG traverse tests are compared with previous measurements, Table V. The differences could be attributed to reverberant effects in the wind tunnel, except for the resolution of the non-ideal slope anomaly and previous observed variability of the sound power output of the ILG with time. In short, the best evaluation of the direct field acoustic radiation of the ILG was probably that which was performed in the wind tunnel.

In addition to the tests described, two boom acoustic treatments were evaluated with the ILG source and traversing microphone. The first treatment consisted of reflector or tent placed on the top side of the boom. The tent had its apex along the centerline of the boom, and sloped to either side at an angle of 20° from the horizontal. The purpose of the tent was to scatter acoustic waves being reflected from the boom and thus attenuate the acoustic energy arriving at the microphone via this extraneous path. The second boom acoustic treatment consisted of covering the boom with one-inch (2.5cm) thick, high flow resistance, acoustic absorptive foam. A subsequent 3/8 inch (1.0cm) foam covering is referred to as thin.

The results of traverses with the tent and thick foam on the boom were essentially identical with the results obtained from traverses above the untreated boom. This tends to substantiate

TABLE IV

Slopes of Sound Pressure Level Reduction
with Distance*, ILG Source, Radial Traverse Test

Orientation $\alpha + \beta$, deg	Octave Band Center Frequency, Hz					
	250	500	1K	2K	4K	8K
-113	21.3	18.3	19.3	19.5	14.9	17
-34	17.4	13.2	16.5	16.5	16.8	15.4
-16	14.5	13	17.5	16.5	16.7	14.8
0	-	14.2	17.5	16.5	17.6	15.3
15	14	16.1	16.1	16.5	17.2	15.7
34	12.8	16.5	15.2	15.5	16.5	15
90	12.5	15.5	17.5	17.1	16.5	18.5
131	16.7	15.3	18.3	17.0	15.8	17.4
Average	-	15.2	17.2	16.9	16.5	16.1

* $SPL_r = SPL_{r_{ref}} - x \log r/r_{ref}$, where $r_{ref} = 1.0$ ft (0.305m) and

x is the slope

TABLE V

Sound Pressure Levels*at One Foot (0.305m),
ILG Source, Radial Traverse Test, dB

Orientation $\alpha + \beta$, deg	Octave Band Center Frequency, Hz					
	250	500	1K	2K	4K	8K
-113	86.3	84.5	85.2	83.3	79	76.8
-34	83.5	80	84.6	85	81.7	76.4
-16	82.5	81	85.2	84.8	80	73.6
0	80	81.7	84.7	83.5	79.2	72.8
+15	79.7	81.3	84.2	84.6	80	73.3
+34	81.5	80.5	82.9	83.3	80.5	79.8
+90	80.5	82.2	83.4	83.4	81.5	78.8
+131	83.2	81.7	83.8	82.4	77.8	74.2
Average	82.2	81.6	84.3	83.8	80	75.7
BBN Cal (Ref 20)	78.5	80	80.5	81.5	79	75.5

* SPL, dB re 20μ N/m²

the conclusion that the non-ideal slopes of the traverse plots are attributable to the source, not boom reflections.

3.2.2 Radial Traverses, Speaker Source, Octave Band Noise

Another set of radial traverse tests was conducted with a speaker source. Typical on-line plots are reproduced as Figure 9. Only the 250 and 500 Hz octave band curves deviate appreciably from ideal behavior, indicating that the wind tunnel test section acoustic wall treatment is quite adequate to permit directionality measurements of sources similar to the speaker used. The measured slopes of the radial traverse plots are listed in Table VI. The values listed approach the ideal minus 20 dB. However, note that the speaker is somewhat directional, and the traverses were taken along the speaker centerline. Subsequent, worst case tests show that if the speaker is directed off-axis, measurements can be affected by reflections.

In addition to the bare boom traverses, a series of tests was performed with a combination tent reflector covered with thin, 3/8 inch (1.0cm) foam. The results, also presented in Table VI, are essentially identical with the bare boom results. This similarity supports the conclusion that the test section acoustic wall treatment is adequate for directionality measurements of sources similar to the speaker used, if the source is directed horizontally.

Table VII compares the one-foot (0.305m) levels measured in the radial traversing tests with the results of a calibration performed in an anechoic room in BBN's Canoga Park facility. The agreement, averaging ± 1.5 dB, is considered indicative of the accuracy which can be expected from the measurement system.

TABLE VI

Slopes of Sound Pressure Level Reduction with Distance*
Five Inch Speaker Source, Radial Traverse Test

Orientation $\alpha + \beta$, deg	Acoustic Center	Boom Surface	Octave Band Center Frequency, Hz					
			250	500	1K	2K	4K	8K
45°	Face	Bare	19.7	21/14	18	18.6	19	18.8
45°	Face + 0.5 in.	Bare	20	20.5	17.7	18.6	18.8	19.7
45°	Face + 0.5 in.	Tent + Foam	22	18.6	18.5	19.8	19.2	19.7
45°	Face + 1.5 in.	Bare	18.7	15.3	20	19.4	19.2	19.8

* $SPL_r = SPL_{r_{ref}} - x \log r/r_{ref}$, where $r_{ref} = 1.0$ foot (0.305m) and

x is the slope

TABLE VII

Sound Pressure Levels*at One Foot (0.305m),
Five Inch Speaker Source, Radial Traverse Test
Speaker Current 0.25 Ampere

Orientation $\alpha + \beta$, deg	Acoustic Center	Boom Surface	Octave Band Center Frequency, Hz					
			250	500	1K	2K	4K	8K
45°	Face	Bare	100	100	101	100.3	104	106.3
45°	Face + 0.5 in.	Bare	101	100	101.2	100.3	104	107.3
45°	Face + 0.5 in.	Tent + Foam	101.2	99.1	100.9	100.3	103.4	106.8
45°	Face +	Bare	101.5	98	102.3	100.6	104	107.3
BBN Cal	Face	-	-	101.7	100.7	101.7	106.7	106.7

* SPL, dB re 20μ N/m²

3.2.3 Radial Traverses, Wall and Boom Reflections, Speaker Source With Sine Wave Excitation, Omni-Directional Microphone

As previously noted, the traverses along the centerlines of both the ILG and speaker sources did not show standing wave patterns indicative of reflections. However, inlet sources may direct acoustic energy off of either the test section wall or the microphone boom. In addition, the octave band random noise signals of the ILG and speaker sources may not represent the quasi-sinusoidal nature of a fan. In order to understand the effect of the resulting reflections and take corrective action, a series of worst-case experiments was conducted by LeRC. The tests involved directing the speaker source towards the wall and the boom to evaluate wall and boom reflections respectively. In addition, evaluations of various acoustic absorption treatments for the boom were evaluated. Approximately 15 tests were conducted, each test consisting of traverses with sine wave excitation at 250, 500, 1000, 2000, 4000 and 8000 Hz.

Typical on-line plots of wall reflection test levels are reproduced as Figure 10. Definite cancellation and reinforcement patterns are evident for all frequency bands. This undesirable acoustic behavior may be due in part to acoustic reflections from the boom and traversing mechanism which were not covered with absorptive foam during these measurements. However, even if the cancellations and reinforcements were due entirely to wall reflections, the situation would not be critical. The peak to valley ratios are about 6 dB for this contrived situation where the source is within three feet of the wall and directed towards the wall. The potential measurement error will decrease rapidly, either as the source is removed from the proximity of

the wall, or as the source is directed upstream. Therefore, corrective action is not advised, but if situations approximating the test conditions are encountered during inlet directionality measurement, the resulting accuracy should be critically evaluated.

Note that only the plots including 2000 Hz and 8000 Hz are presented in Figures 10-13. These octave bands were chosen because they cover the principal frequency ranges of interest for 20-inch (0.51m) and 5.5-inch (0.14m) fans respectively.

3.2.4 Radial Traverses, Boom Reflections, Speaker Source With Sine Wave Excitation, Omni-Directional Microphone

Boom reflections are potentially more serious because the boom is always in proximity to the source and microphone and because the cancellation/reinforcement patterns are more severe, Figure 11. The plot representing the traverse with the source set at 2000 Hz appears unusually flat with large excursions. However, this behavior is considered to be due in large measure to the directionality of the source. Note that the 2000 Hz source output at r_{ref} (1.0 ft. or 0.305m) is approximately 82 dB, compared with the centerline octave band output of 100.3 dB, Table VII. Thus, the speaker output which is directed towards the microphone, when the speaker is pointed towards the boom, is approximately 18 dB down from the centerline output. This extreme source directionality is not evidenced at other frequencies, and is not expected for typical inlets.

Various boom treatments including hard tent reflectors, tent reflectors with acoustically absorptive thin foam (3/8 inch or 1.0cm), and thick foam (1.0 inch or 2.5cm) were evaluated. Figure 12 shows the results of thick foam. Variation of level

from ideal attenuation with distance is evident, but the situation is improved over the untreated boom, Figure 11. In conclusion, the measurement system with the boom treatment is considered as good as can be achieved short of rebuilding the entire facility. More importantly, wall and boom reflections are not expected to interfere with normal measurements. However, situations where relatively high level acoustic energy is directed towards either the wall or boom should be anticipated and resulting data critically evaluated.

3.2.5 Radial Traverses, Boom Reflections, Speaker Source With Sine Wave Excitation, Directional Porous Strip Sensor

All traversing tests discussed thus far have employed an omnidirectional microphone. Figure 13 shows the results of employing the directional porous strip sensor. The improvement over the omnidirectional microphone result, Figure 12, is evident. However, subsequent wind-on tests demonstrate the inherent limitations of the porous strip sensor in flow.

3.2.6 Use of Radial Traverses to Evaluate Boom Reflection Effects, Test Inlets

A real inlet will have a distribution of sources and the noise will be varying in amplitude and frequency. The vertical plane directionality is likely to be stronger than that of the five-inch (13cm) speaker used for the radial traverses. All these factors will tend to reduce the effect of the boom reflection. A static radial traverse along with a static directionality measurement is recommended for each inlet tested in order to separate boom reflection effects from finite sized source effects.

3.3 Directionality Measurement Demonstration Tests

The directionality of various sources was measured with sword microphones and a porous strip sensor mounted on the rotating microphone boom. These microphones are shown installed in a normal configuration, Figure 14. For the directionality measurement demonstration either the sword or porous strip sensor was usually mounted at the six foot (1.8m) position on the boom. Since sword microphones normally weathervane so as to point directly into the wind stream, they were strung together with a parallelogram arrangement so as to keep their normal wind-on orientation. The output of the individual microphones was detected, scaled logarithmically and plotted as a function boom angle, Figure 3c. These plots were subsequently compared with the known source directionality patterns.

3.3.1 Sweep Rate

In order to establish the maximum sweep rate which would still preserve the patterns of highly directional sources, a limited number of angular sweeps was performed at various sweep rates. Typical on-line generated plots are presented in Figures 15 and 16 for rates of 10 and 2.5 degrees per second, respectively.

The faster rate, Figure 15, shows noticeable "hysteresis" which is absent at 2.5 degrees per second, Figure 16. The slower rate was adopted for the majority of subsequent sweeps.

3.3.2 Test Conditions and Centerline Levels

The test conditions for the directionality demonstration plots are summarized in Table VIII. A total of 216 measurements were made using an ILG centrifugal fan (18), a five inch (13cm) speaker,

and a calibrated horn (19). With some variation, each source was directed along the tunnel centerline and towards the tunnel wall. The angle in the tunnel is given by $\alpha + \psi$ where α is the inlet angle of attack and ψ is the source angle relative to the inlet. The directionality of the ILG and speaker sources were measured in octave bands from 250 to 8000 Hz. Six measurements were also made with the horn source at each configuration, but with different bands of noise. (Octave bands centered at 1000, 2000, and 4000 Hz plus one-third octave bands centered at 6300, 8000, and 10,000 Hz.)

The levels measured along the centerline of each acoustic source for each test condition are compared with the appropriate source calibration, Table VIII. The correspondence between the measured and calibration values is an indication of the measurement accuracy of the complete instrumentation - wind tunnel system. A range of ± 2 dB encompasses virtually all of the measurements from 2000 to 8000 Hz. A measurement standard deviation of ± 1.0 dB is estimated.

One aspect of these data is the obvious presence of 10 dB errors in some measurements. These were preserved and recorded in order to emphasize the necessity of maintaining complete histories of instrument settings so that calibrations can be reconstructed.

3.3.3 Comparison of Measured Directionality With Anechoic Room Measurements

The faithful reproduction of source directivity patterns which have ranges of levels as great as 20 dB is as important as the accurate measurement of the centerline levels. The results of the directivity measurement demonstration tests, Table VIII, show that this is indeed possible with either omni-directional or directional microphones. Virtually no variation was noted with

TABLE VIII

Summary of Measured Source Centerline Levels
Corrected to One Foot Radius†
Directionality Measurement Demonstration, Softwall Condition

Source	MIC	Rate °/Sec	RAD ft	α deg	ψ deg	Band Center Frequency							
						250	500	1K	2K	4K	6.3	8	10
ILG	BBN-Cal	-	3	-	-	78.5	80	80.5	81.5	79		75.5	
ILG	OMNI	2.3	6	30	0	84.2	81.3	83.9	83.6	78.8		73.5	
ILG	Porous	2.5	6	30	-30	83.7	81.8	84.4	83.1	76.8		71.5	
ILG	LAT	-	2.3	-	-	83.3	78.8	82.3	80.8	80.3		79.3	
LE5-2	BBN-Cal	-	4.58	-	-	-	101.7	100.7	101.7	106.7		106.7	
LE5-2	OMNI	2.3	2	30	0	-	-	-	116*	119*		105.5	
		8	2	30	0	-	-	-	116*	120*		106	
		2.3	6	30	0	-	-	-	111*	114.6*		111*	
		8	6	30	0	-	-	-	111*	114.6*		111*	
LE5-2	OMNI	2.3	6	30	0	102.5	102.5	104.5	112.5*	116.5*		113*	
LE5-2	OMNI	2.3	6	30	40	103.5	103.5	106	113*	117.5*		114*	
LE5-2	Porous**	2.5	6	30	-30	104	101.5	102.5	101.3	104		104.6	
LE5-2	Porous	2.5	6	30	-30	104	101.5	102.8	101	104.4		104.4	
LE5-2	Porous	2.5	6	30	48	103	101.7	102.2	101	104.4		104.4	
Horn	Cal (19)	-	9	-	-	-	-	132	129.5	121	119.5	120	117.5
	OMNI	2.5	6	30	-30	-	-	133	128.5	121.5	120.4	122	117.8
		10	6	30	-30	-	-	133	128.5	121.5	120.4	122	118.3
		2.8	6	30	40	-	-	134.3	128.5	122	120.3	122.5	118.6
Horn	Porous	2.5	6	30	-30	-	-	131.6	127.6	121	118	119	116
		10	6	30	-30	-	-	131.6	127.6	121	118	118.5	116
Horn	Porous**	2.5	6	30	-30	-	-	132	128	122	118.3	118.4	117
Horn	Porous	2.5	6	30	-45	-	-	132	129	122.6	119	120	118.5
		10	6	30	45	-	-	132	129	122.6	119	120	118

** With aluminum support at tip of porous strip sensor.

† Table I is for ILG, 20 log r for other data.

* Apparent 10 dB error in plot scaling.

angle of the source in the tunnel; so only the more critical configurations with the sources angled towards the wall are presented. Measured directionality plots are compared with corresponding anechoic measurements in Figures 17 through 20 for the following source/microphone combinations:

<u>Figure</u>	<u>Source</u>	<u>Microphone</u>
17	speaker	omni-directional
18	speaker	porous strip sensor
19	horn	omni-directional
20	horn	porous strip sensor

These curves show that faithful reproductions of source directionality can be obtained in the 9 x 15 foot wind tunnel test section for sources which have directivity patterns which are representative of the inlet directivity patterns. Comparison of these curves with similar data measured in the hardwall condition (5) shows significant improvement.

3.4 Wind-On Tests

Structural problems arose when wind was blown over the microphone support boom with a porous strip sensor and weathervaning sword in place. Corrective action was handled by LeRC. Definitive steps included:

1. Reduction of boom gear backlash
2. Addition of structural support at tip of porous strip sensor
3. Reduction of tunnel flow instabilities

Subsequent tests evidenced satisfactory behavior. The remainder of the wind-on tests involved inlet directionality and tunnel ambient noise measurement.

3.4.1 Inlet Directionality Measurement

Wind-on tests were conducted by LeRC with the one-quarter inch sword microphone, the porous strip sensor, and the lateral microphone, Figure 14. In addition to the sword microphone, a standard one-quarter inch microphone connected directly to a cathode follower and mounted on top of a weather-vaning sword was used.

Data from these tests lead to two observations:

1. Directionality can be measured accurately in the wind tunnel with omni-directional microphones
2. The output of the porous strip sensor is seriously degraded in the presence of flow at 9600 Hz

Specifically, comparative results for a B&K 1/4 inch microphone and the porous strip sensor for test section Mach numbers $M = 0, 0.12$ and 0.15 are presented as Figures 21 through 26. Note that the frequency of the siren (23) is 9600 Hz. At no flow, the outputs of both microphones are quite similar in shape with the porous strip sensor levels lower by 6 dB. (Fig. 21 & 24) This is in accordance with the calibrated frequency response of the porous strip sensor, reference 22. At a test section Mach number $M = 0.12$, the porous strip sensor's output is further reduced relative to the omni-directional microphone output (Fig. 22 & 25). At $M = 0.15$, the porous strip sensor's output bears little resemblance, in form, to that of the omni-mic (Fig. 23 & 26). This result is attributable to attempting to

utilize the porous strip sensor beyond its useful envelope of frequency and Mach number. With Mach number of the order of 0.15, the output is seriously degraded above 4000 Hz, Appendix B. In that appendix, the theoretical sensitivity of the continuous line array in the presence of flow is presented. Interestingly, there is an angle, which is a function of Mach number, at which the sensor's output should be equal to the no flow output. This angle is given by:

$$\cos \phi = \frac{-M}{2}$$

where ϕ is the orientation of the sensor as it is rotated about the source, starting upstream of the source. The porous strip sensor's output in the wind tunnel, Figure 26, does not approach the correct output as it should at $\phi = \alpha + \beta = \pm 94.3^\circ$ (for $M=0.15$).

Therefore, the problems in utilizing the porous strip sensor are twofold:

1. The response is severely modified by the presence of flow, Appendix B.
2. The theoretical response was not confirmed by LeRC measurements.

The latter problem may be overcome by evaluation at frequencies well removed from the sensor's upper frequency limit. This approach is encouraged on the basis of yet unpublished results from a similar effort at NASA Ames Research Center (24). In that program, a test was performed with a source on the test section wall and a porous strip sensor positioned slightly

downstream and oriented at $\phi = 109^\circ$. For the worst flow condition tested, $q = 40$ psf (1914 kg/m^2), the sensor's output averaged 3 dB down from 500 to 8000 Hz. This result agrees reasonably well with the theoretical result, Appendix B.

If subsequent tests verify the theoretical response for all angles, the porous strip sensor may be useful in reducing the effect of wind noise. Note that the theoretical response is least affected by flow for cross wind configurations. These are the most important configurations since they measure simulated downward propagating noise from test inlets.

3.4.2 Settling Chamber Wind-On Noise

With the tunnel running, the settling chamber microphones evidence levels in excess of the electrical noise floor (except in the highest frequency bands). Typical settling chamber measurements are presented as Figure 27 for test section dynamic pressures (q) ranging from 14.5 to 72.5 psf (694 to 3469 N/m^2). Normalizing these data by the third power of the dynamic pressure yields a good fit, Figure 28. Subsequent data are presented as Figure 29. The two sets of data are nominally identical with fewer irregularities in the later measurements. This is attributed to improvement in the tunnel flow stability.

However, these settling chamber levels show only a 1.0 dB to 3 dB reduction from hardwall levels (Figure 28, Reference 5). The expectation was that settling chamber noise would be reduced by as much as 10 dB with the addition of the test section acoustic treatment. Two factors are hypothesized:

1. Air flow through the settling chamber cooler coils

generates more noise than predicted.

2. Tunnel noise coming from the diffuser is making a greater contribution than previously predicted.

The latter hypothesis is supported by the fact that the theoretical reduction of a lined duct of the dimensions of the test section decreases rapidly from 6 dB at 100 Hz to 0.4 dB at 400 Hz (25). This is similar to the improvement noted.

3.4.3 Free Stream Microphone Test Section Wind-On Noise

Normalized test section microphone levels for a sword in the free stream, are given in Figure 30. These results were verified by extensive subsequent measurements (26). Figure 30 also shows the envelope of hardwall test section wind-on noise measurements. The softwall results are consistently 10 dB lower than the previously measured hardwall results.

The 10 dB reduction in the test section wind-on noise levels is attributed to three factors:

1. The aerodynamic shape of the sword microphone holder reduces turbulence induced pseudo-noise.
2. The aerodynamic shape of the sword microphone holder reduces turbulence induce acoustic radiation in close proximity to the microphone.
3. The test section acoustic lining reduces the reverberant acoustic level in the test section.

The model for turbulence induced pseudo-noise shows level variation with velocity to the fourth power or dynamic pressure squared (5). Since the results, Figure 30, collapse nicely when normalized by dynamic pressure to the third power, the first factor is ruled out.

Reduction of acoustic noise generation in proximity of the microphone, factor two, is considered likely. However, estimation of the expected improvement due to the aerodynamic shape of the sword is not feasible.

Evaluation of the third factor, reduction of reverberation, depends on the source location. If the dominant source were in the test section, the reduction would depend on the source location relative to the microphone. In the hardwall configuration, the reverberant and direct fields are equal in level at 3 feet (1.0 m). Therefore, if the source were that distance away from the microphone, the level would drop 3 dB with the removal of the reverberant field. The source would have to be 9 feet (2.7 m) from the microphone for the 10 dB improvement noted. This suggests the exhaust stand, which has not been considered a candidate source based on the analytic noise model (5).

If the dominant source were in the diffuser, the reduction would depend on how much the diffuser acted as a wave guide, creating plane waves going up through the test section.

This uncertainty can be alleviated by performing cross spectral analyses on signals from pairs of microphones located longitudinally in the wind tunnel. The phase relationship as a function of frequency will give a strong indication of the direction of propagation of noise.

3.4.4 Obstructed Microphone Test Section Wind-On Noise

Normalized test section measured wind-on noise levels for an obstructed microphone and the lateral microphone are presented in Figures 31 and 32 respectively. The measurements are compared with the free-stream levels in Figure 33. Clearly, the small profile sword microphone evidences the lowest wind noise, and making measurements in the wake of other microphones increases wind noise dramatically. The wind noise for those measurements made in turbulent flow is attributed solely to turbulence.

3.4.5 Porous Strip Sensor Wind-On Noise

Normalized wind-on noise levels measured with the porous strip sensor in the test section are presented in Figure 34. Above 500 Hz, the wind-on noise levels measured with the porous strip sensor, Figure 34, are consistently lower than obstructed microphone levels and previously measured levels, Reference 5. However, the porous strip sensor does not effect significant reduction of wind-on noise levels relative to the free stream sword microphone measured levels, Figure 31. The poor performance of the porous strip sensor may be due, in part, to the vibration of the boom and sensor during the measurements. Subsequently, a snubber was added to the tip of the sensor, and the flow stability in the test section was improved. Another set of wind-on noise measurements is recommended in order to evaluate the porous sensor's measurement potential.

These results along with previous evaluations and calibrations suggest that the most benefit would be realized by using the porous strip sensor in a high turbulence situation, such as down stream of a simulator.

3.4.6 Diffuser Wind-On Noise

Normalized diffuser levels are presented as Figure 35. These diffuser ambient noise measurements are unique, no other diffuser data have been taken to date. The levels are higher than the settling chamber levels, and comparable to test section levels. The result adds credibility to the hypothesis that the dominant noise source is located in the general area of transition from test section to diffuser, with the majority of sound energy going down the diffuser.

The noise levels in the shop or preparation room are greatly reduced from the hardwall configuration levels, a result expected because of the acoustic treatment in the slots in the test section. No data are presented.

4.0 CONCLUSIONS AND RECOMMENDATIONS

The wind tunnel modifications and the evaluation program described have been multi-faceted and have extended across a time period of over one year. Procedures have evolved and various deficiencies have been defined and corrected during this period. However, in spite of these complicating factors, a number of particularly important conclusions and recommendations require statement:

1. The tunnel anechoic treatment is basically adequate to permit direct field acoustic measurements with a measurement standard deviation ± 1.0 dB from 2000 to 8000 Hz (when the source level significantly exceeds the combined wind, tunnel and ambient level).
2. Measurements at 1000 Hz will have a somewhat larger associated error.
3. Measurements at 250 and 500 Hz are definitely affected by tunnel reflections and reverberation.
4. The softwall treatment along with the use of aerodynamically clean microphone supports has served to reduce the test section wind-on noise level by 10 dB.
5. Direct field acoustic measurements are limited in radius only by the size of the test section.
6. Hall radius is not an adequate descriptor in an almost--anechoic space with reflecting surfaces.

7. The treated test section wall serves as an acoustic reflector which would be important only in special combinations of source location and directivity.
8. The boom serves as an acoustic reflector. Treatment with sound absorbing material is recommended. The importance of the reflections depends on the directionality of the inlet noise source. Traverses with real inlets are recommended to evaluate the extent of the problem.
9. The diffuser termination wall serves as an acoustic reflector hampering measurements of inlets of simulators having downstream propagating noise. Treatment with sound absorbing treatment equivalent to fiberglass of a density of 4 lb/ft^3 (64 kg/m^3) is considered necessary (presently implemented by LeRC).
10. The decay rate test reported herein should be repeated following the acoustic treatment of the diffuser termination to quantify the resulting improvements (already implemented by LeRC).
11. The ILG source is not a point source. Also, vertical support brackets probably effected extra dipole sources. The use of a time invariant omni-directional and directional speaker sources is recommended for subsequent acoustic evaluations and calibrations.
12. Wind tunnel, wind-on, determination of the far field properties of finite sized inlets with distributed internal sources requires prior knowledge of the geometric near field attenuation with distance. This prior knowledge may be obtained in part from wind-off radial traverses.

13. Standard and straightforward bookkeeping procedures are necessary to keep track of microphone calibrations.
14. On-line plotting of results permits immediate evaluation. However, a priori estimation of the results is necessary to detect anomalies and trends.
15. Transient mechanical inputs to the microphone--cathode follower--cable system produces large, unwanted outputs. The exact cause is undetermined at this time.
16. The porous strip sensor does not perform well above 4000 Hz with flow Mach numbers above $M = 0.1$. Within an envelope of frequency and Mach number, prescribed by the theoretical response of a line array, the porous strip sensor should function effectively and significantly reduce the effect of high turbulence wind-on noise, especially in cross wind configurations.
17. Settling chamber and test section wind-on noise levels are attributed to noise generated in the diffuser. Cross spectral density phase analyses are recommended to verify the direction of propagation.
18. Microphones obstructed by other microphones exhibit significantly higher apparent noise in the presence of wind. The use of streamlined microphones is recommended.

5.0 SYMBOL DEFINITION

The symbols used throughout this report are principally defined with English units because the wind tunnel dimensions and dynamic pressure are described in English units. However, non-dimensional and engineering relations are expressed in both English and SI units for reference as follows:

<u>Symbol</u>	<u>Definition</u>	<u>Units</u>
c_o, c	Speed of sound	ft/sec (m/sec)
d	Diameter of noise sources	ft (m)
f	Frequency	Hz
k	Wavenumber	1/ft (1/m)
L	Length of directional microphone	ft (m)
M	Mach number	-
n	Index	-
q	Dynamic pressure	lb/ft ² (kg/m ²)
r	Radius	ft (m)
x	Slope,	-
x	Distance	ft (m)
SPL	Sound pressure level, dB re 20 μ N/m ²	-
V_T	Trace Velocity	ft/sec (m/sec)
E_s	Speaker Shunt Voltage	volt, rms
U	Flow Velocity	ft/sec (m/sec)

<u>Symbol</u>	<u>Definition</u>	<u>Units</u>
α	Angle of attack	degrees
α'	Angle between axis of line sensor and direction of propagation of plane wave	degrees
β	Angle of microphone boom relative to inlet centerline	degrees
ξ	Acoustic center offset	degrees ft (m)
θ'	Angle between flow velocity and direction of propagation of plane wave	degrees
λ	Wavelength	ft (m)
ϕ	Angle between direction of flow and centerline of directional microphone	
ω	Radial frequency	1/sec
ψ	Angle of source relative to inlet	degrees
τ	Time delay	seconds

REFERENCES

1. NASA TM X-2305, "Lewis 9- By 15-Foot V/STOL Wind Tunnel", by Joseph A. Yuska, James H. Diedrich, and Nestor Clough, July 1971.
2. BBN Technical Memorandum No. 19410-1, "Oblique Incidence Absorption and Scattering Measurements of NASA Lewis 9 x 15 Foot V/STOL Wind Tunnel Wall Material", Krishna Aravamudan, 20 May 1975.
3. BBN Technical Memorandum No. 19410-2, "Norman-Incidence Absorption Coefficients of Wall Material for NASA Lewis 9 x 15 Foot V/STOL Wind Tunnel", John F. Wilby, 16 June 1975.
4. BBN Report 2743, "Utilization and Enhancement of the NASA Lewis 2 x 15 Foot V/STOL Wind Tunnel for Inlet Noise Research", by Allan G. Piersol and Peter E. Rentz, 10 May 1974.
5. BBN Report 3174 (NASA CR-135026), "Hardwall Acoustical Characteristics and Measurement Capabilities of the NASA Lewis 9 x 15 Foot Low Speed Wind Tunnel", Peter E. Rentz, June 1976.
6. Bies, D.A., "Investigation of the Feasibility of Making Model Acoustic Measurements in the NASA Ames 40 x 80 Foot Wind Tunnel", BBN Report 1870 (Contract NAS2-5742), April 1970.
7. Bies, D.A., "Investigation of the Feasibility of Making Model Acoustic Measurements in the NASA Ames 40 x 80 Foot Wind Tunnel", BBN Report 2088 (Contract NAS2-6206), 1971.

8. Arndt, R.E.A., Boxwell, D.A., "A Preliminary Analysis of the Feasibility of Rotor Noise Measurements in the AMRDL-Ames 7 x 10 Foot Wind Tunnel", NASA Working Paper, October 1971.
9. Arndt, R.E.A., Boxwell, D.A., "A State-of-the-Art Report on Aeroacoustical Testing in Conventional Wind Tunnels", Paper at 84th Meeting Acous. Soc. Amer., Miami Beach, Florida, November 1971.
10. Vér, I.L., Malme, C.I., Meyer, E.B., "Acoustical Evaluation of the NASA Langley Full-Scale Wind Tunnel", BBN Report 2100 (NAS1-9559), January 1971.
11. Vér, I.L., "Acoustical Modeling of the Test Section of the NASA Langley Research Center's Full-Scale Wind Tunnel", Bolt Beranek and Newman Report 2280 (Contract NAS1-9559), November 1971.
12. Vér, I.L., "Acoustical Evaluation of the NASA Langley V/STOL Wind Tunnel", BBN Report 2288 (Contract NAS1-9559), December 1971.
13. Holbeche, T.A., Williams, J., "Acoustic Considerations for Noise Experiments at Model Scale in Subsonic Wind Tunnels", Royal Aircraft Establishment Rech. Rep. 72155, September 1972.
14. Oetting, R.B., "Preliminary Noise Measurements in the Open-Jet of the VKI Low Speed Wind Tunnel, L-1", Von Karman Institute for Fluid Dynamics Tech., Note 89, May 1973.

15. Vér, I.L., Franken, Peter A., "Conceptual Design Study of the Noise Control Treatment for the NASA Full-Scale Subsonic Wind Tunnel", BBN Report 2368, 15 June 1972.
16. Wilby, J.F., Scharton, T.D., "Evaluation of the NASA Ames #1 7 x 10 Foot Wind Tunnel as an Acoustic Test Facility", BBN Report 2936, 30 June 1975.
17. Hayden, R.E., Murray, B.S., Galaitsis, A.G., "Preliminary Investigation of Acoustic Requirements for NLR 8 x 6 m Low Speed Wind Tunnel", BBN Report 3087, June 1975.
18. Beranek, L.L., Noise and Vibration Control, McGraw Hill Book Company, New York, 1971, Page 144.
19. BBN Technical Memorandum No. 19410-3, "Directional Acoustical Source Characteristics", Peter E. Rentz and John F. Wilby, July 1975.
20. Rentz, P.E., Scharton, T.D., Wilby, E., "Shotgun and Cannon Directional Microphone Calibrations and Wind Tunnel Acoustic Measurements", BBN Technical Memorandum 19410-4, 18 July 1975.
21. BBN Report 2600 (NASA CR-114756), "Relation Between Near Field and Far Field Acoustic Measurements", D.A. Bies and T.D. Scharton, 29 March 1974.
22. BBN Report 3022 (NASA CR-137652), "Development, Fabrication and Calibration of a Porous Surface Microphone in an Aerofoil", D.U. Noiseux, N.B. Noiseux, Y. Kadman, March 1975.

23. NASA TM X-71767, "Experimentally Determined Aeroelastic Performance and Control of Several Sonic Inlets", B.A. Miller, Presented at the Eleventh Propulsion Conference cosponsored by The American Institute of Aeronautics and Astronautics and the Society of Automotive Engineers, Anaheim, California, September 29 - October 1, 1975.
24. Contract NAS2-8382, Task 7, Technical Monitor - Paul Soderman.
25. Beranek, L. L., "Noise and Vibration Control", McGraw-Hill Book Company, New York, 1971, Page 383.
26. Telephone communication with D. Dietrich, in reference to 20 inch fan tests conducted in June 1976, 11 August 1976.

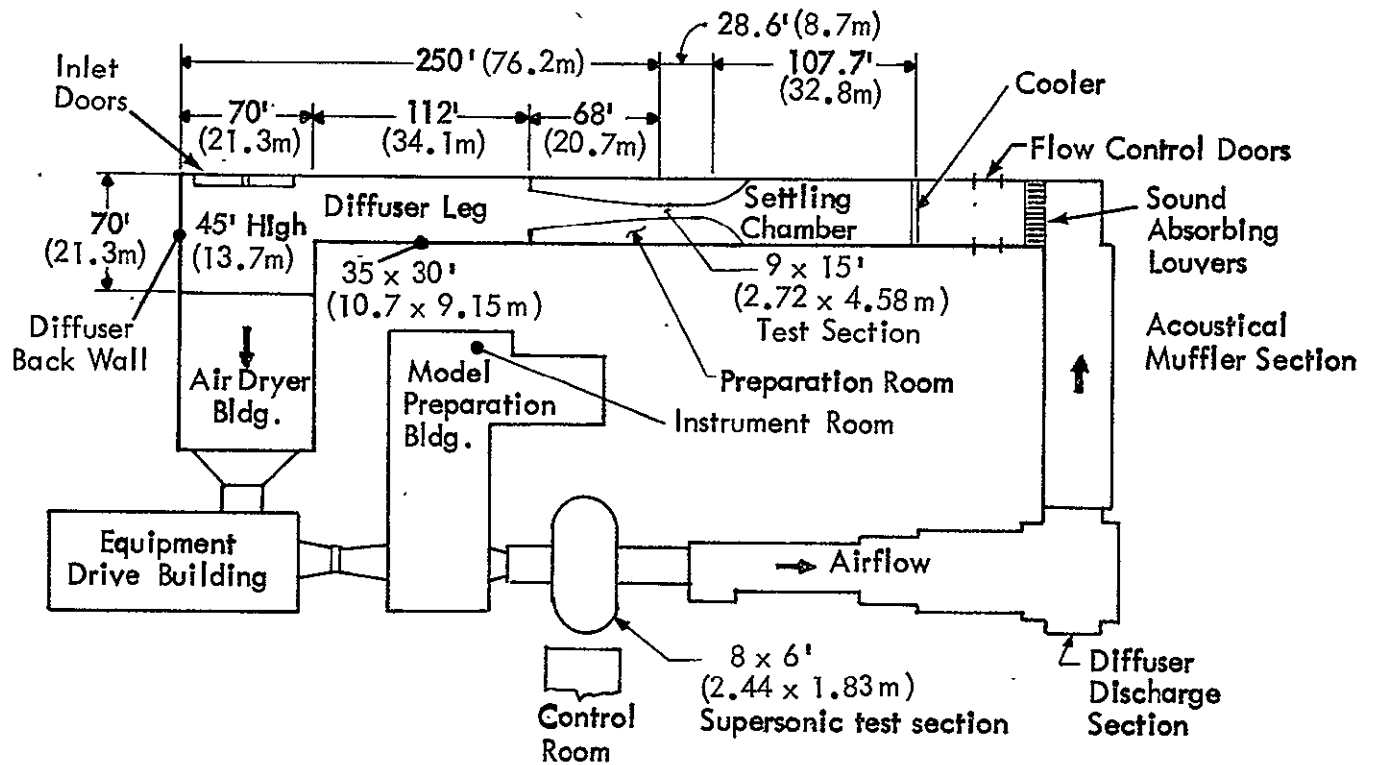


FIGURE 1. OVERALL PLAN VIEW OF NASA LEWIS 9 x 15 FOOT LOW SPEED TEST SECTION IN THE RETURN LEG OF THE 8 x 6 FOOT SUPERSONIC WIND TUNNEL

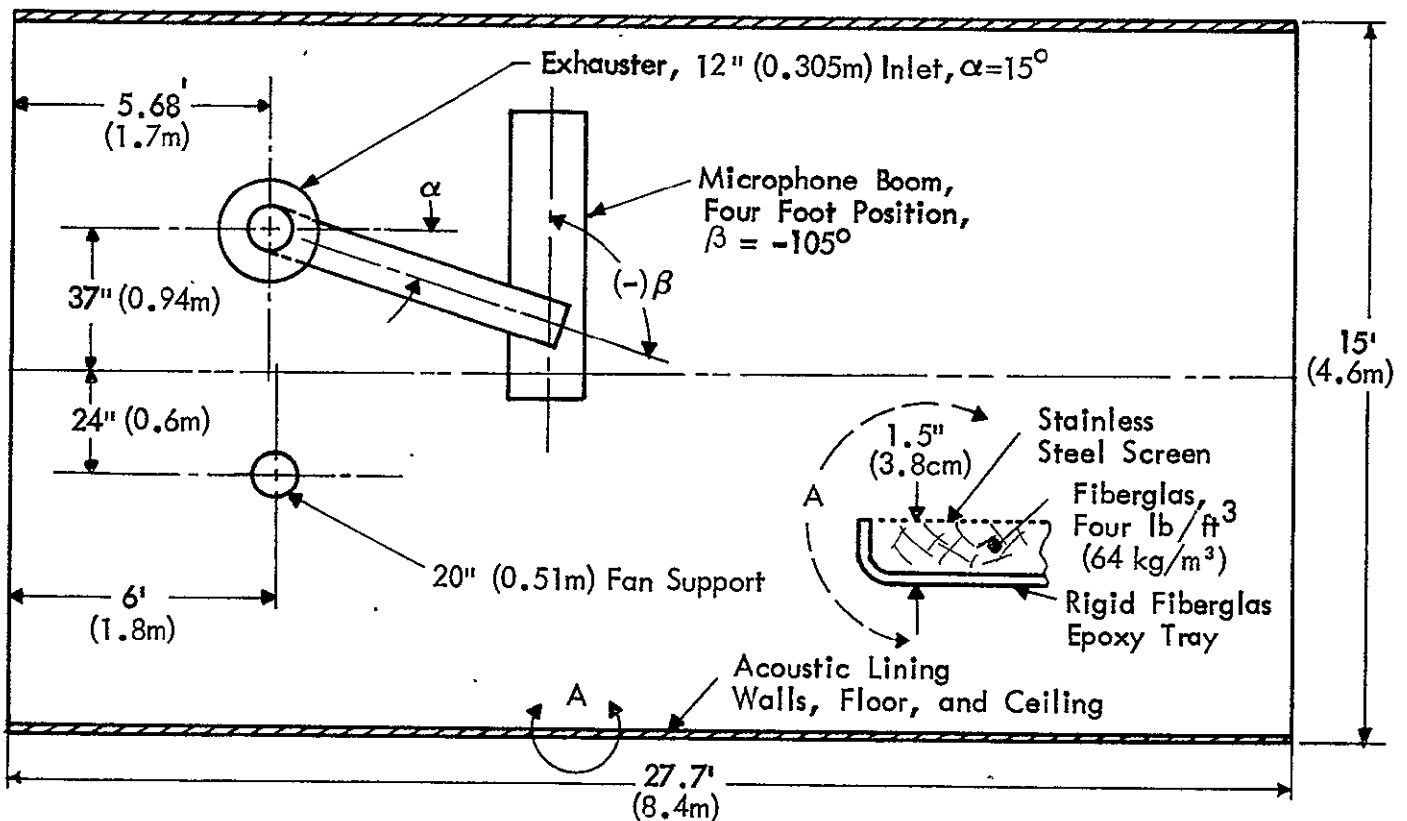
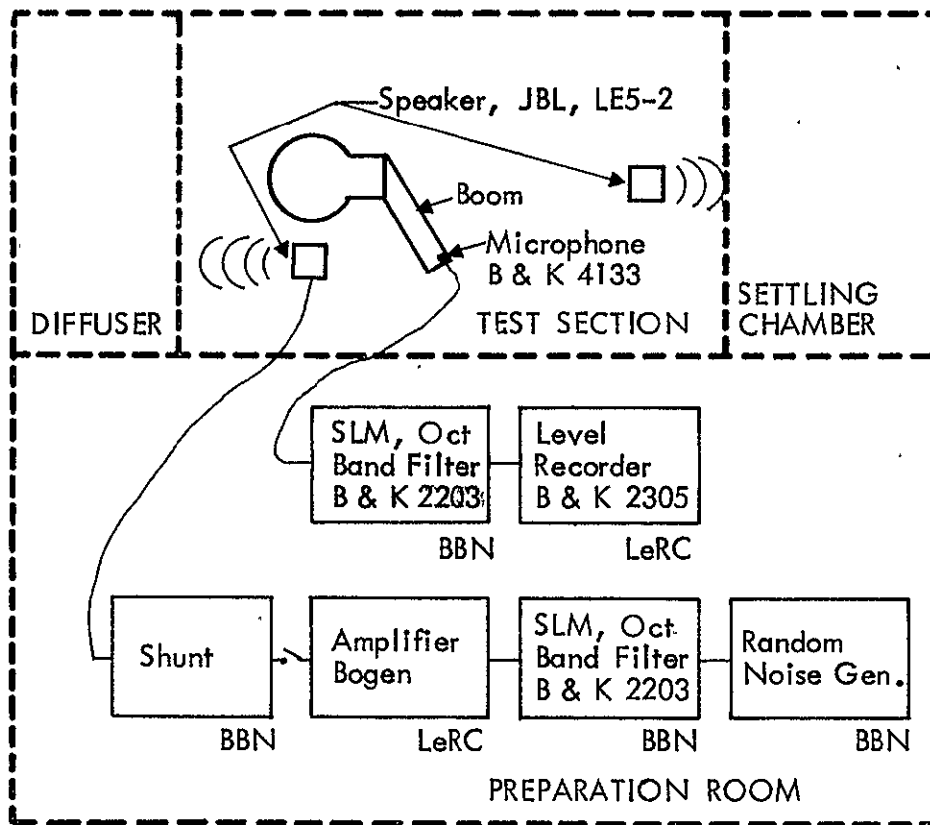


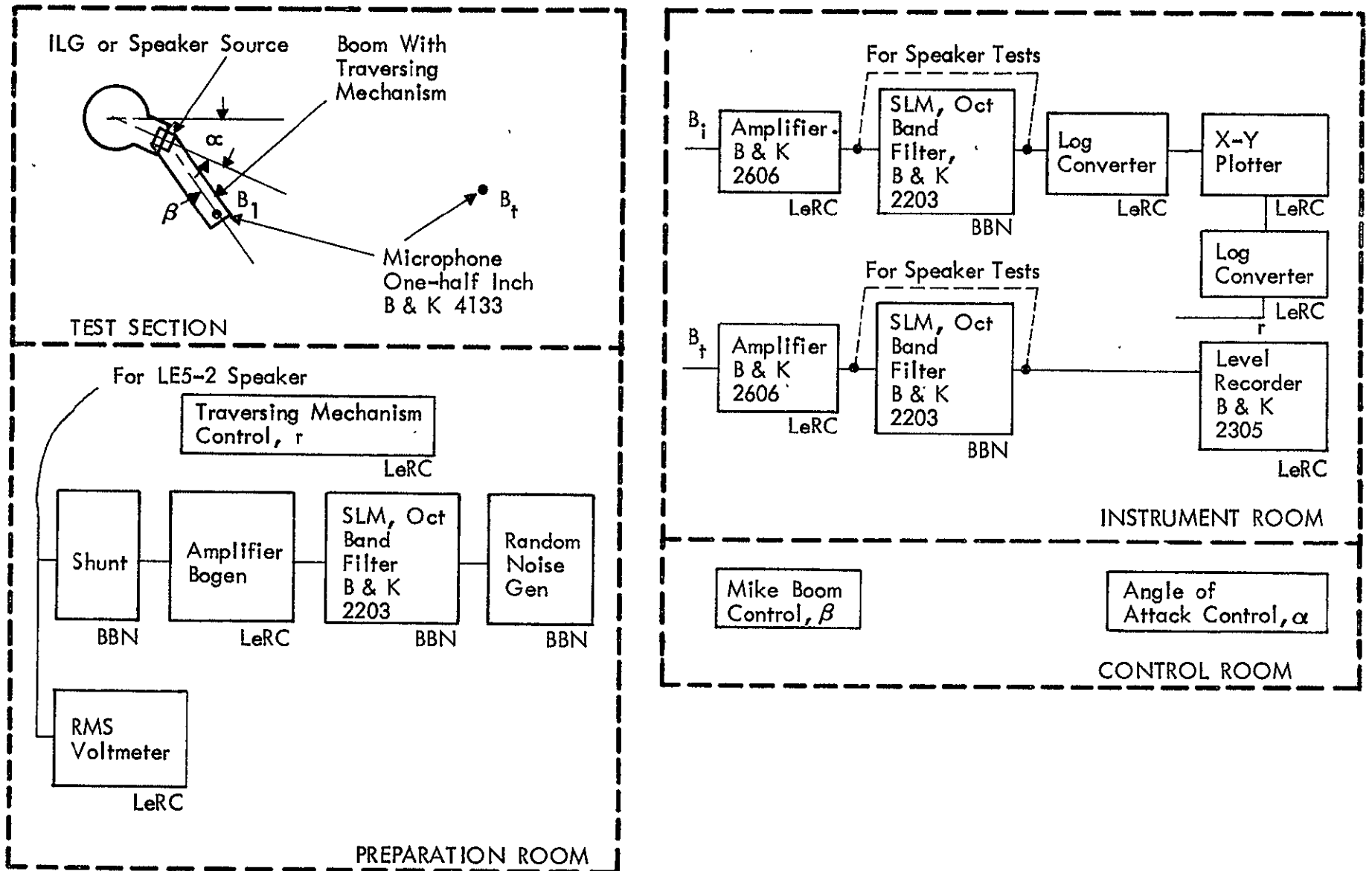
FIGURE 2. WIND TUNNEL TEST SECTION PLAN VIEW SHOWING EXHAUSTER, 20" INLET STAND (TO BE INSTALLED) MICROPHONE BOOM AND SPEAKER LOCATION

PRECEDING PAGE BLANK NOT FILMED



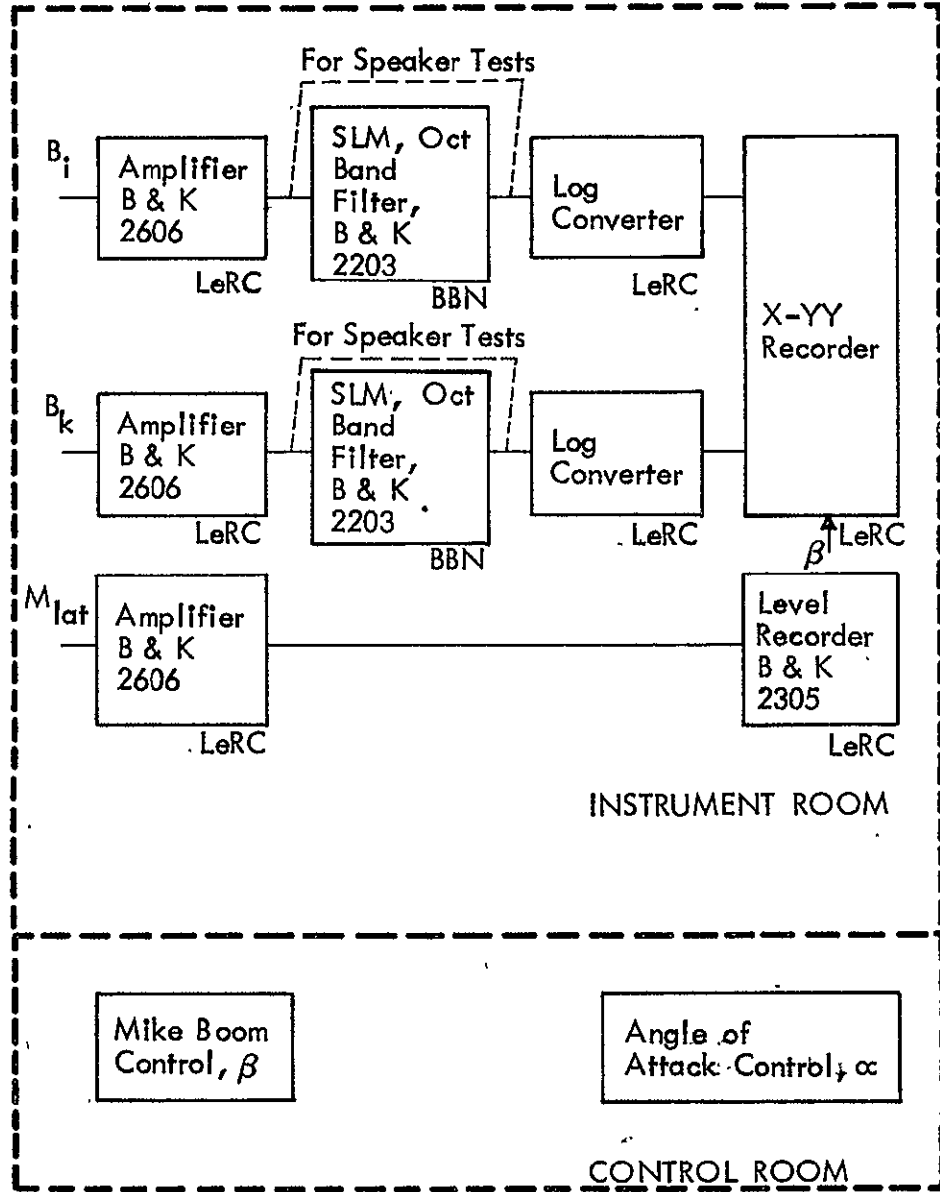
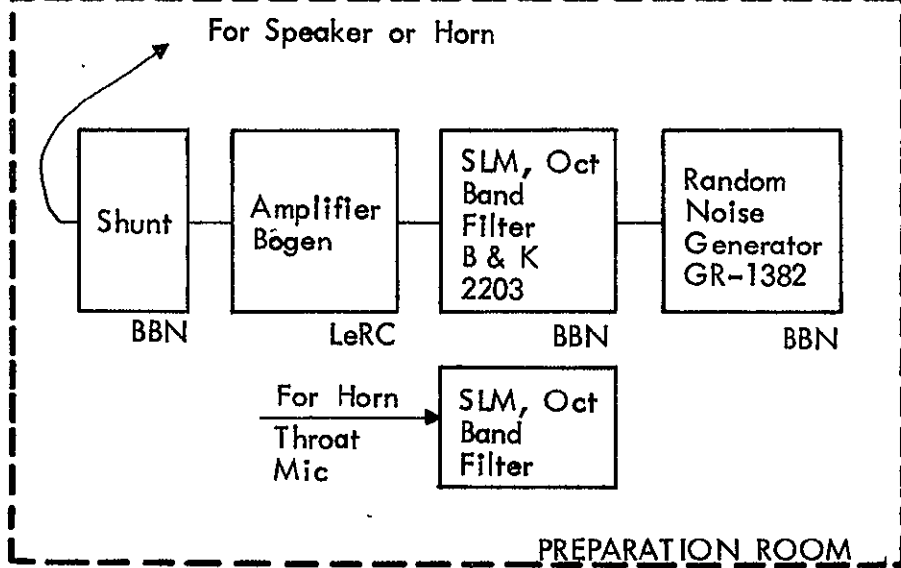
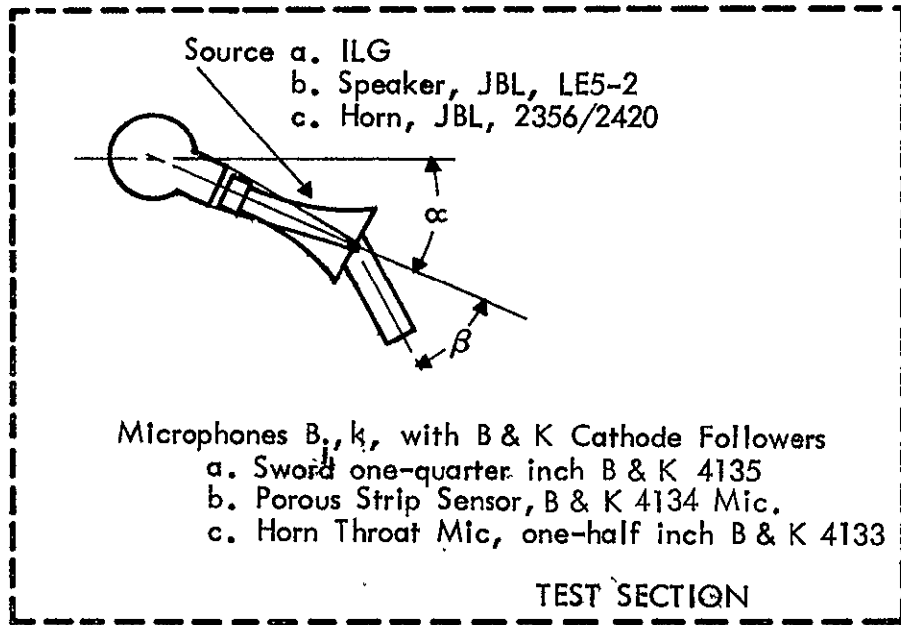
(a) Decay Rate Test

FIGURE 3. TEST APPARATUS AND INSTRUMENTATION BLOCK DIAGRAMS, SOFT WALL EVALUATION, 9 x 15 FOOT LOW SPEED WIND TUNNEL



(b) Radial Traverse Tests

FIGURE 3. (Cont)



(c) Directionality Measurement Tests



FIGURE 3. (Cont)

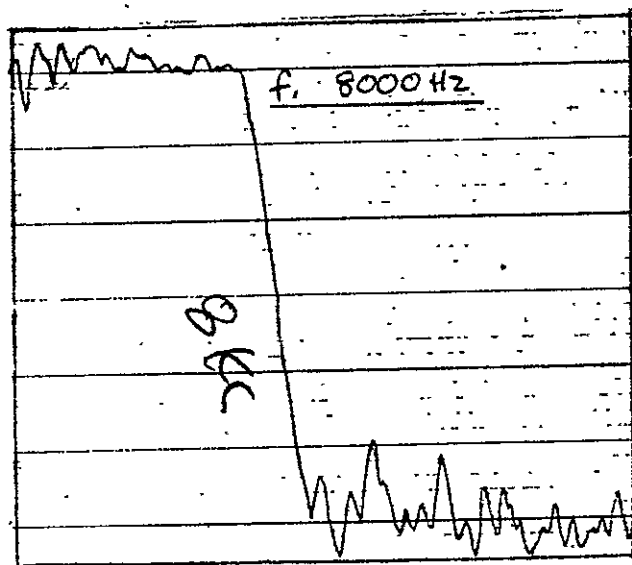
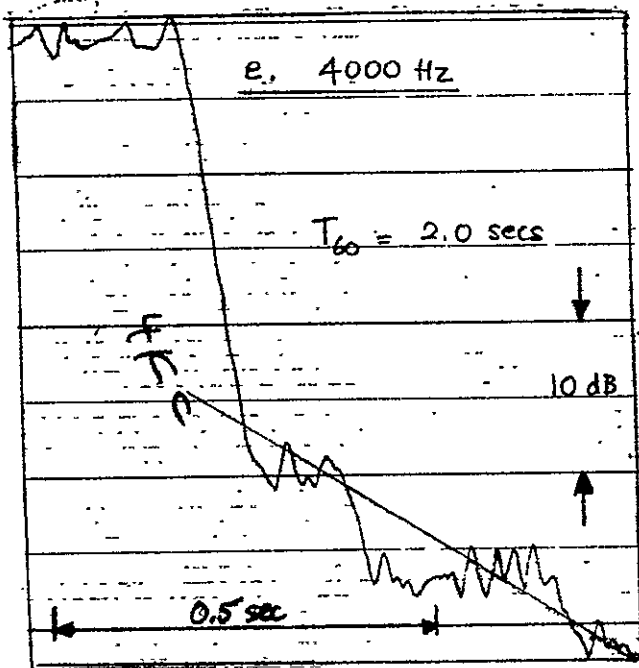
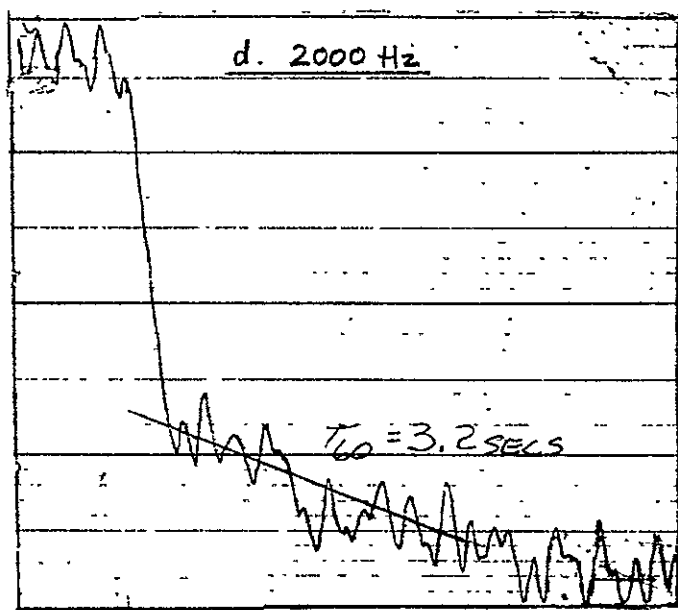
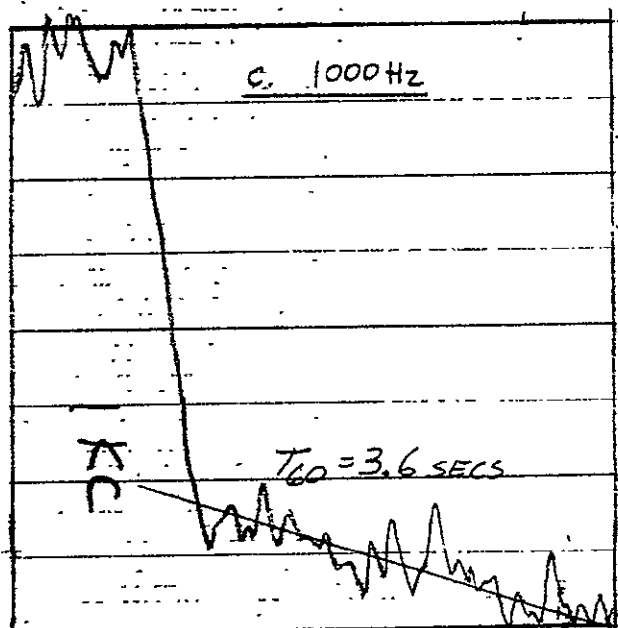
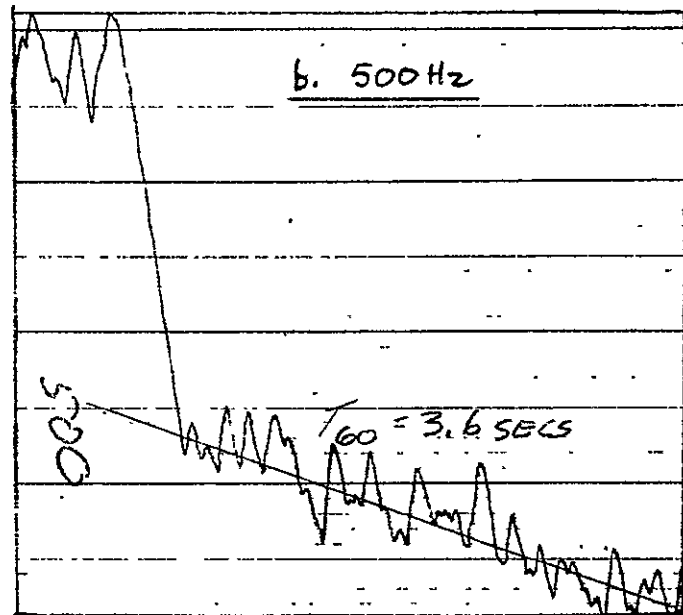
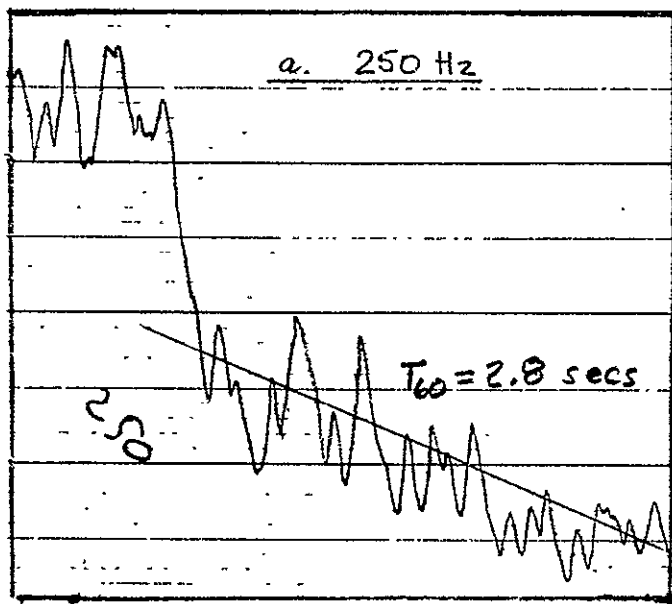


Figure 4. Octave Band Decays. Speaker Source At Inlet, Pointing Towards Settling Chamber, Microphone At 6' (1.8 m) Position On Boom in Softwall Test Section

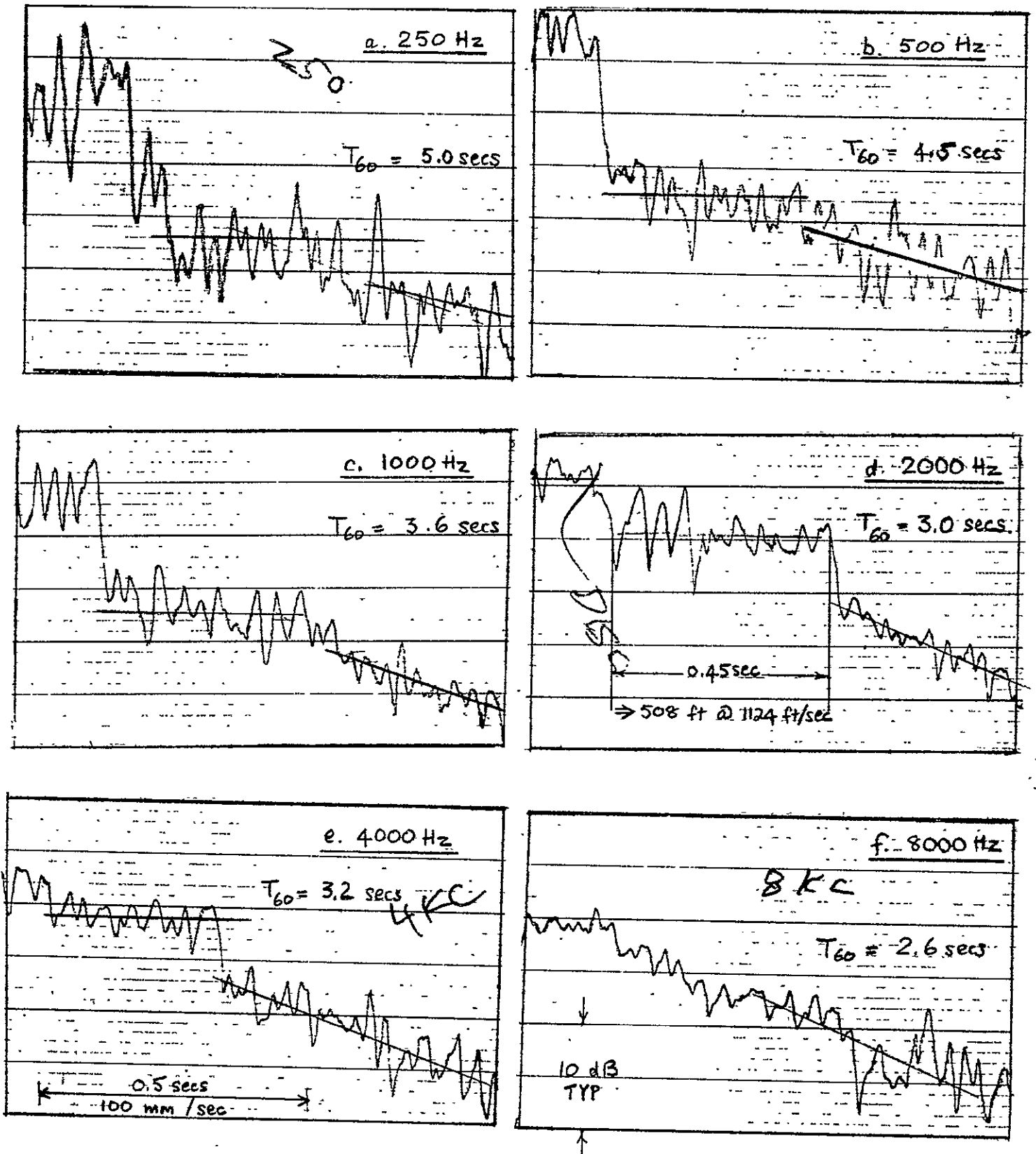


Figure 5. Octave Band Decays, Speaker Source At Simulator Exit, Pointing Towards Diffuser, Microphone At 6' (1.8 m) Position On Boom In Softwall Test Section

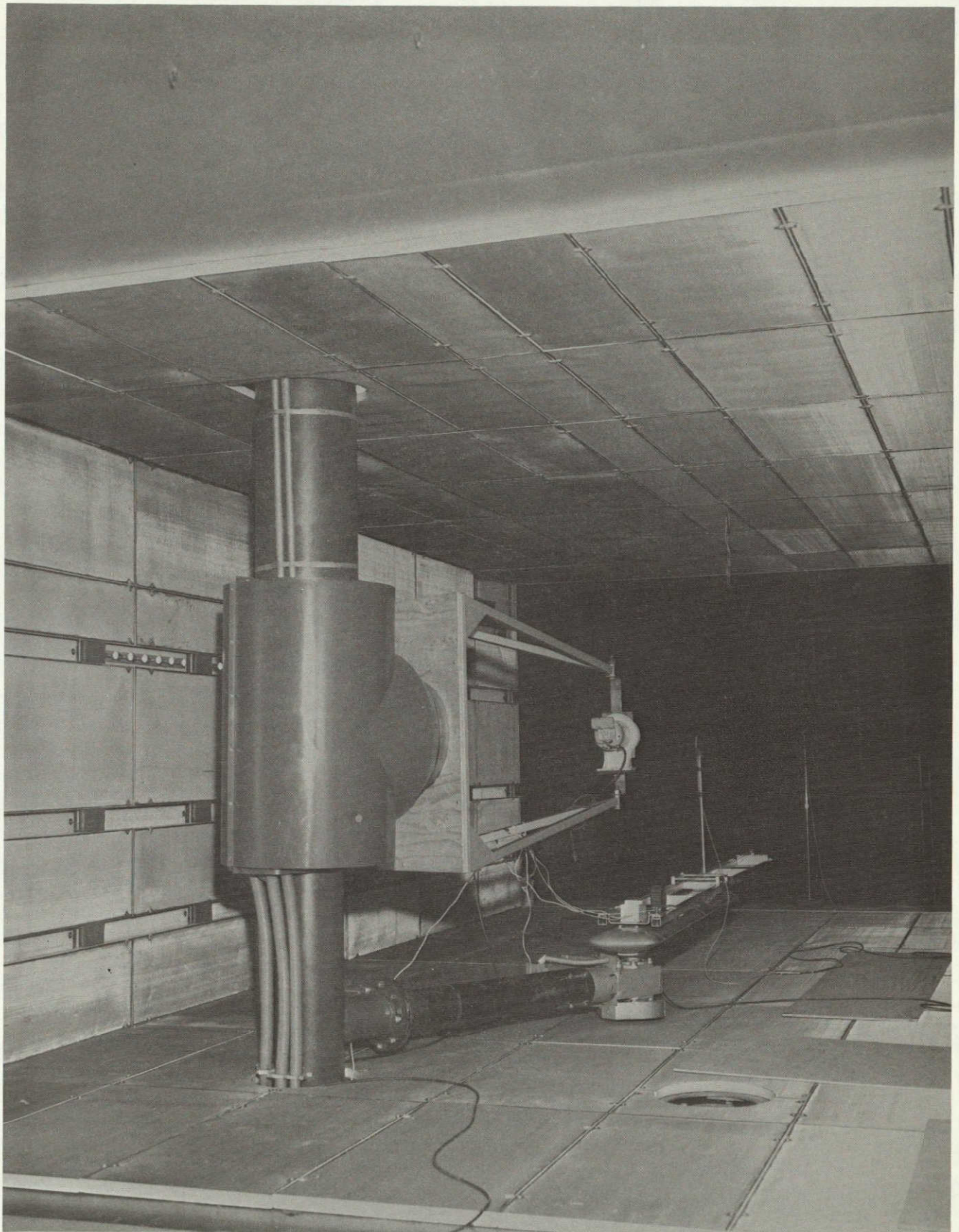
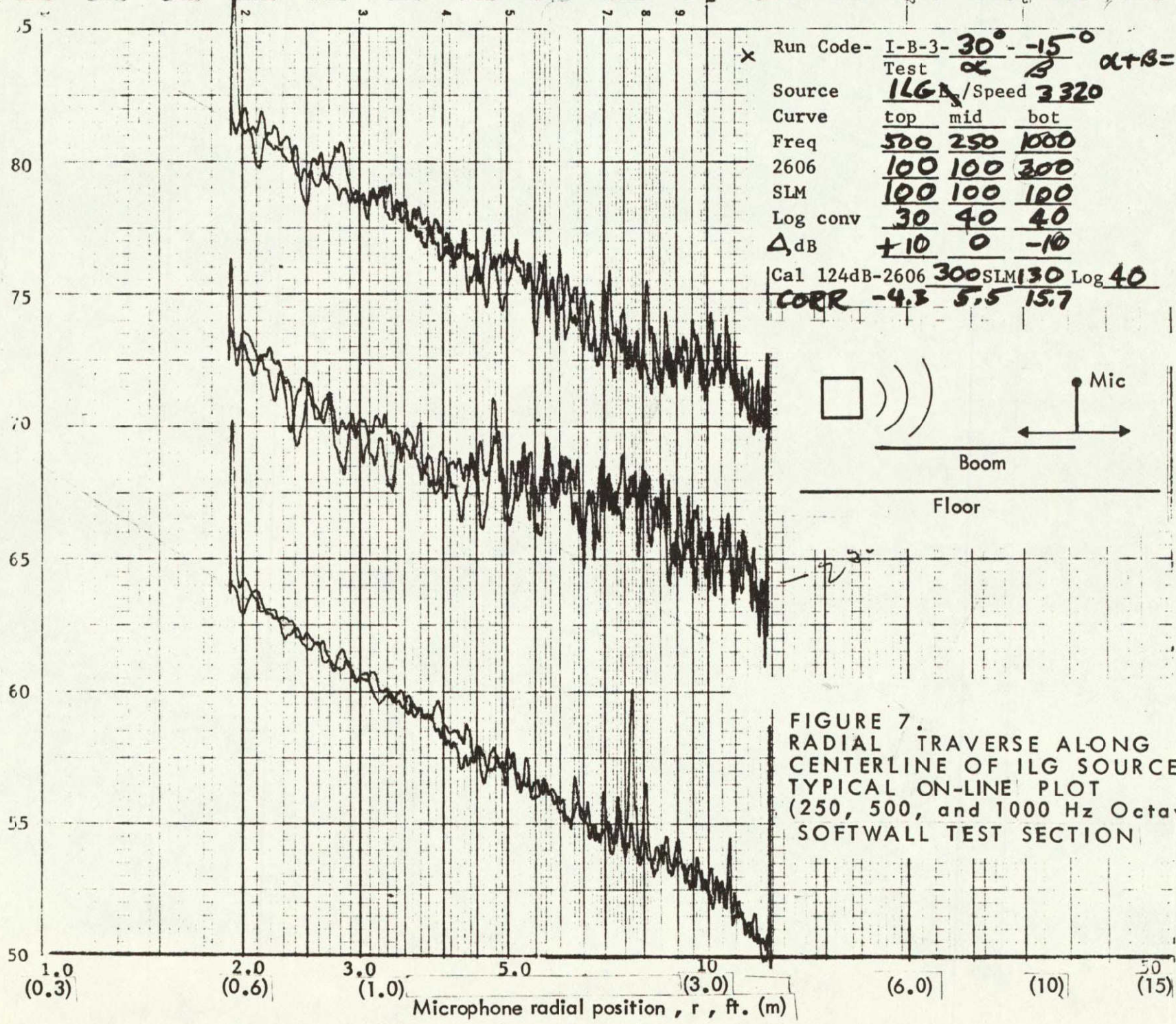


FIGURE 6. ILG SOURCE WITH MICROPHONE TRAVERSING MECHANISM, ACOUSTICALLY TREATED(SOFT WALL) 9 x 15 FOOT WIND TUNNEL TEST SECTION

ORIGINAL PAGE IS
OF POOR QUALITY

Traversing microphone sound pressure level, dB re 20 $\mu\text{N}/\text{m}^2$



Run Code- I-B-3- $30^\circ - 15^\circ$
 Test α β $\alpha + \beta = 15^\circ$
 Source ILG / Speed 3320
 Curve top mid bot
 Freq 500 250 1000
 2606 100 100 300
 SLM 100 100 100
 Log conv 30 40 40
 Δ dB +10 0 -10
 Cal 124dB-2606 300 SLM 130 Log 40
 CORR -4.3 5.5 15.7

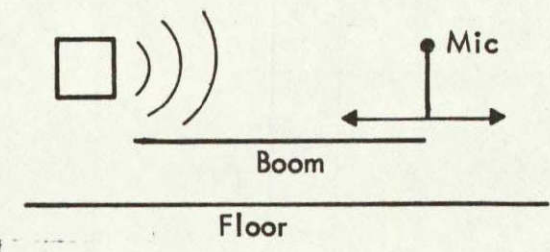


FIGURE 7.
 RADIAL TRAVERSE ALONG
 CENTERLINE OF ILG SOURCE,
 TYPICAL ON-LINE PLOT
 (250, 500, and 1000 Hz Octaves)
 SOFTWALL TEST SECTION

Traversing microphone sound pressure level, dB re 20 $\mu\text{N}/\text{m}^2$

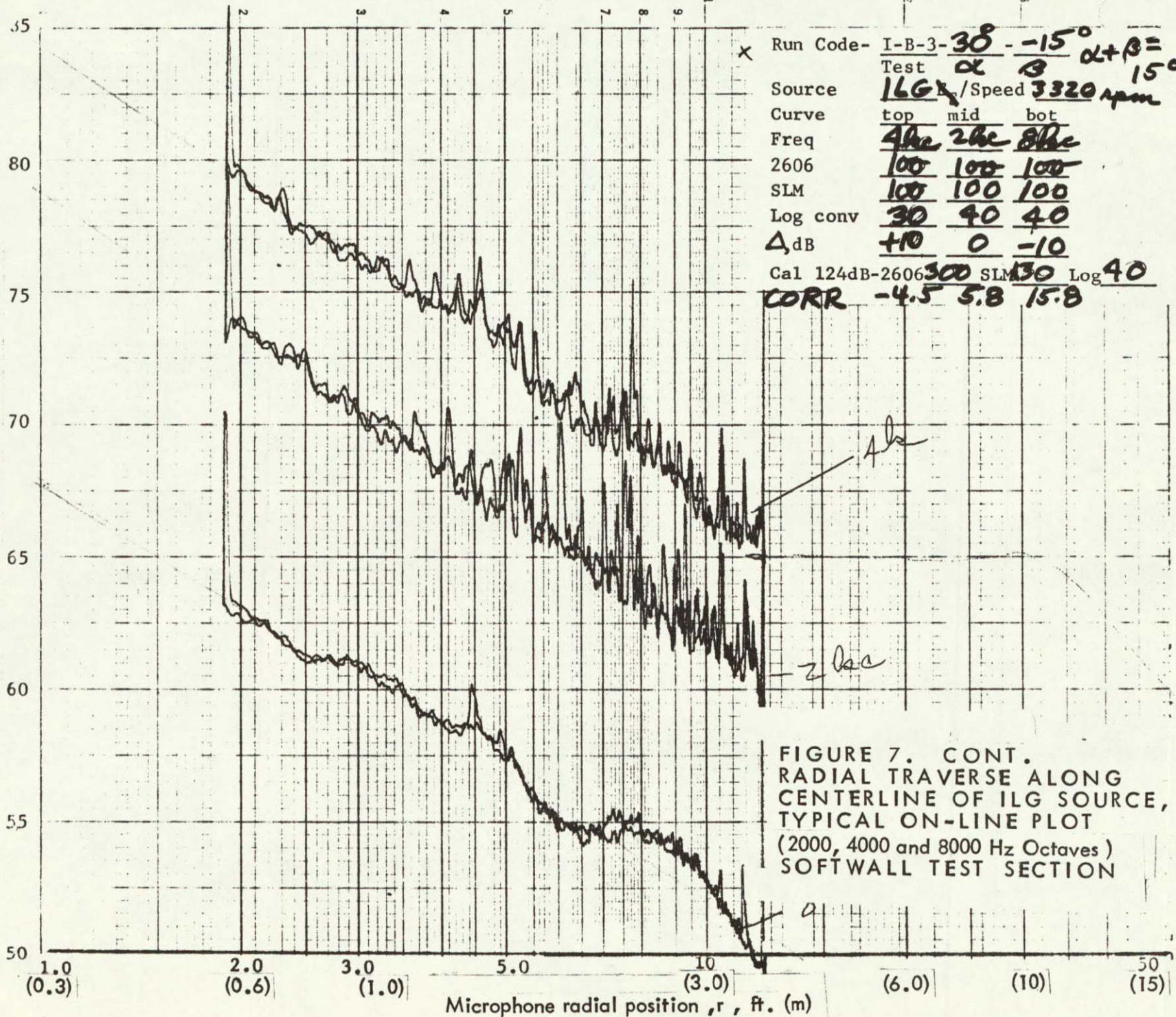
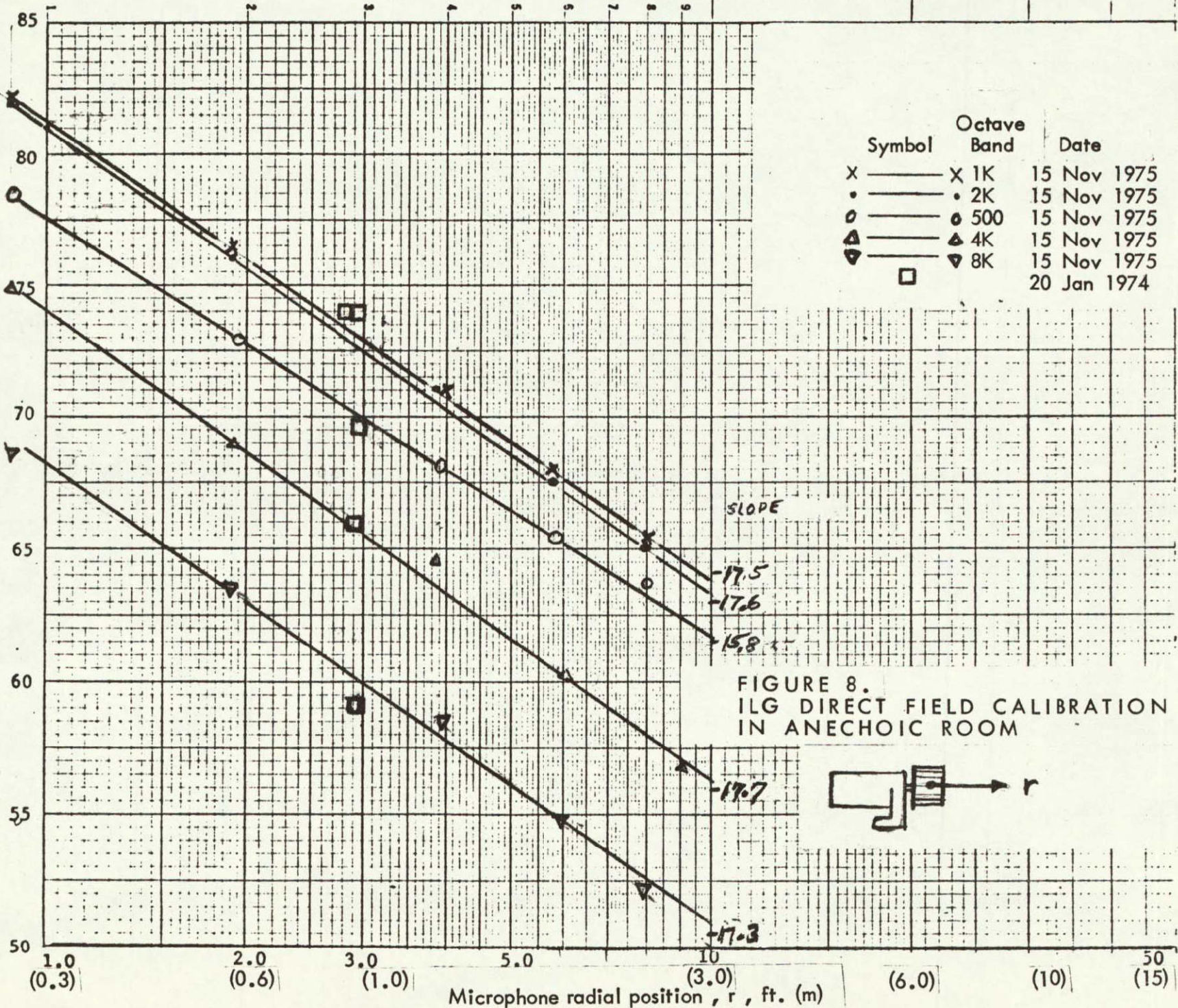
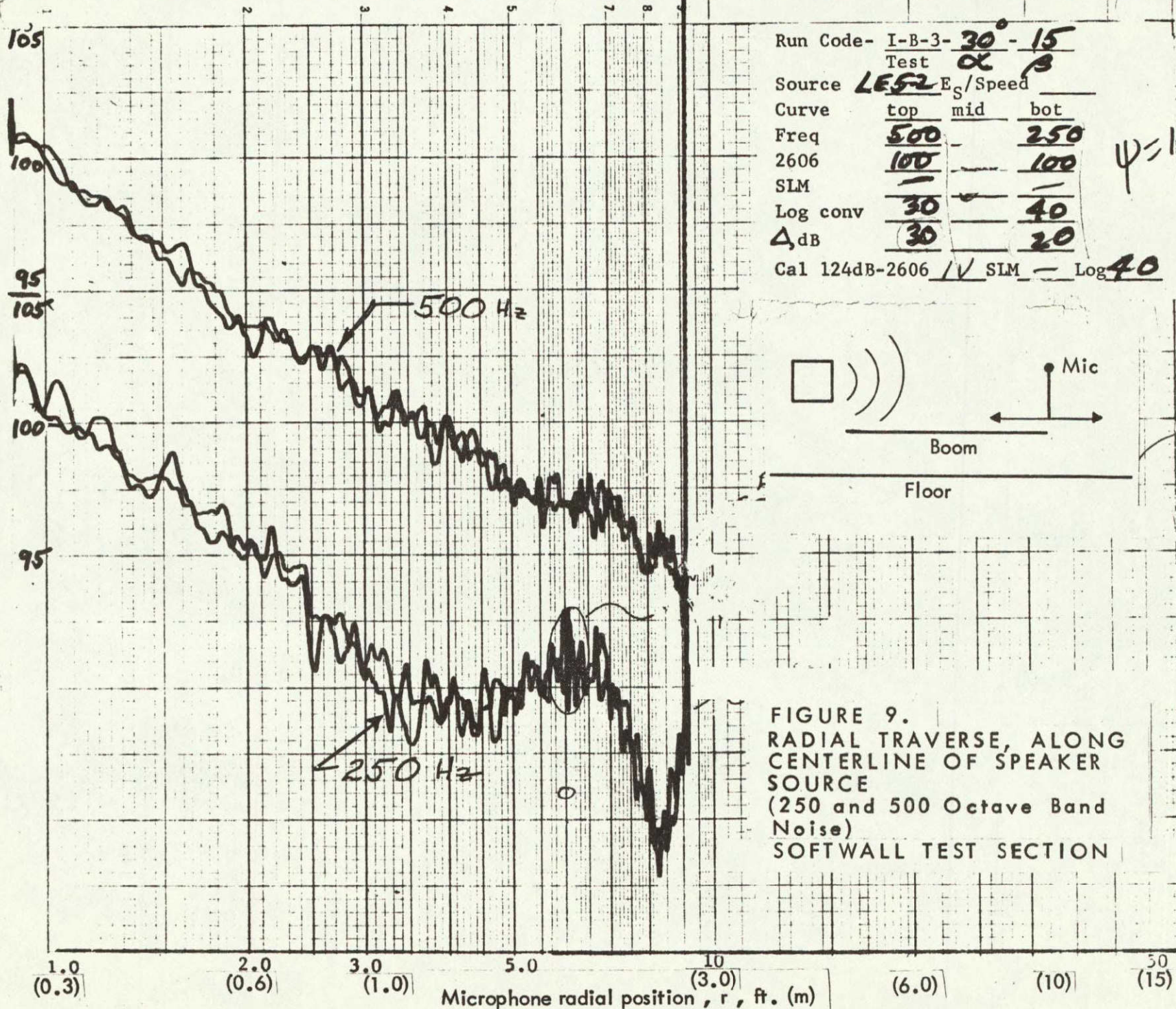


FIGURE 7. CONT.
 RADIAL TRAVERSE ALONG
 CENTERLINE OF ILG SOURCE,
 TYPICAL ON-LINE PLOT
 (2000, 4000 and 8000 Hz Octaves)
 SOFTWALL TEST SECTION

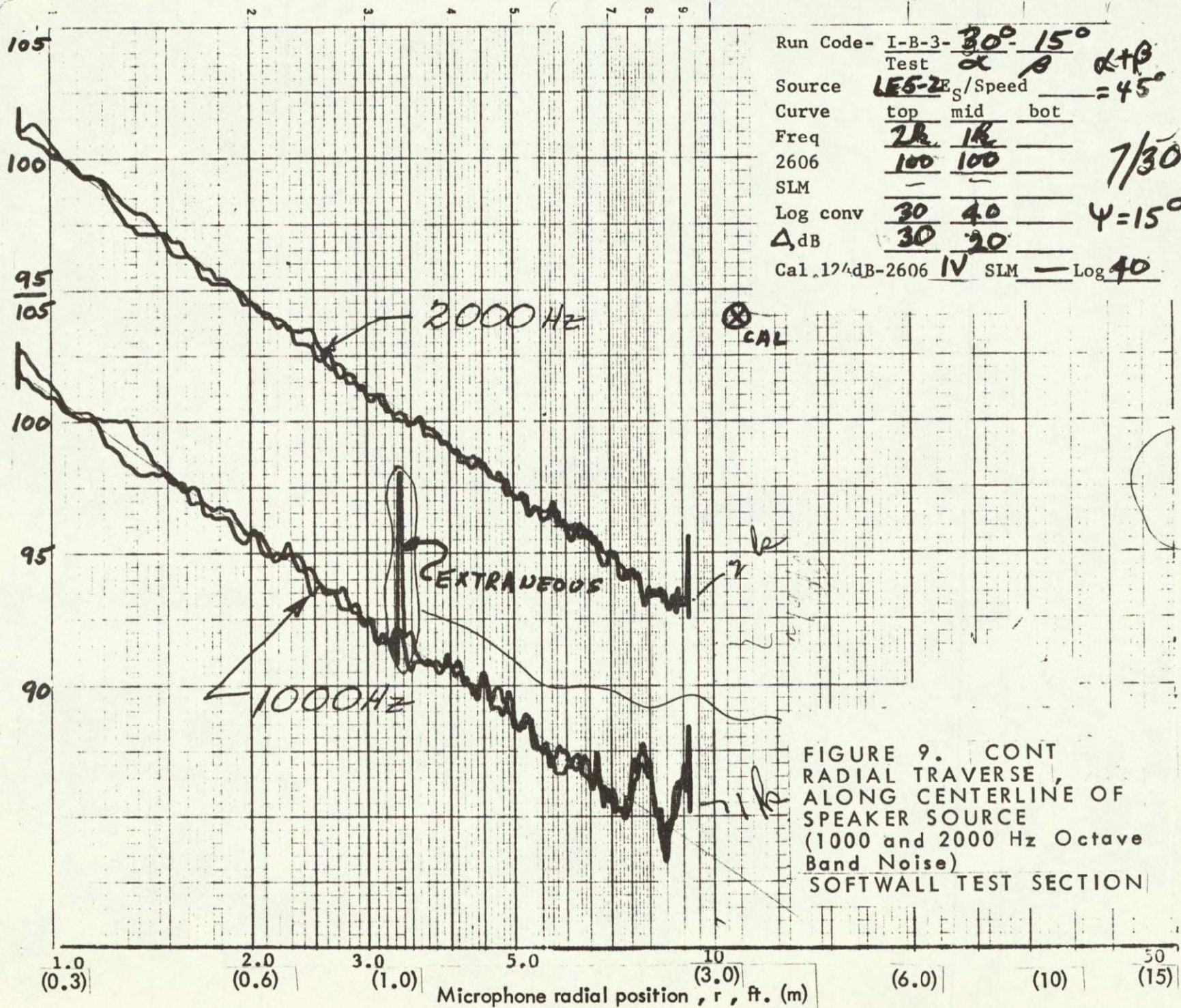
Traversing microphone sound pressure level, dB re 20 $\mu\text{N}/\text{m}^2$



Traversing microphone sound pressure level, dB re 20 $\mu\text{N}/\text{m}^2$



Traversing microphone sound pressure level, dB re $20 \mu\text{N/m}^2$



Traversing microphone sound pressure level, dB re 20 $\mu\text{N}/\text{m}^2$

105
100
95
105
100
95
90
85

1.0 (0.3) 2.0 (0.6) 3.0 (1.0) 5.0 (3.0) 10 (6.0) 50 (15)

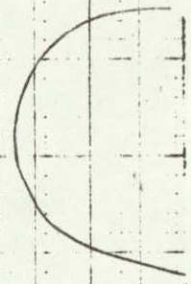
Microphone radial position, r, ft. (m)

Run Code- I-B-3- $30^\circ - 15^\circ$ $\alpha + \beta = 45^\circ$
 Test α β
 Source E_s /Speed
 Curve top mid bot $\psi = 15^\circ$
 Freq 8A 4A
 2606 100 100 7/30
 SLM
 Log conv 30 40
 Δ , dB 30 20
 Cal 124dB-2606 1.1 V SLM Log 40

8000 Hz

4000 Hz

FIGURE 9. CONT
 RADIAL TRAVERSE,
 ALONG CENTERLINE OF
 SPEAKER SOURCE
 (4000 and 8000 Hz Octave
 Band Noise)
 SOFTWALL TEST SECTION



Traversing microphone sound pressure level, dB re 20 $\mu\text{N}/\text{m}^2$

95

90

85

95

90

85

80

1.0
(0.3)

2.0
(0.6)

3.0
(1.0)

5.0

10
(3.0)

(6.0)

(10)

50
(15)

Microphone radial position, r, ft. (m)

Run Code- I-B-3-10°-10°-35
 Test α β γ
 Source SP E_g /Speed 1.0V ψ
 Curve top mid bot $\Gamma=0^\circ$
 Freq 1k 2k Γ_{ref} 45°
 2606 30mV 30mV TO WALL
 SLM
 Log conv 30 40
 Δ ,dB 40 30
 Cal 124dB-2606 1.0 SLM — Log 40

41

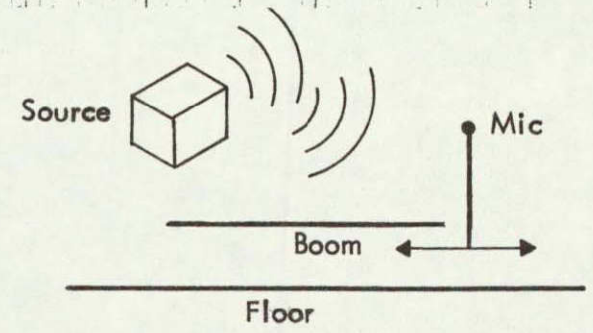
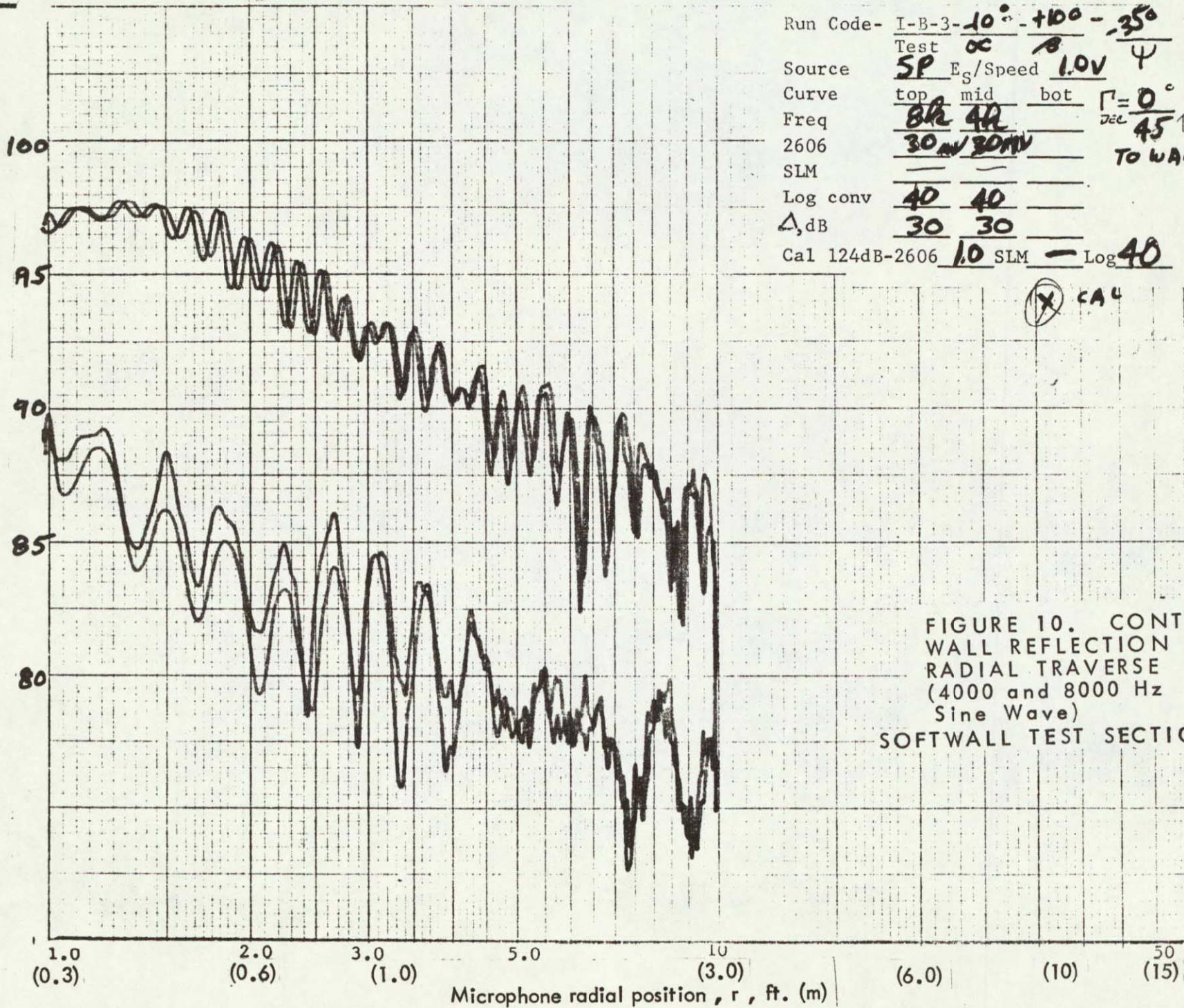


FIGURE 10.
 WALL REFLECTION
 RADIAL TRAVERSE
 (1000 and 2000 Hz
 Sine Wave)
 — SOFTWALL TEST SECTION

-2k

Traversing microphone sound pressure level, dB re 20 $\mu\text{N}/\text{m}^2$



Run Code- I-B-3-10°-+100-35° - 43
 Test ∞ β ψ
 Source SP E_s /Speed 1.0V ψ
 Curve top mid bot $\Gamma = 0^\circ$
 Freq 8R 4R $\frac{1}{2}c$ 45 TO WALL
 2606 30mV 30mV TO WALL
 SLM
 Log conv 40 40
 Δ , dB 30 30
 Cal 124dB-2606 1.0 SLM - Log 40

(X) CAL

FIGURE 10. CONT WALL REFLECTION RADIAL TRAVERSE (4000 and 8000 Hz Sine Wave) SOFTWALL TEST SECTION

Traversing microphone sound pressure level, dB re 20 μ N/m²

Run Code- I-B-3- 30° - 30° - 30°
 Test α β ψ
 Source SP E_s /Speed 1.0 ψ
 Curve top mid bot $\Gamma = 45^\circ$
 Freq 2.0k 2.2k Δ_{rel}
 2606 10mV 30mV
 SLM
 Log conv 40 40
 Δ , dB 40 30
 Cal 124dB-2606 1.0 SLM \times Log 40

0.2 k
 0.6
 0.2 k
 0.2 k
 0.8 k
 0.1 k

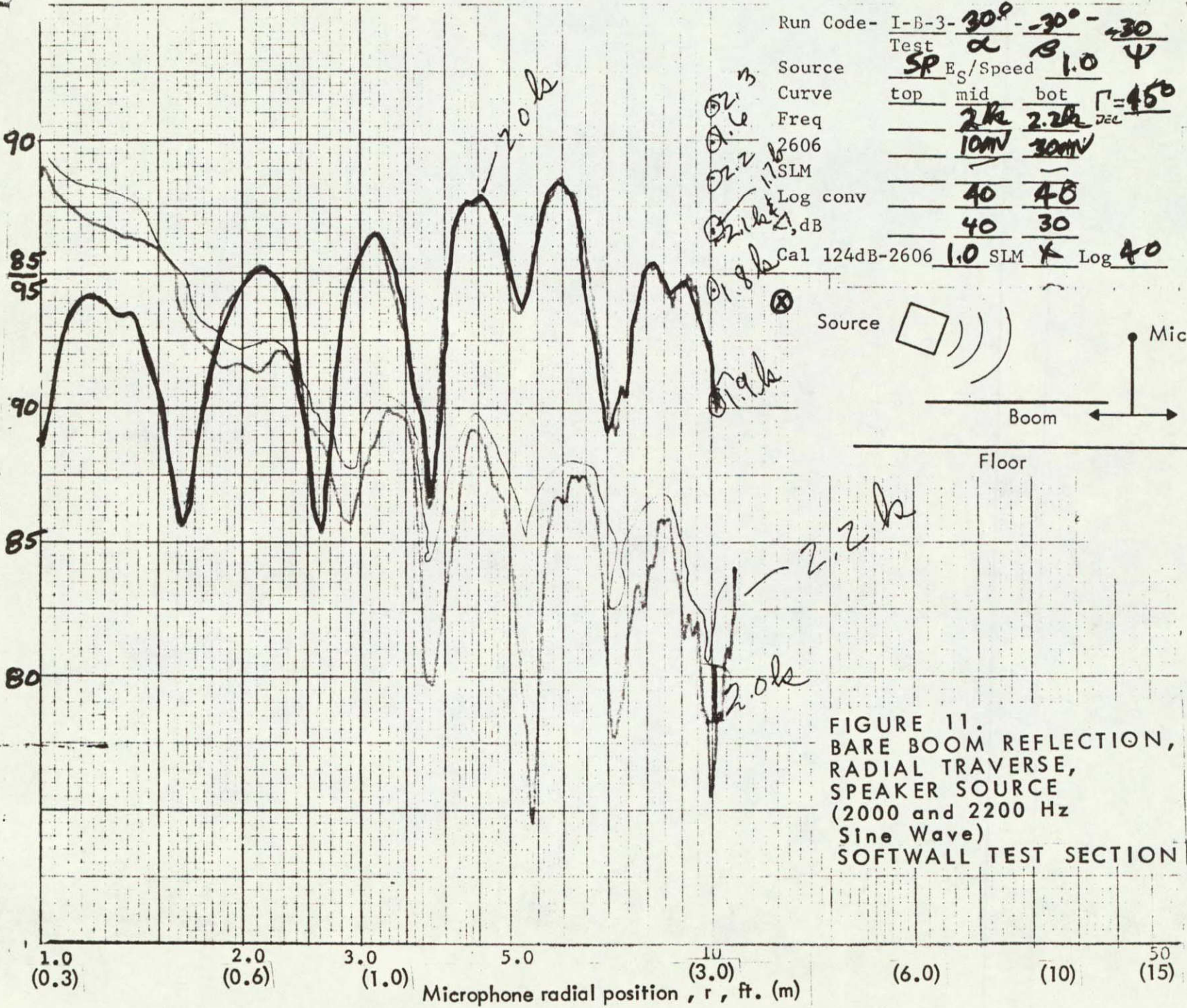
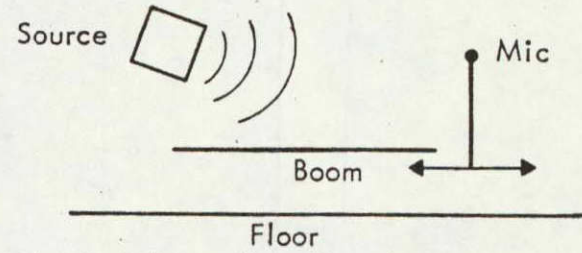
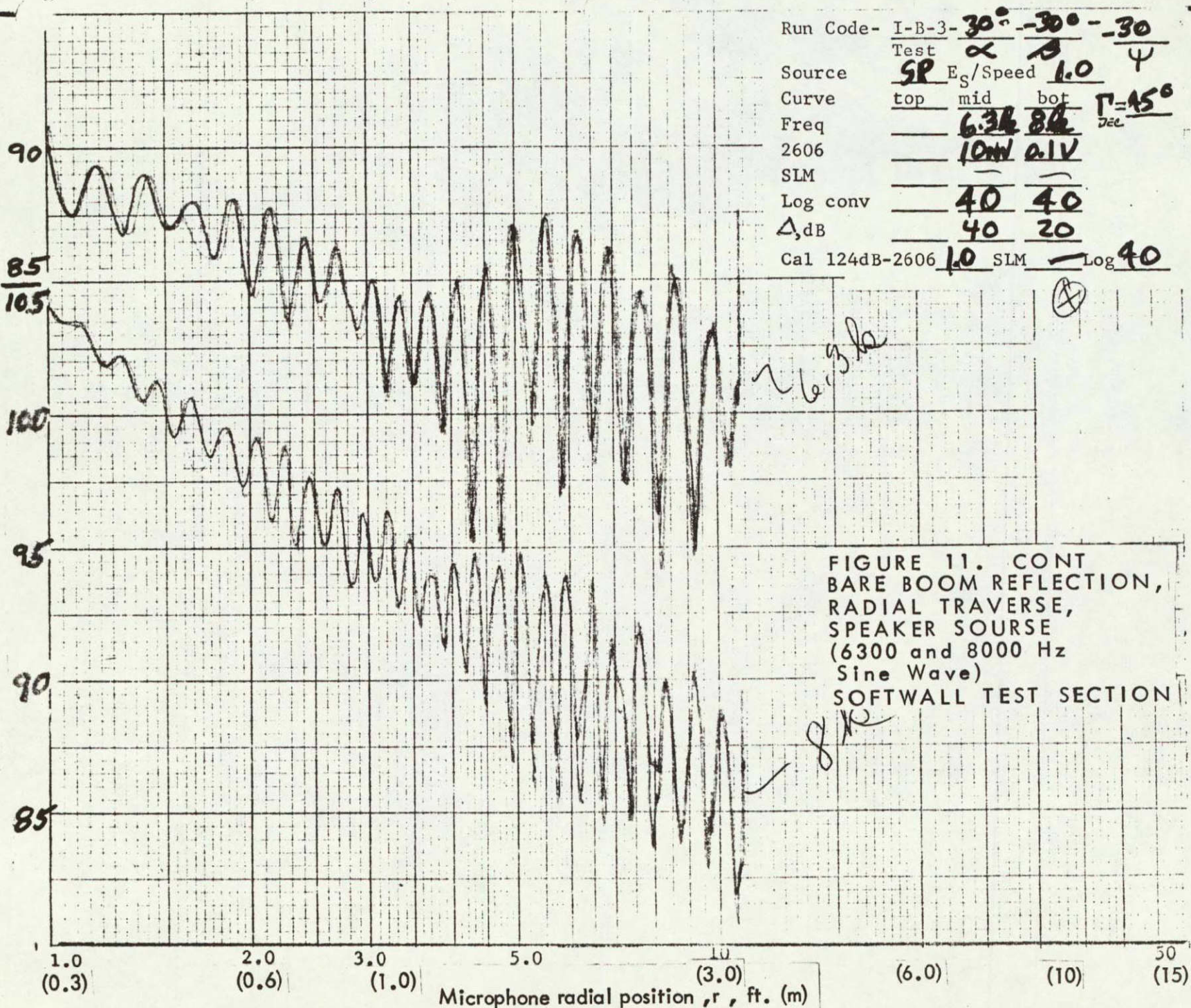


FIGURE 11.
 BARE BOOM REFLECTION,
 RADIAL TRAVERSE,
 SPEAKER SOURCE
 (2000 and 2200 Hz
 Sine Wave)
 SOFTWALL TEST SECTION

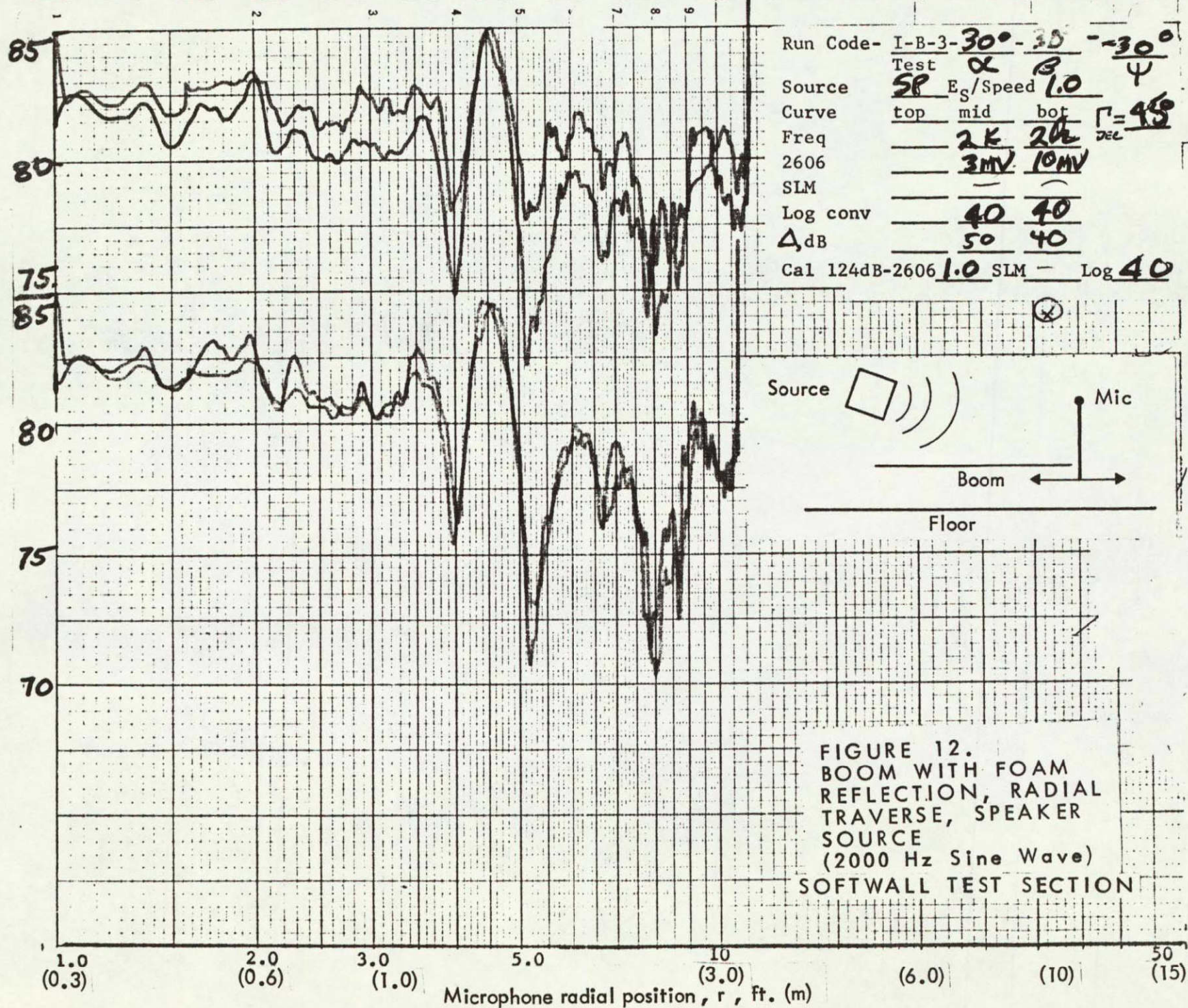
Traversing microphone sound
pressure level, dB re 20 $\mu\text{N}/\text{m}^2$



Run Code- I-B-3- 30° -30° -30° -77
 Test ∞ ∞ ∞
 Source SP E_s /Speed 1.0 ∞
 Curve top mid bot $\Gamma=15^\circ$
 Freq 6.3 kHz 8 kHz Dec
 2606 10W 0.1V
 SLM — —
 Log conv 40 40
 Δ ,dB 40 20
 Cal 124dB-2606 1.0 SLM — Log 40

FIGURE 11. CONT
 BARE BOOM REFLECTION,
 RADIAL TRAVERSE,
 SPEAKER SOURCE
 (6300 and 8000 Hz
 Sine Wave)
 SOFTWALL TEST SECTION

Traversing microphone sound pressure level, dB re $20 \mu\text{N}/\text{m}^2$



Run Code- I-B-3-30°-30°-30° 68
 Test α β γ
 Source SP E_s/Speed 1.0
 Curve top mid bot $r = 45$
 Freq 2K 20K DEL
 2606 3MV 10MV
 SLM
 Log conv 40 40
 ΔdB 50 40
 Cal 124dB-2606 1.0 SLM - Log 40

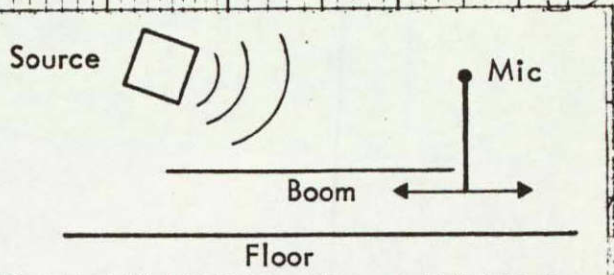


FIGURE 12.
 BOOM WITH FOAM REFLECTION, RADIAL TRAVERSE, SPEAKER SOURCE (2000 Hz Sine Wave) SOFTWALL TEST SECTION

Traversing microphone sound pressure level, dB re 20 $\mu\text{N}/\text{m}^2$

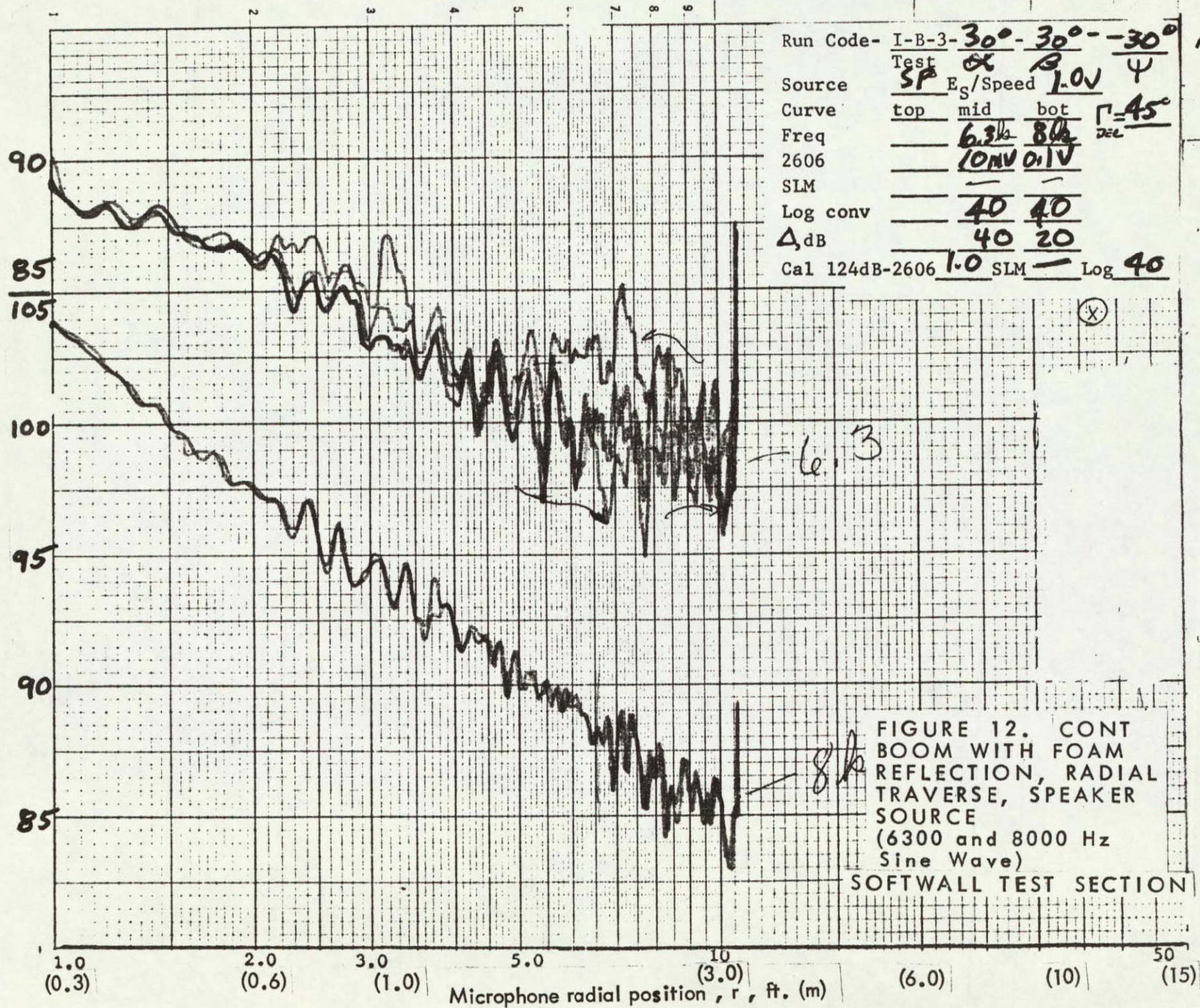
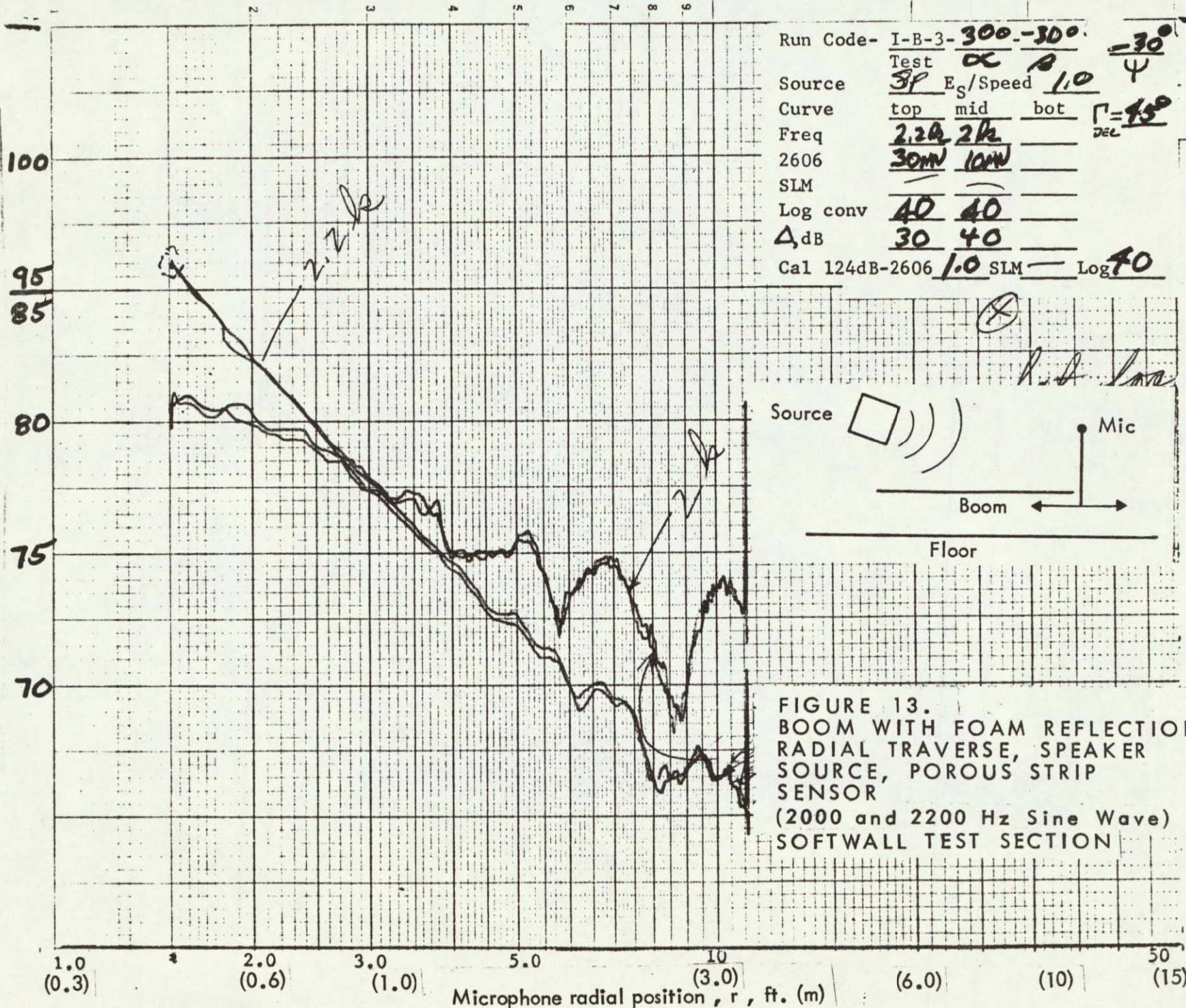


FIGURE 12. CONT BOOM WITH FOAM REFLECTION, RADIAL TRAVERSE, SPEAKER SOURCE (6300 and 8000 Hz Sine Wave) SOFTWALL TEST SECTION

Traversing microphone sound pressure level, dB re 20 $\mu\text{N}/\text{m}^2$



Run Code- I-B-3-300-30° -30° 117
 Test ∞ ρ 1.0 ψ
 Source 3P E_s /Speed 1.0
 Curve top mid bot $\Gamma=150$
 Freq 2.2k 2k DEL
 2606 30mV 10mV
 SLM
 Log conv 40 40
 Δ ,dB 30 40
 Cal 124dB-2606 1.0 SLM Log 40

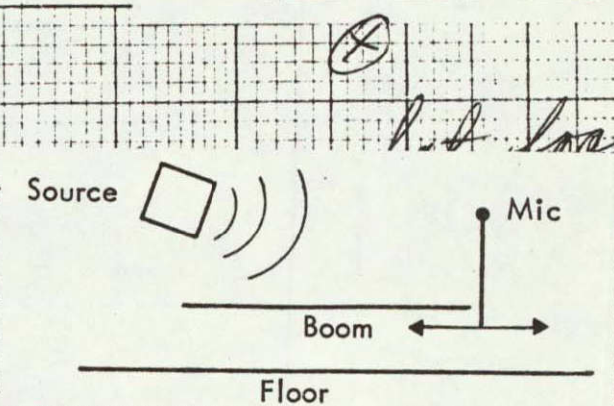
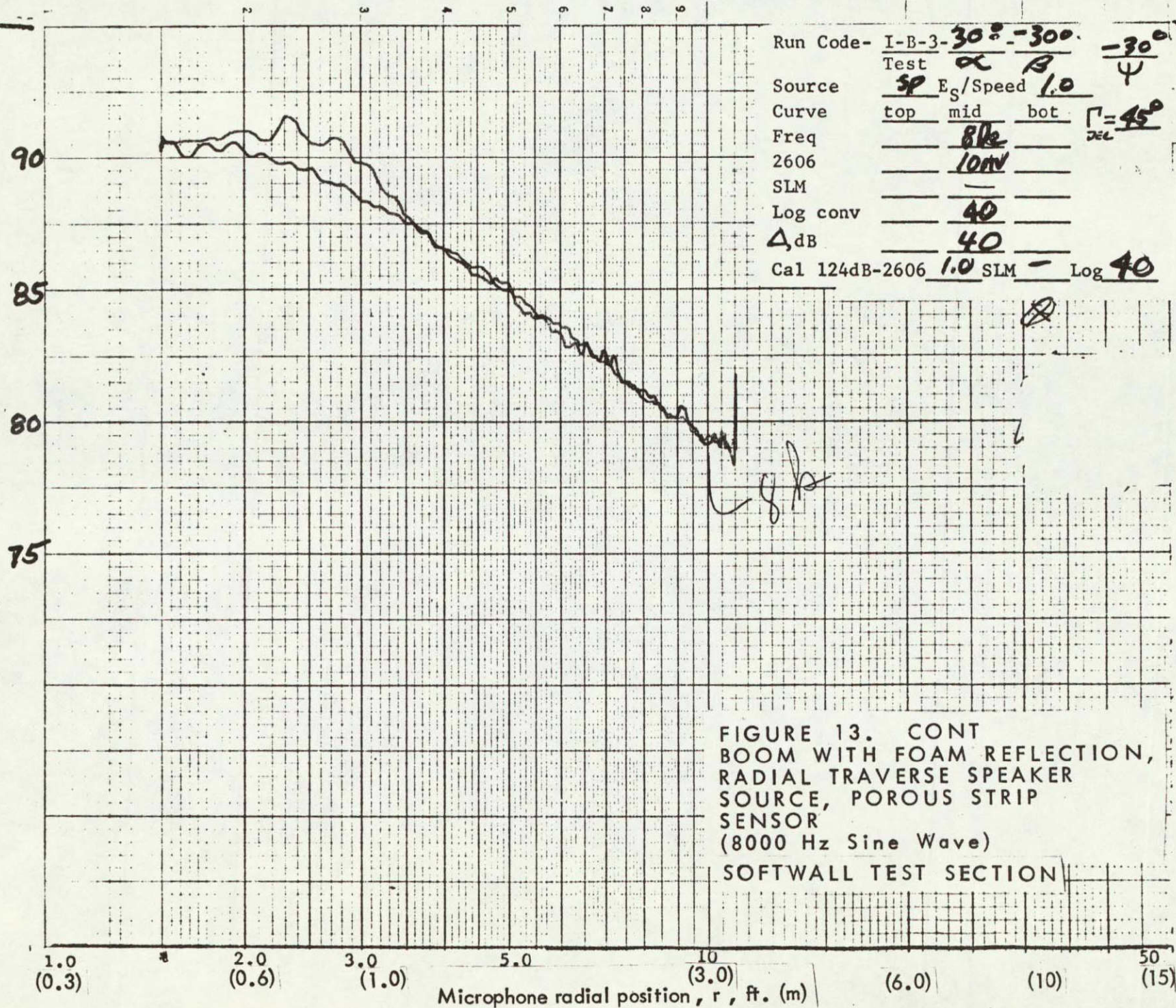


FIGURE 13.
 BOOM WITH FOAM REFLECTION,
 RADIAL TRAVERSE, SPEAKER
 SOURCE, POROUS STRIP
 SENSOR
 (2000 and 2200 Hz Sine Wave)
 SOFTWALL TEST SECTION

Traversing microphone sound pressure level, dB re $20 \mu\text{N}/\text{m}^2$



Run Code- I-B-3-30°-300. -30° 12)

Test α B ψ

Source SP E_s /Speed 1.0

Curve top mid bot $\square = 45^\circ$

Freq 8ke $\frac{1}{2} \text{CEL}$

2606 10mV

SLM

Log conv 40

Δ dB 40

Cal 124dB-2606 1.0 SLM - Log 40

FIGURE 13. CONT
 BOOM WITH FOAM REFLECTION,
 RADIAL TRAVERSE SPEAKER
 SOURCE, POROUS STRIP
 SENSOR
 (8000 Hz Sine Wave)
 SOFTWALL TEST SECTION

ORIGINAL PAGE IS
OF POOR QUALITY

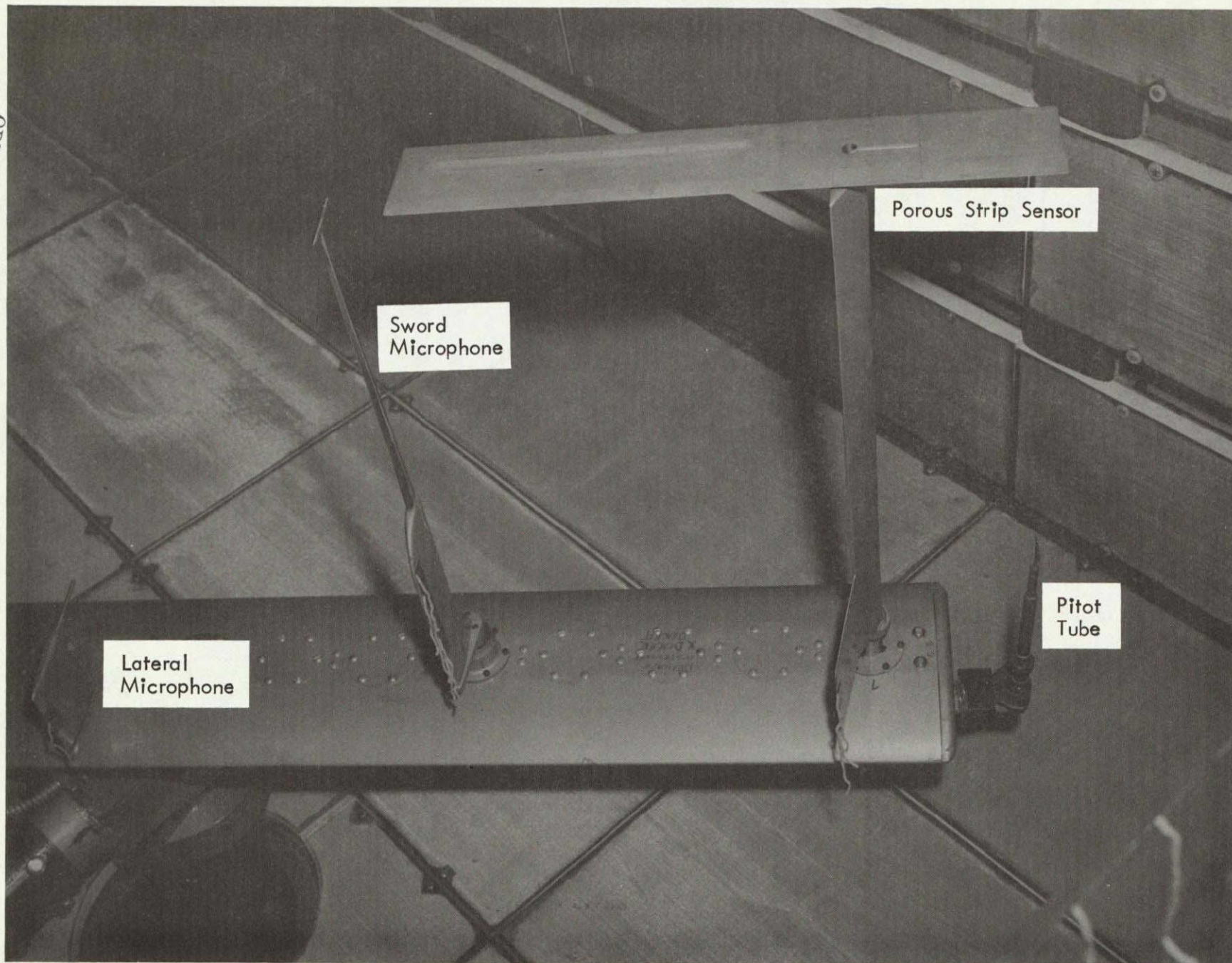
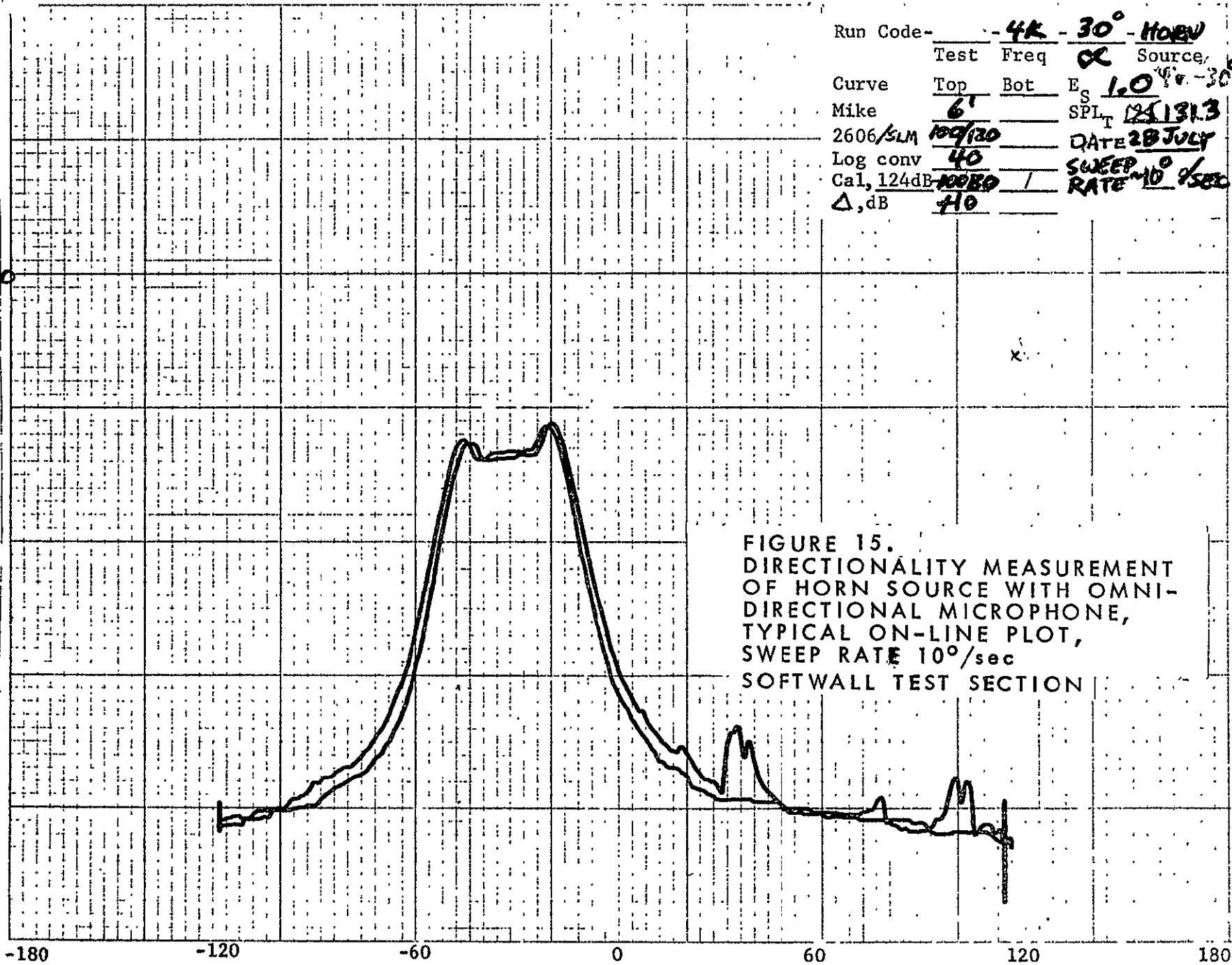


FIGURE 14. POROUS STRIP SENSOR, WEATHERVANING MICROPHONE SWORD,
AND PITOT TUBE ON ROTATING MICROPHONE BOOM

Omni Directional Microphone Sound Pressure Level,
dB re 20 μ N/m²

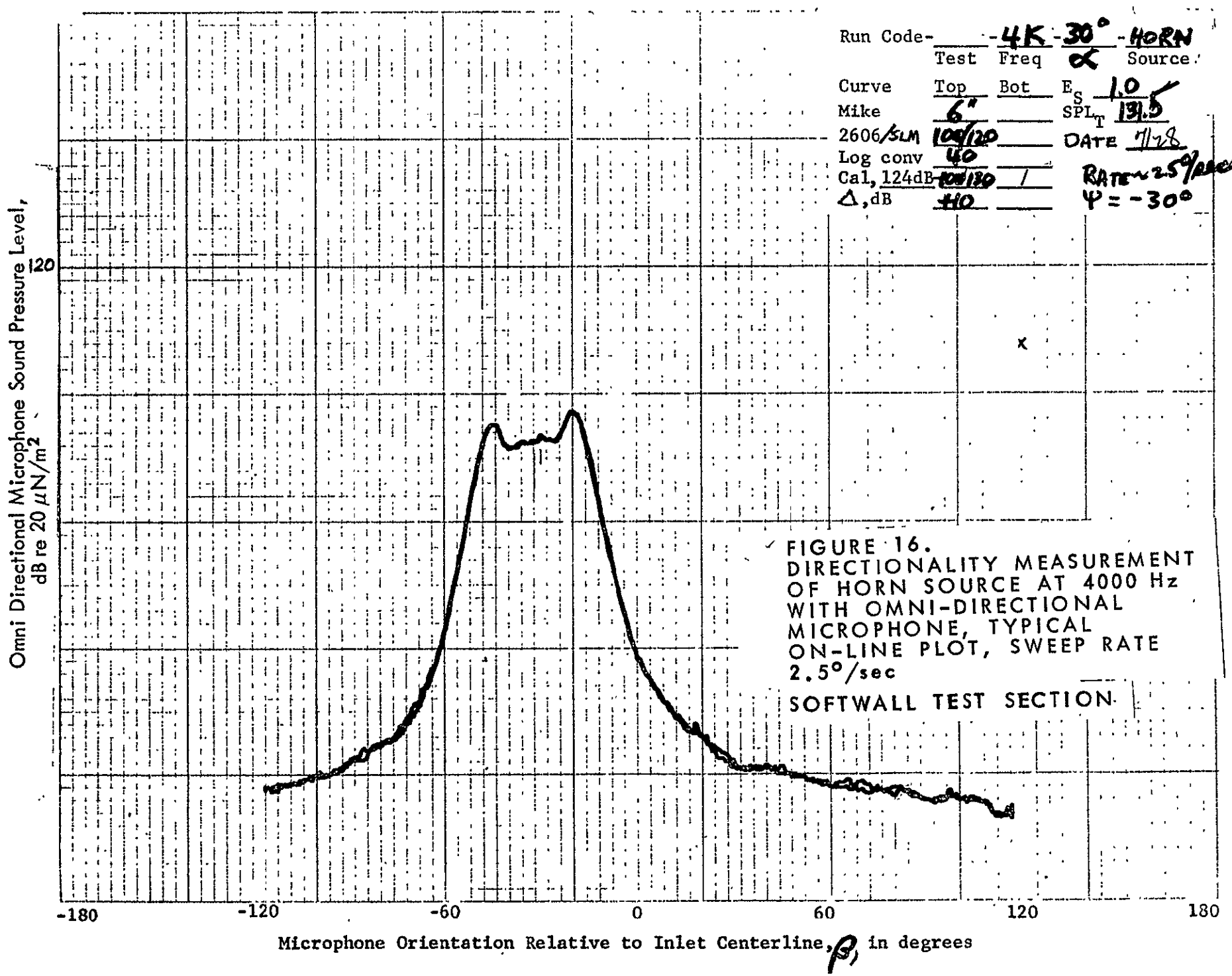


Run Code-	- 4K - 30° - HORN		
Test Freq	OK	Source	
Curve	Top	Bot	E _s 1.0 ⁴ - 30°
Mike	6'	SPL _T	125.131.3
2606/SLM	100/30	DATE	28 JULY
Log conv	40	SWEEP	10°/sec
Cal, 124dB	10000	RATE	10°/sec
Δ, dB	10		

FIGURE 15.
DIRECTIONALITY MEASUREMENT
OF HORN SOURCE WITH OMNI-
DIRECTIONAL MICROPHONE,
TYPICAL ON-LINE PLOT,
SWEEP RATE 10°/sec
SOFTWALL TEST SECTION

Microphone Orientation Relative to Inlet Centerline, β , in degrees

Run Code- 4K-30°-HORN
 Test Freq 4 Source α
 Curve Top Bot E_S 1.0
 Mike 6" SPL_T 131.5
 2606/SLM 100/120 DATE 7/28
 Log conv 40 RATE 2.5°/sec
 Cal, 124dB 100/130 / 1 ψ = -300
 Δ, dB 410



✓ FIGURE 16.
 DIRECTIONALITY MEASUREMENT
 OF HORN SOURCE AT 4000 Hz
 WITH OMNI-DIRECTIONAL
 MICROPHONE, TYPICAL
 ON-LINE PLOT, SWEEP RATE
 2.5°/sec
 SOFTWALL TEST SECTION.

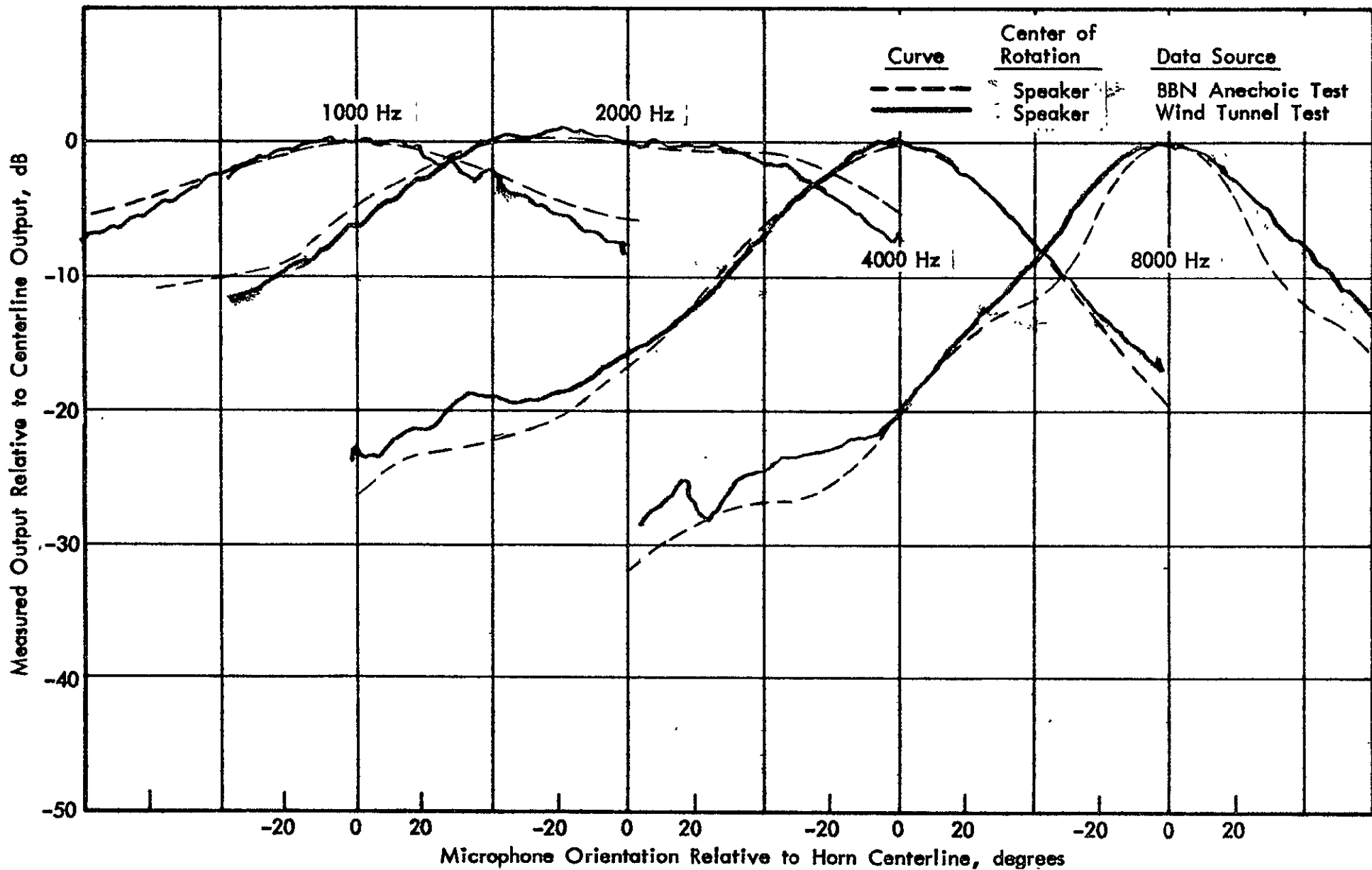


FIGURE 17. COMPARISON OF LE5-2 SPEAKER DIRECTIONALITY MEASUREMENTS WITH OMNI MICROPHONE AT SIX FOOT RADIUS IN SOFTWALL TEST SECTION, ANGLED TOWARDS WALL ($\alpha=30, \psi=40$), AND IN ANECHOIC CHAMBER

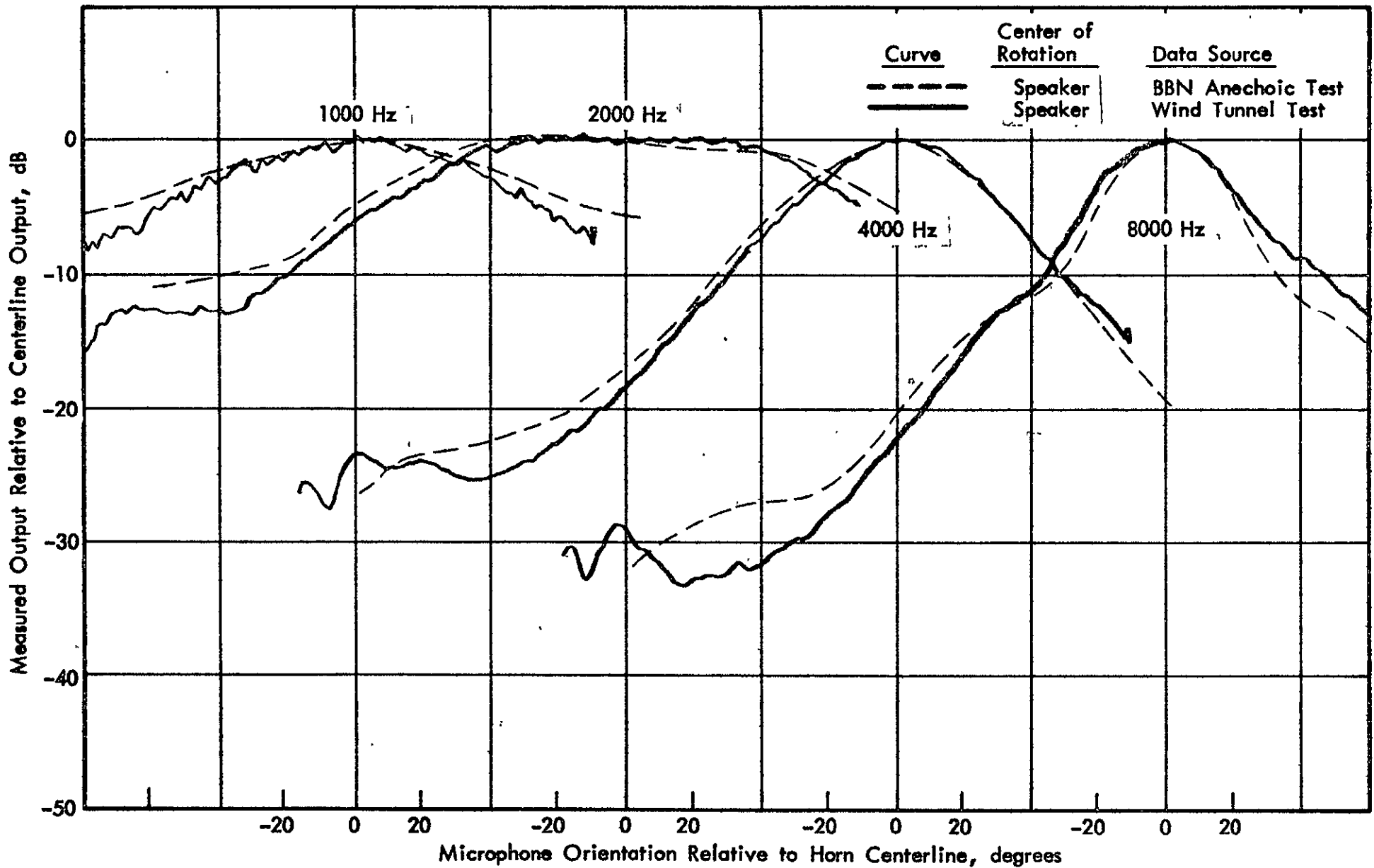


FIGURE 18. COMPARISON OF LE5-2 SPEAKER DIRECTIONALITY MEASUREMENTS WITH POROUS STRIP SENSOR IN SOFT WALL TEST SECTION, ANGLED TOWARDS WALL ($\alpha = 30, \psi = 48$), AND WITH OMNI MICROPHONE IN ANECHOIC CHAMBER

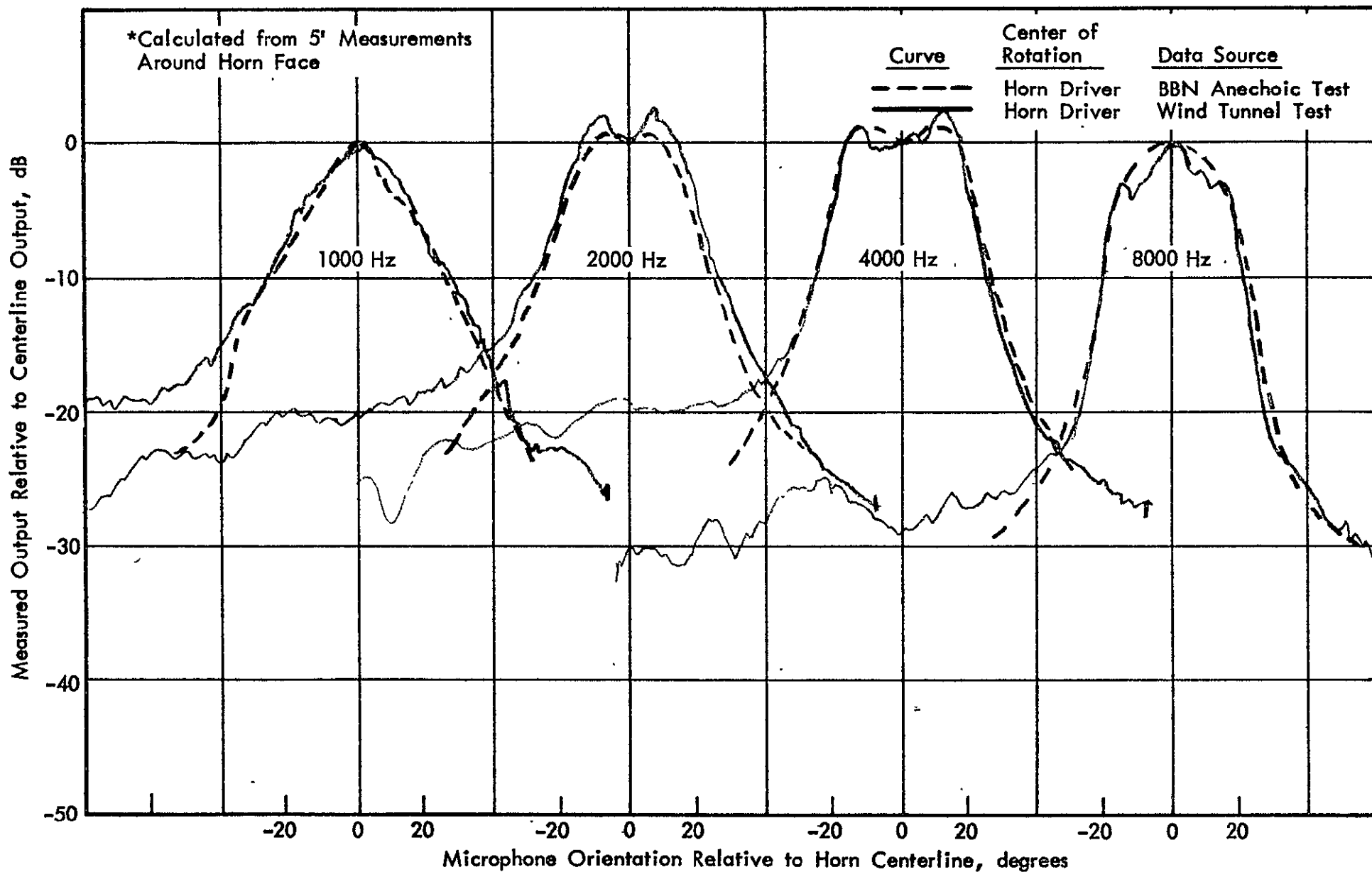


FIGURE 19. COMPARISON OF HORN DIRECTIVITY MEASUREMENTS WITH OMNI MICROPHONE IN SOFTWALL TEST SECTION, ANGLED TOWARDS WALL ($\alpha = 30$, $\psi = 40$); AND IN ANECHOIC CHAMBER

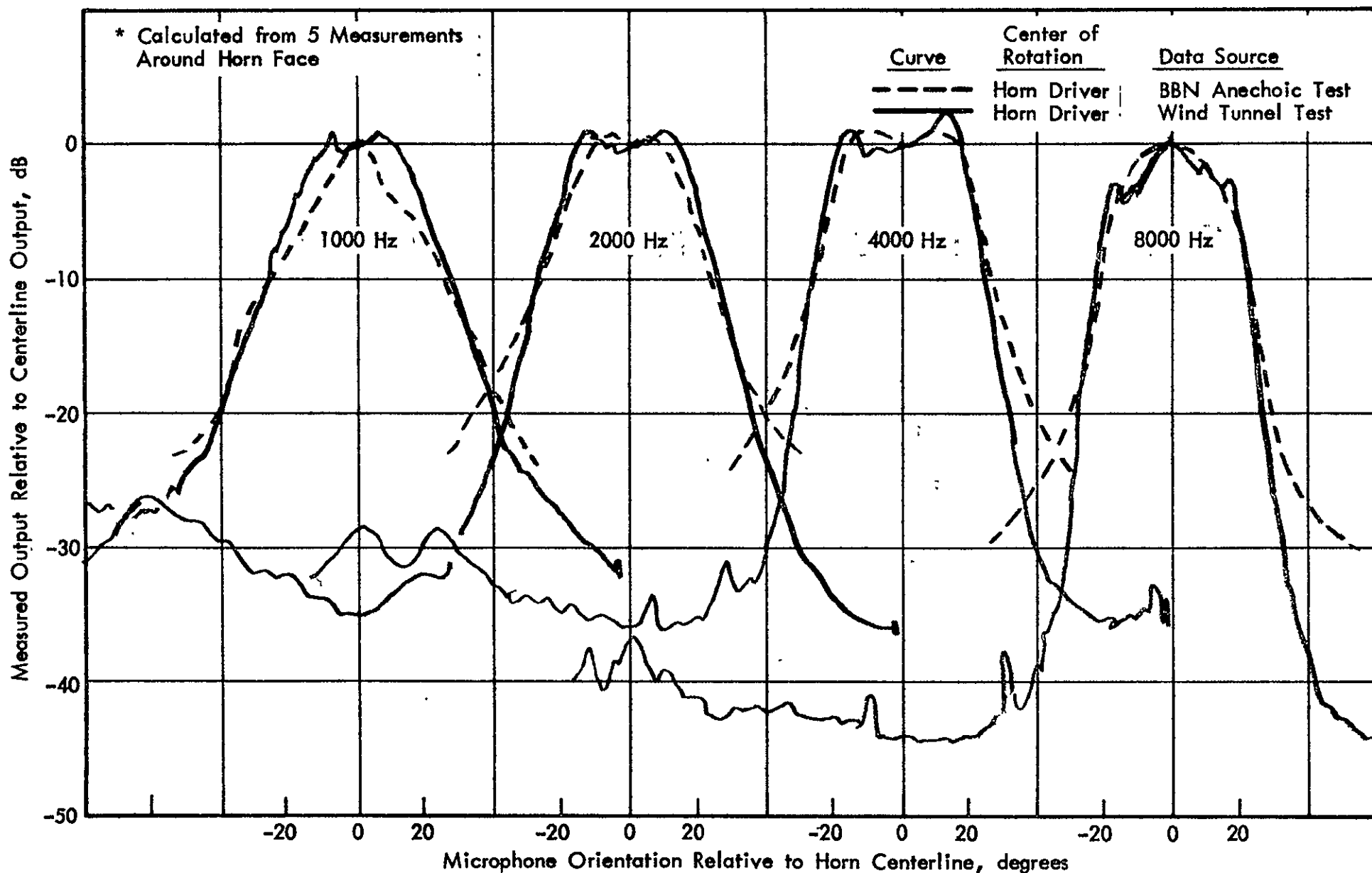
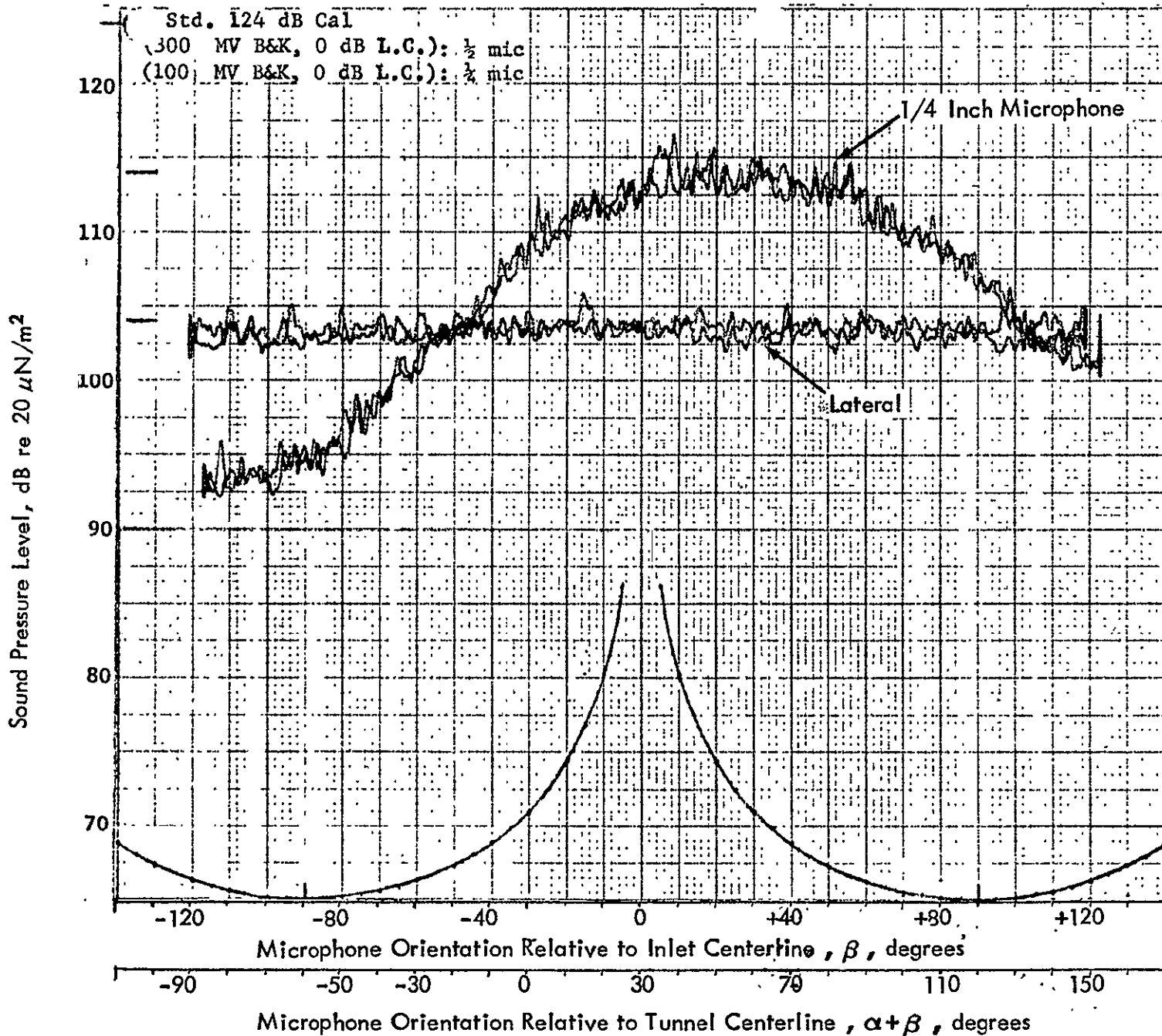


FIGURE 20. COMPARISON OF HORN DIRECTIONALITY MEASUREMENTS WITH POROUS STRIP SENSOR AT SIX FOOT RADIUS IN SOFTWALL TEST SECTION, ANGLED TOWARDS WALL ($\alpha = 30, \psi = 45$), AND WITH OMNI MICROPHONE IN ANECHOIC CHAMBER

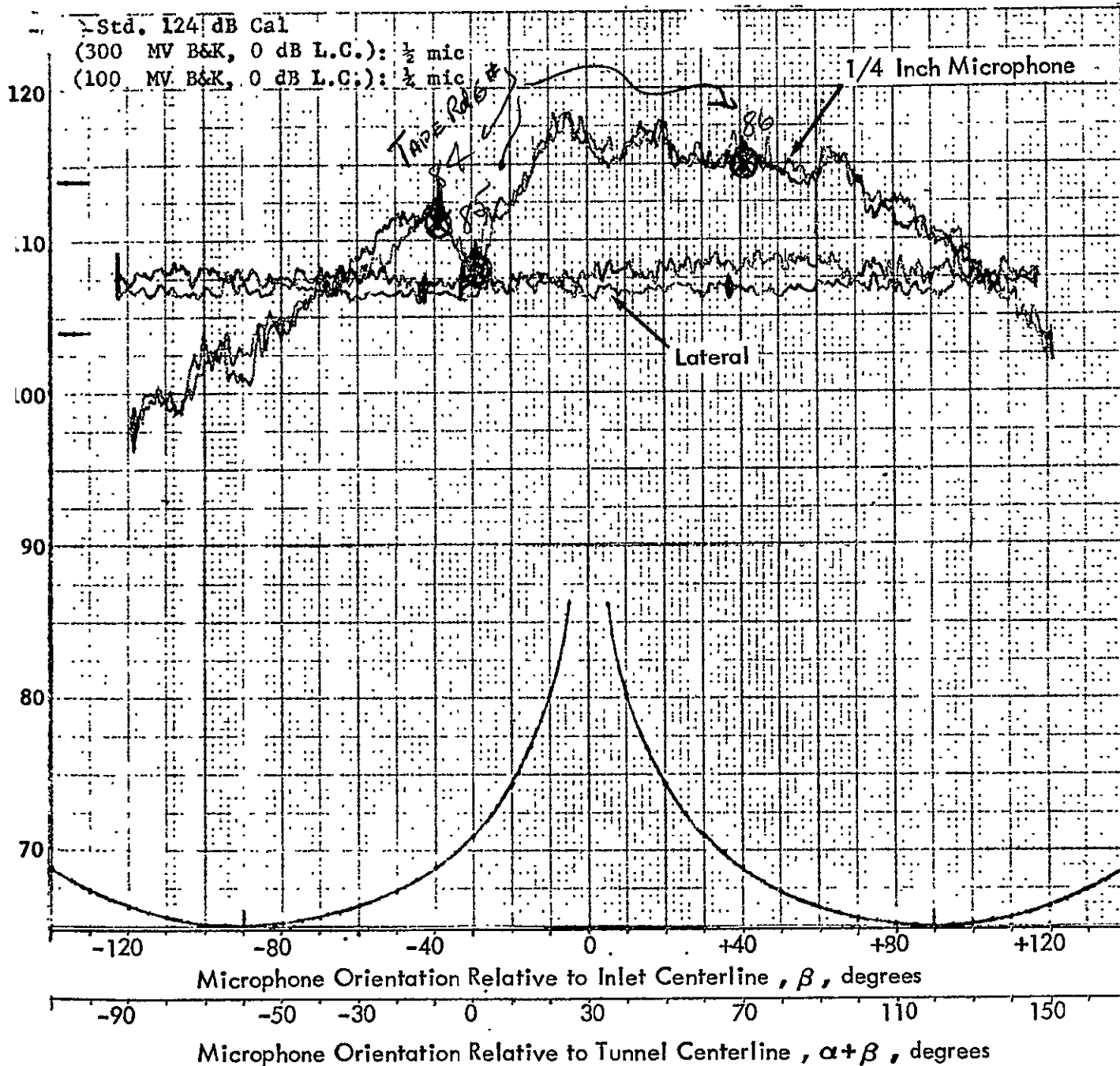


Date: 11/6/75
 Test No.: IIA2
 Plot No.: 165
 Inlet Configuration:
Scrap
SOFTWARE TEST
SECTION
 Run Conditions:
 Rdg. No.*
 α 30 β 2.5
 M_t 0.6 r_m 4
 Siren freq* 9.6K
 Tunnel $q(V_0)$ 0
 Acoustic System:
 Curve G R
 Top Bot.
 Mike* L BU
 B&K* 100 100
 L.C.* 0 0
 Cal(B&K/LC)* ✓ ✓
 Δ dB 0 0
 Fil. Gen. Freq* 10 10 kHz
 Fil. B.W.* 1/3 1/3

*Required information

FIGURE 21.
 B&K MICROPHONE
 OUTPUT, $M = 0$
 INLET DIRECTIONALITY
 TEST

Sound Pressure Level, dB re $20 \mu\text{N}/\text{m}^2$



Date: 11/6

Test No.: HAZ

Plot No.: 186

Inlet Configuration:
SCOOP
SOFT WALL TEST
SECTION

Run Conditions:
 Rdg. No.* _____

α 30° β 2.5

M_t 0.6 r_m 4

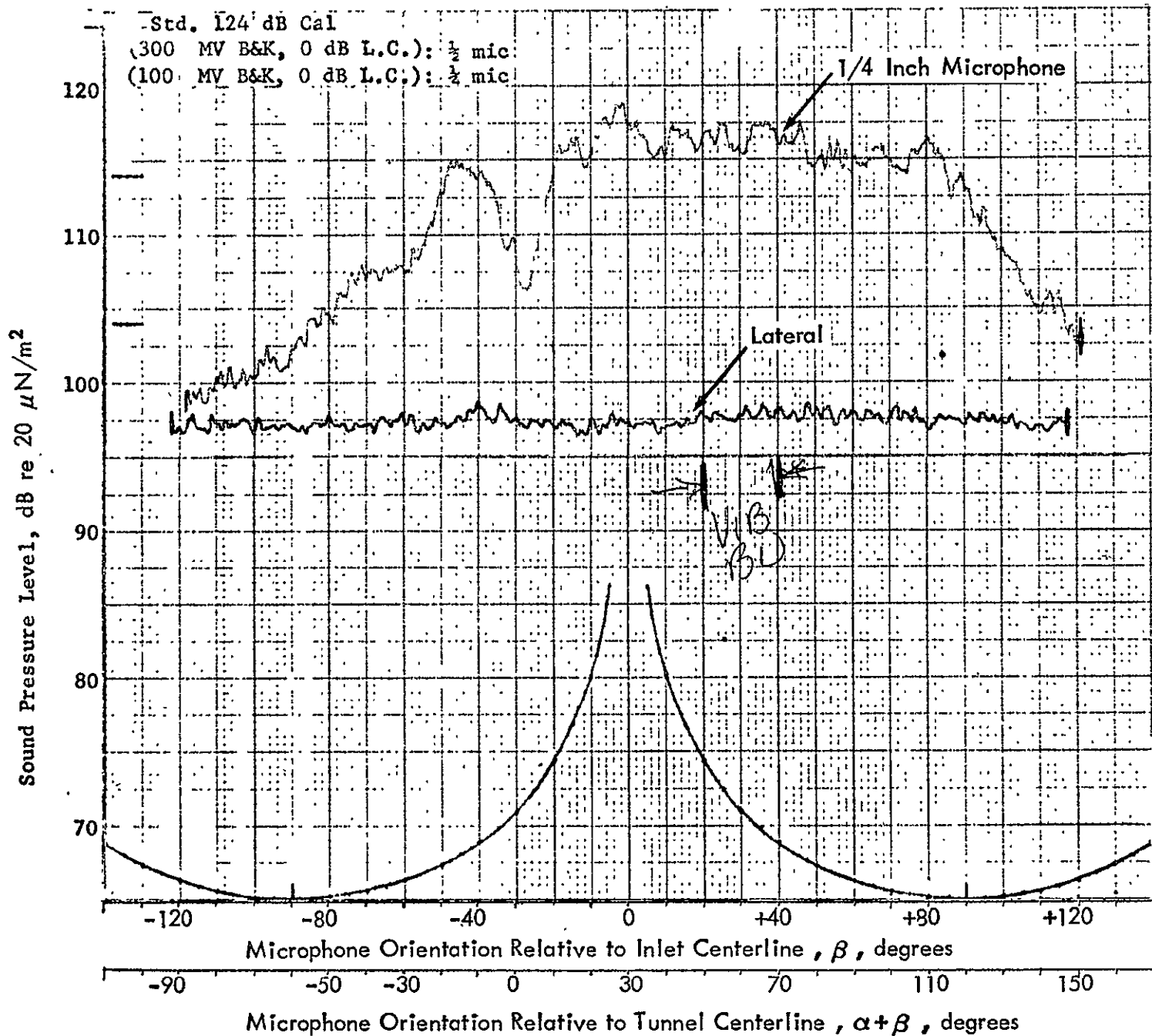
Siren freq* 9.6 K

Tunnel $q(V_0)$ 22

Acoustic System:
 Curve GR
 Mike* L BU
 B&K* 100 100
 L.C.* 0 0
 Cal (B&K/LC)* ✓ ✓
 Δ dB 0 0
 Fil. Gen. Freq* 10 10
 Fil. B.W.* 1/3 1/3

*Required Information

FIGURE 22.
 B & K MICROPHONE
 OUTPUT, $M = 0.12$
 INLET DIRECTIONALITY
 TEST



Date: 1/16
 Test No.: IIA2
 Plot No.: 234

Inlet Configuration:
SLOOP
SOFTWALL TEST
SECTION

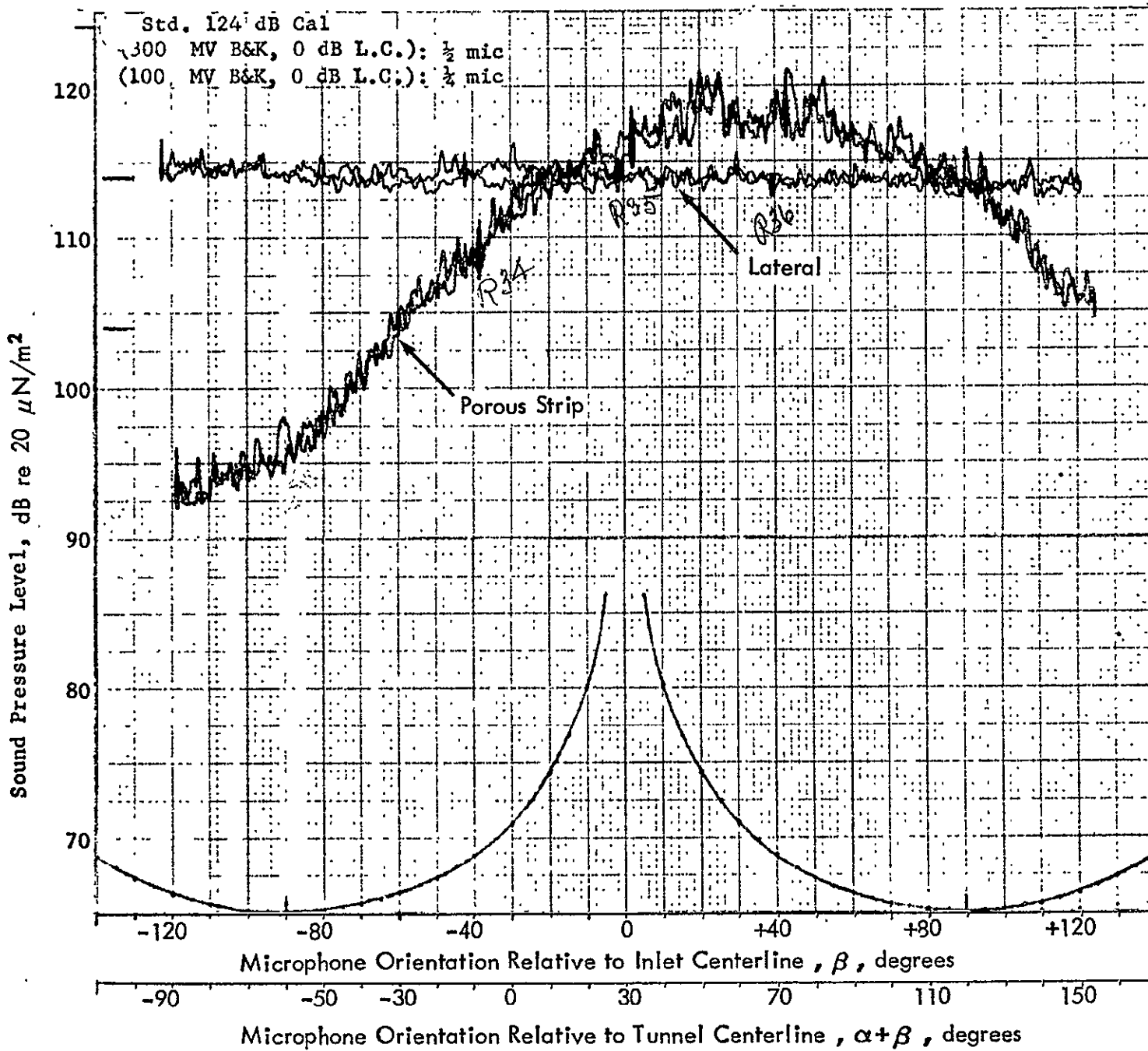
Run Conditions:
 Rdg. No.* —
 α 30° β 2.5
 M_t 0.6 r_m 4
 Siren freq* 9.6K
 Tunnel $q(V_0)$ 3A

Acoustic System:

Curve	Top	Bot
Mike*	<u>L</u>	<u>BU</u>
B&K*	<u>300</u>	<u>100</u>
L.C.*	<u>0</u>	<u>0</u>
Cal (B&K/LC)*	<u>C</u>	<u>V</u>
Δ dB	<u>-10</u>	<u>0</u>
Fil. Cen. Freq*	<u>10K</u>	<u>10K</u>
Fil. B.W.*	<u>1/3</u>	<u>1/3</u>

*Required Information

FIGURE 23.
 B & K MICROPHONE
 OUTPUT, $M = 0.15$
 INLET DIRECTIONALITY
 TEST



Date: 10/22/75
 Test No.: 1B2
 Plot No.: 2A

Inlet Configuration:
SCOOP
SOFTWALL TEST
SECTION

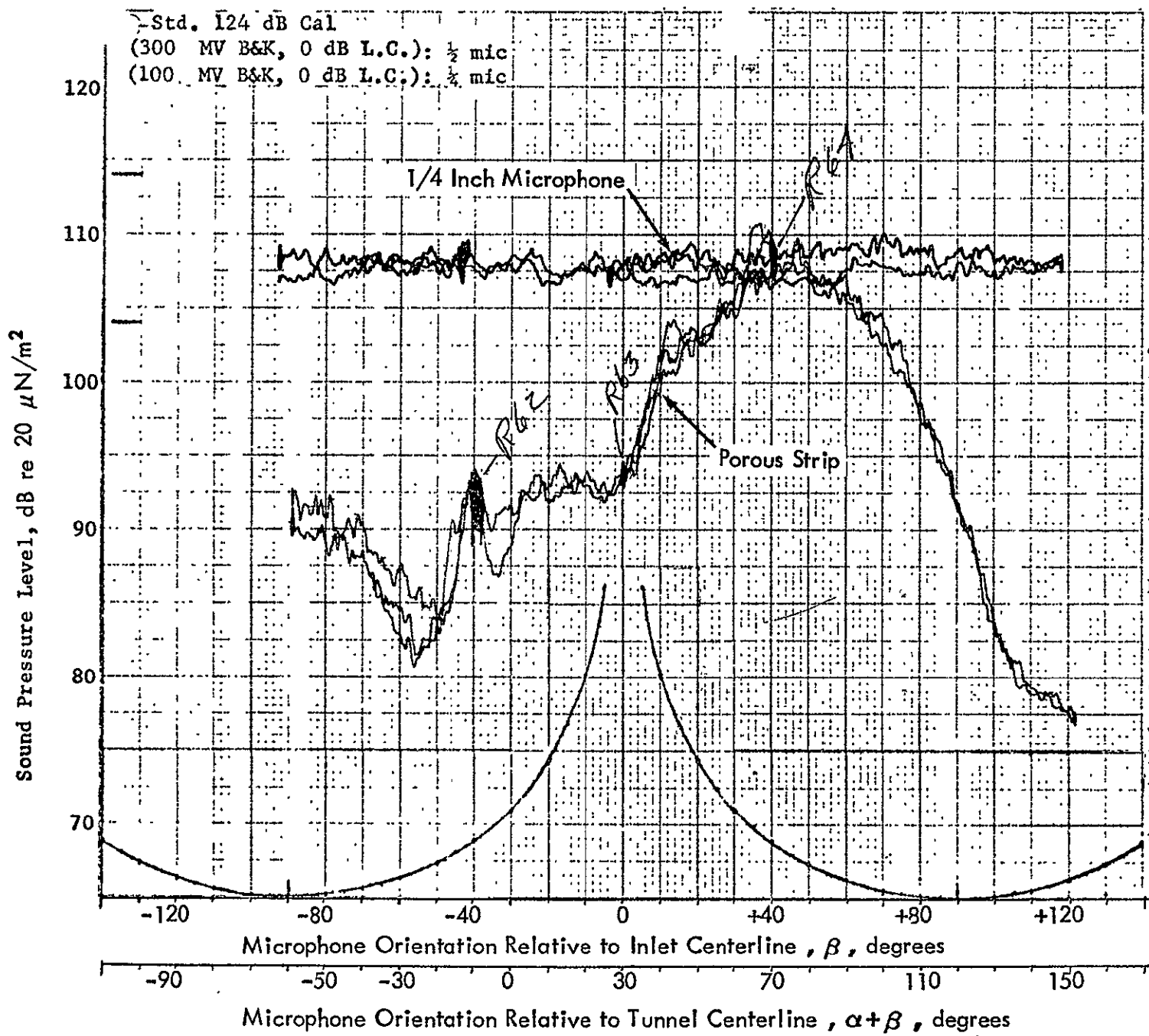
Run Conditions:
 Rdg. No.* ✓
 α 30° β 2.5
 M_t 0.6 r_m 41
 Siren freq* 9.6 K
 Tunnel $q(V_0)$ 0

Acoustic System:
 Curve R_{3A} 60
 Top Bot
 Mike* $P.S.$ LAT
 B&K* 100 30
 L.C.* $\#0$ $\#0$
 Cal (B&K/LC)* ✓ ✓
 Δ dB $+10$
 Fil. Cen. Freq* 10K 10K
 Fil. B.W.* $1/3$ $1/3$

*Required Information

FIGURE 24.
 POROUS STRIP SENSOR
 OUTPUT, $M = 0$

INLET DIRECTIONALITY
 TEST



Date: 11/3
 Test No.: II B
 Plot No.: 55

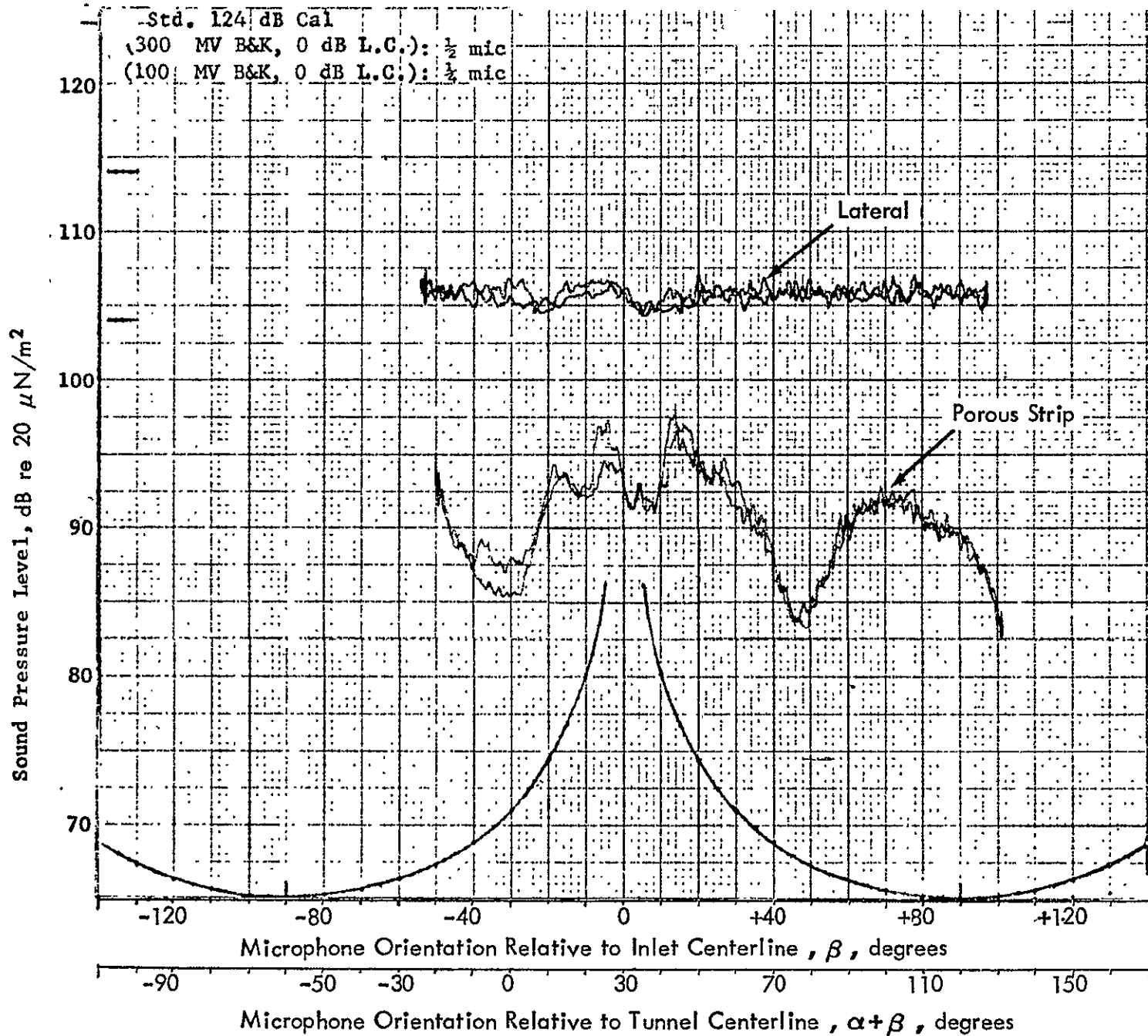
Inlet Configuration:
SCOOP
SOFTWALL TEST
SECTION

Run Conditions:
 Rdg. No.*
 α 30 β 2.5
 M_t 0.6 r_m 41
 Siren freq* 9.6 K
 Tunnel $q(V_0)$ 22

Acoustic System:
 Curve GN RD
 Mike* LAT PS
 B&K* 100 300
 L.C.* 0 0
 Cal (B&K/LC)* ✓ ✓
 Δ dB 0
 Fil. Cen. Freq* 10k 10k
 Fil. B.W.* 1/3 1/3

*Required Information

FIGURE 25.
 POROUS STRIP SENSOR
 OUTPUT, $M = 0.12$
 INLET DIRECTIONALITY
 TEST



Date: 11/5
 Test No.: TEB
 Plot No.: 139

Inlet Configuration:
SCOP 180
SOFTWALL TEST
SECTION

Run Conditions:
 Rdg. No.*
 α 0 β 2.5
 M_t 0.6 r_m 4'
 Siren freq* 9.6 K
 Tunnel $q(V_0)$ 34

Acoustic System:

Curve	Top	Bot
Mike*	<u>L</u>	<u>P</u>
B&K*	<u>100</u>	<u>300</u>
L.C.*	<u>0</u>	<u>0</u>
Cal (B&K/LC)*	<u>✓</u>	<u>✓</u>
Δ dB	<u>0</u>	<u> </u>
Fil. Gen. Freq*	<u>10</u>	<u>106</u>
Fil. B.W.*	<u>1/3</u>	<u>1/3</u>

*Required Information

FIGURE 26.
 POROUS STRIP SENSOR
 OUTPUT, $M = 0.15$
 INLET DIRECTIONALITY
 TEST

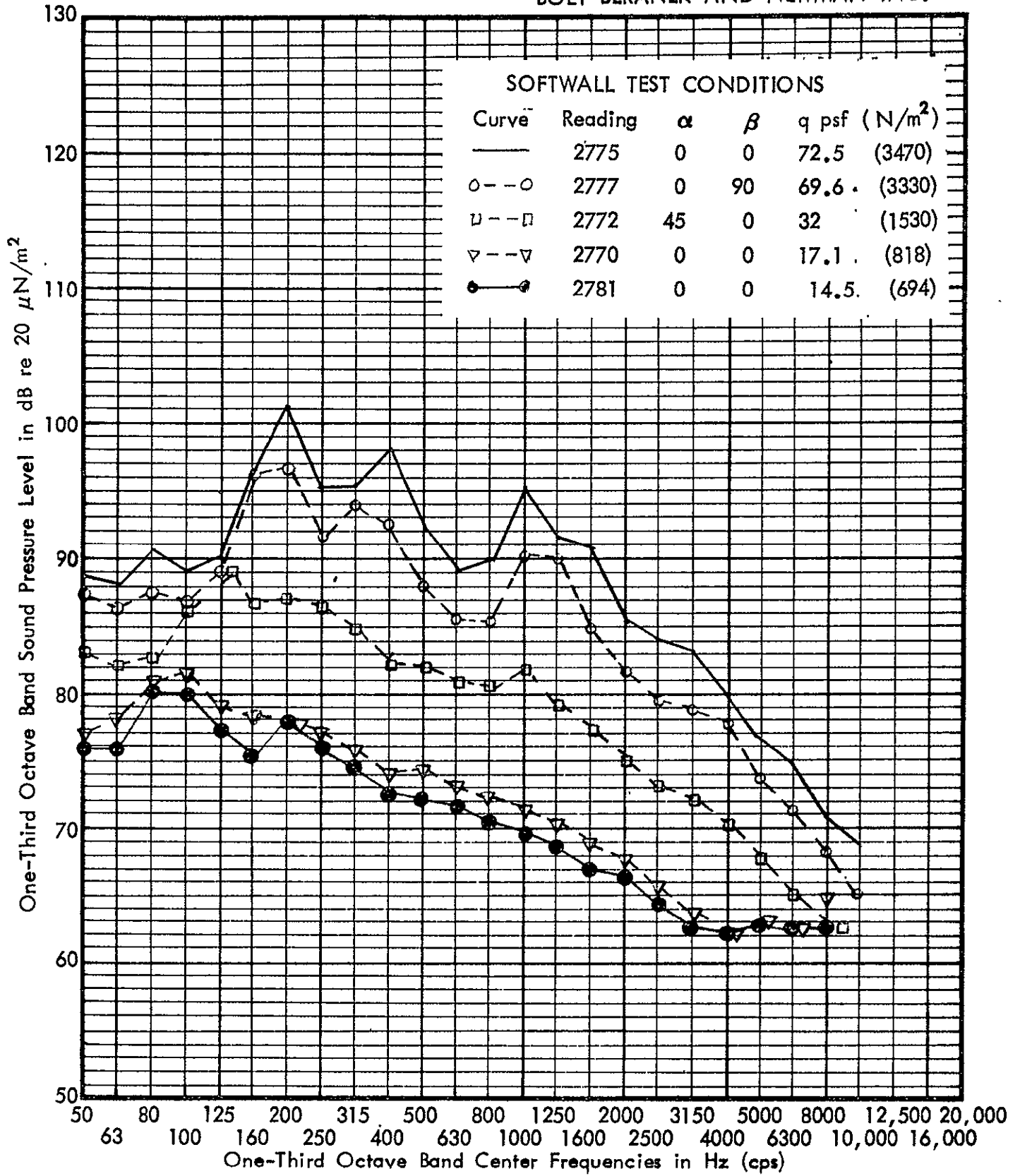


FIGURE 27. SETTLING CHAMBER WIND-ON SOUND PRESSURE LEVELS
SOFTWALL TEST SECTION

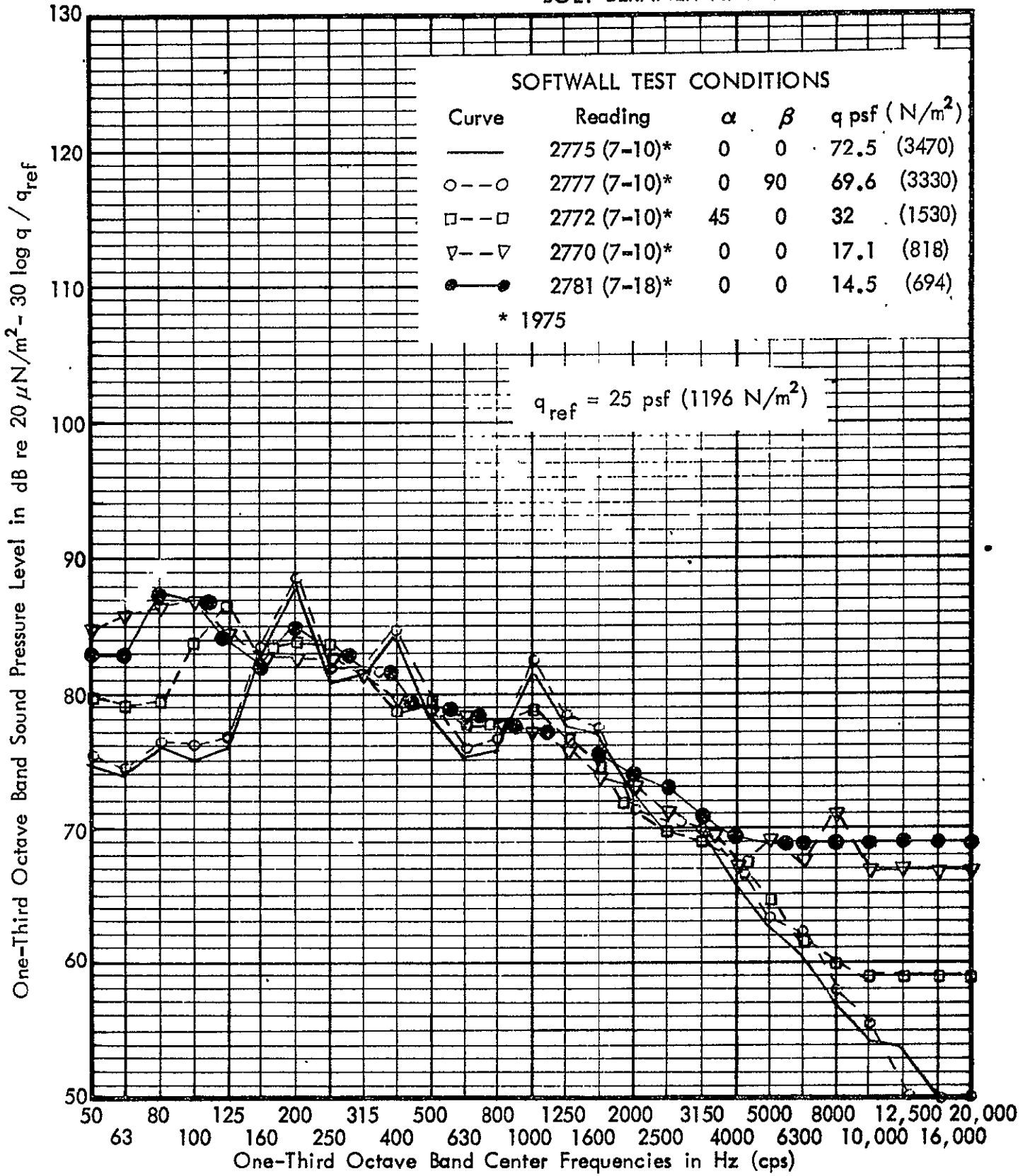


FIGURE 28. NORMALIZED, SETTLING CHAMBER, WIND-ON SOUND PRESSURE LEVELS , SOFTWALL TEST SECTION

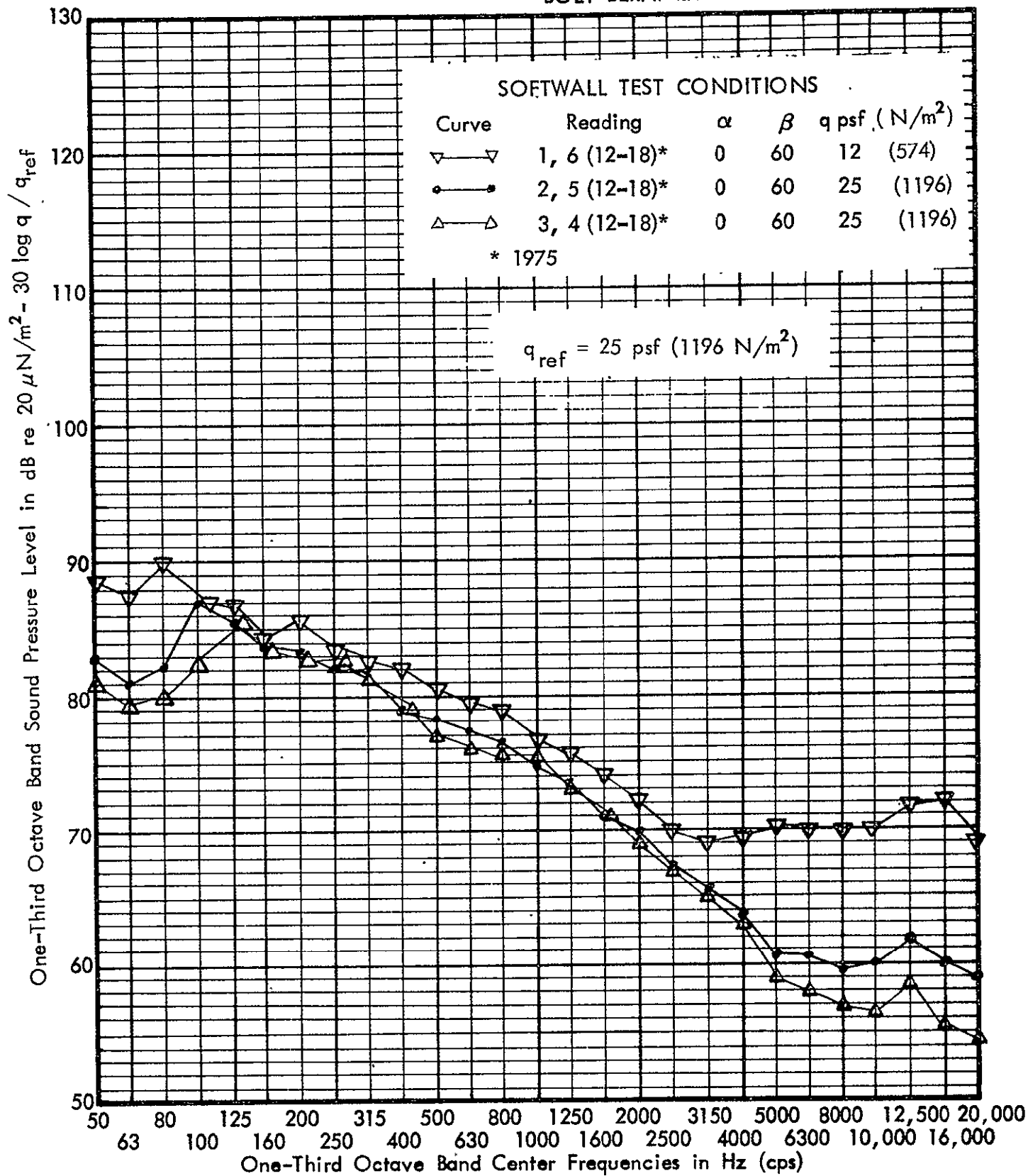


FIGURE 29. NORMALIZED, SETTLING CHAMBER, WIND-ON SOUND PRESSURE LEVELS , SOFTWALL TEST SECTION

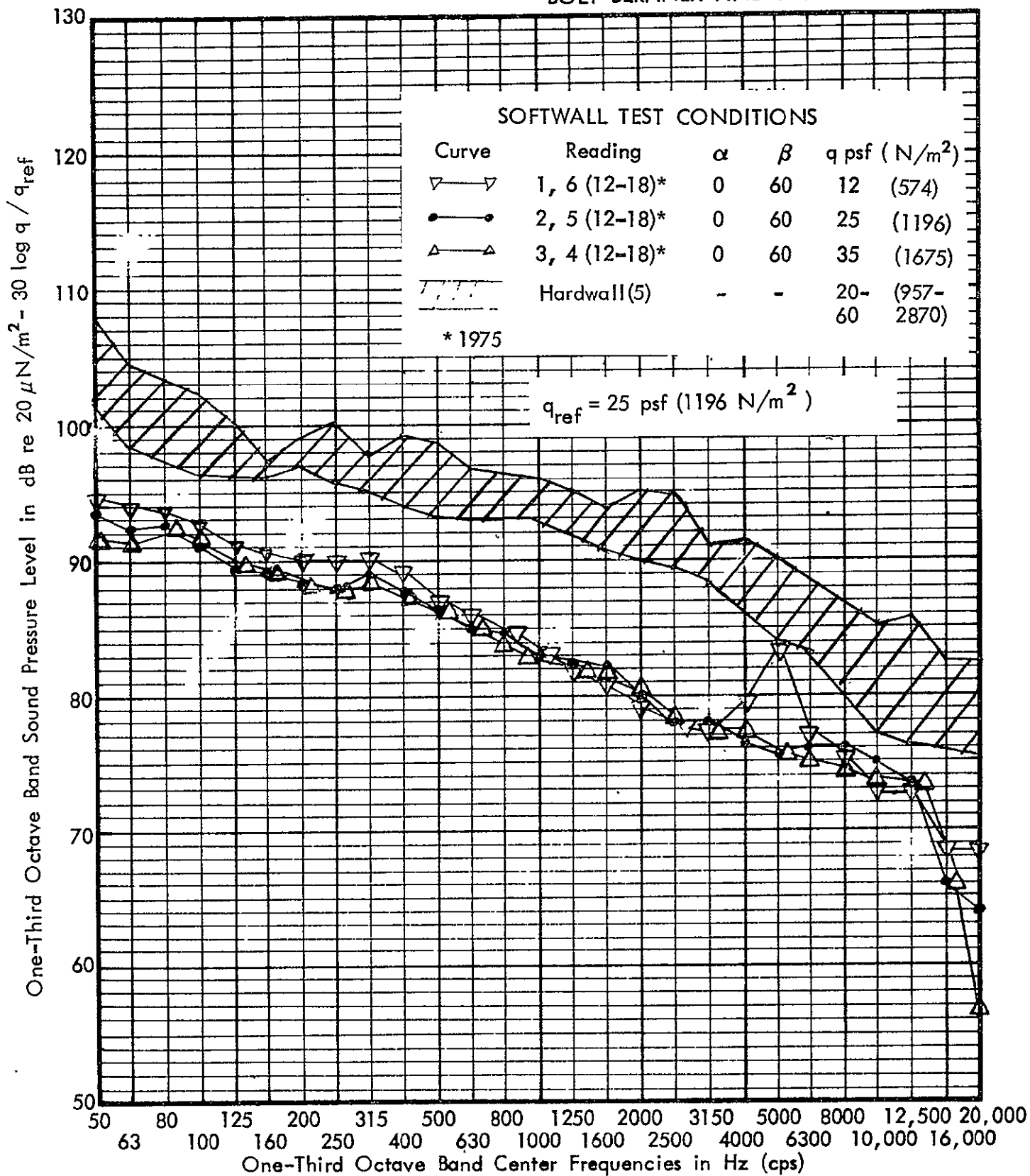


FIGURE 30. NORMALIZED TEST SECTION, FREE STREAM, SWORD MICROPHONE, WIND-ON SOUND PRESSURE LEVELS SOFTWALL TEST SECTION

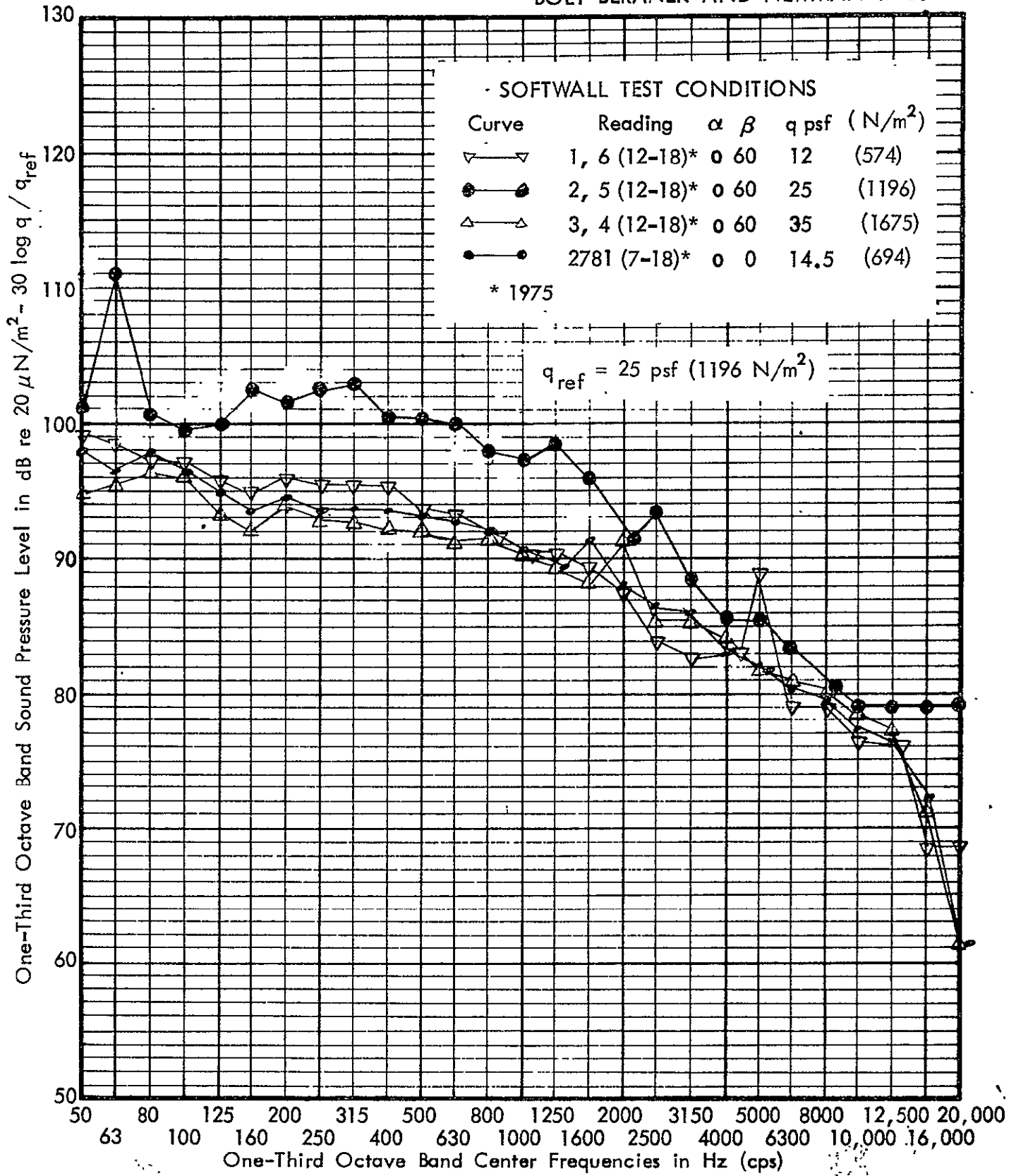


FIGURE 31. NORMALIZED, TEST SECTION, OBSTRUCTED MICROPHONE, WIND-ON SOUND PRESSURE LEVELS, SOFTWALL TEST SECTION

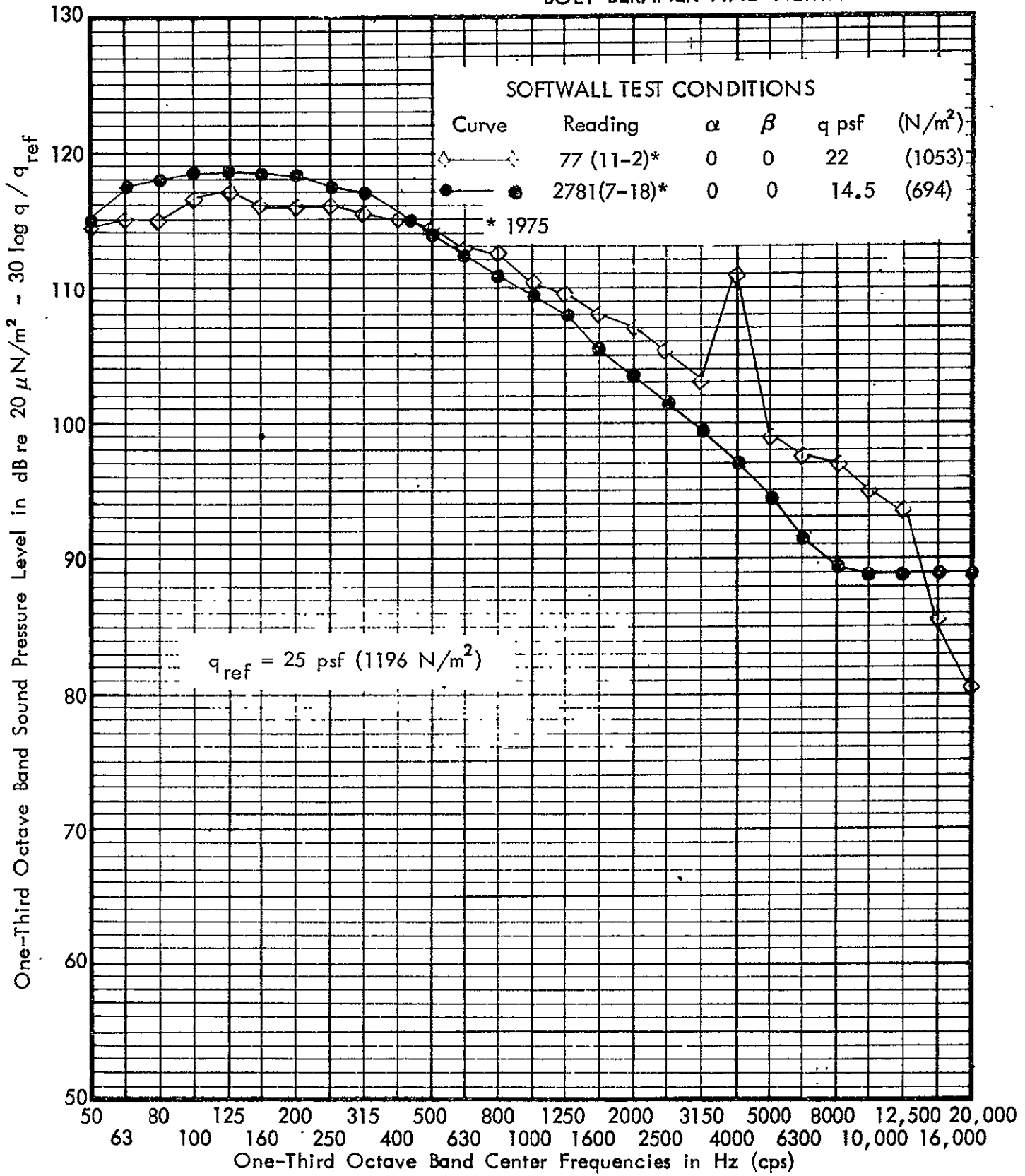


FIGURE 32. NORMALIZED, TEST SECTION, LATERAL MICROPHONE, WIND-ON SOUND PRESSURE LEVELS, SOFTWALL TEST SECTION

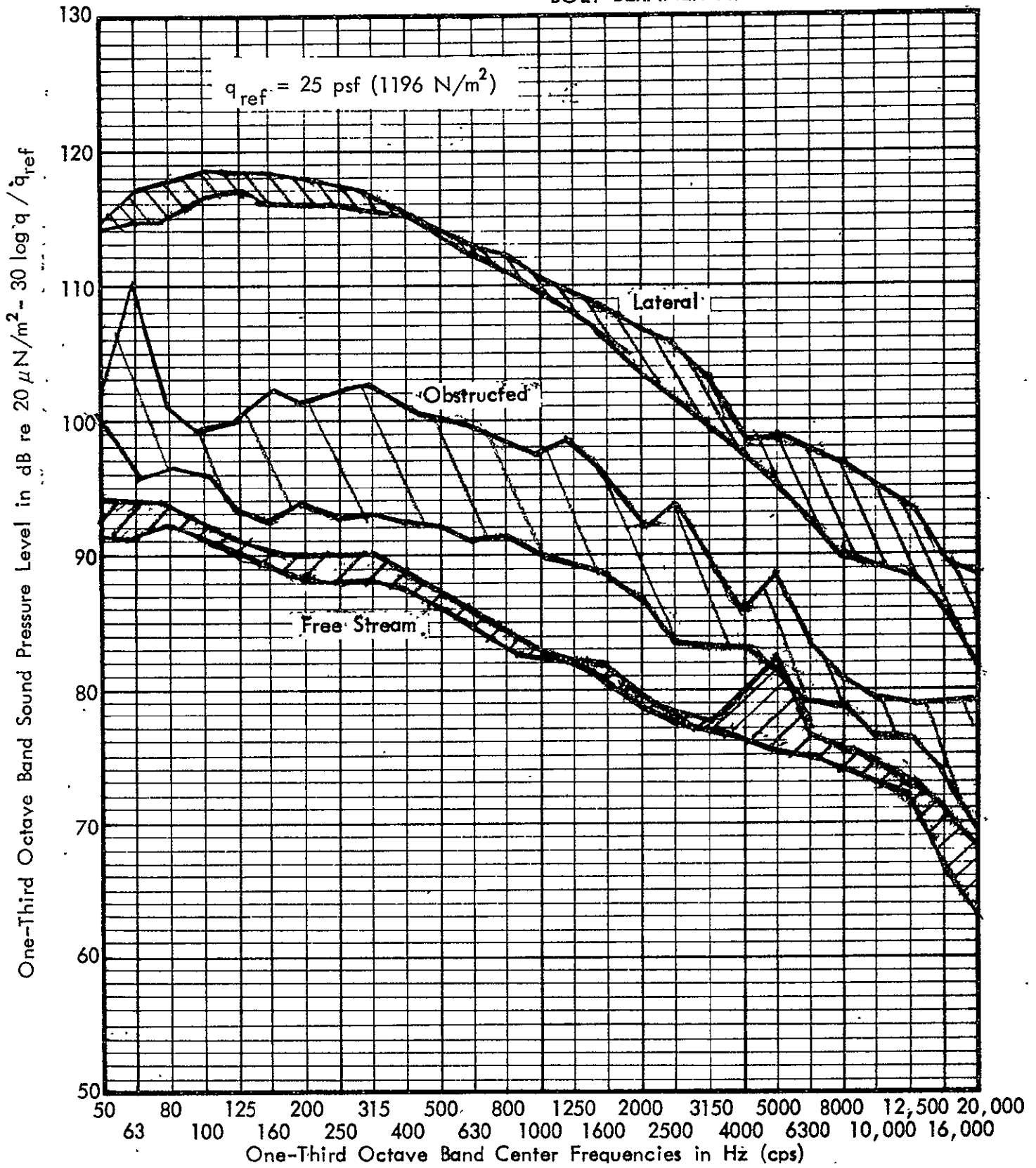


FIGURE 33. COMPARISON OF FREE STREAM, OBSTRUCTED, AND LATERAL MICROPHONE, WIND-ON NORMALIZED SOUND PRESSURE LEVELS, SOFTWALL TEST SECTION

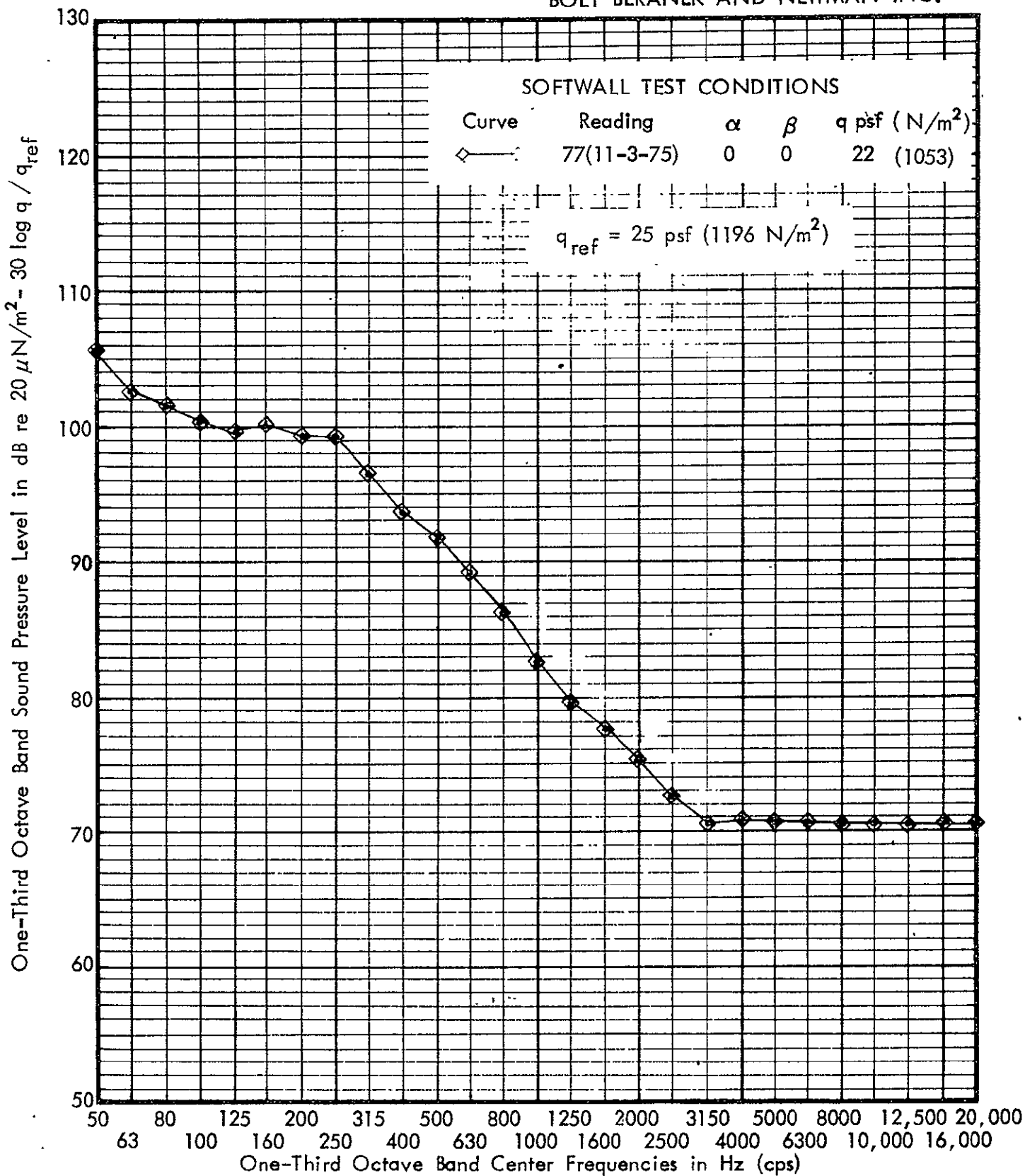


FIGURE 34. NORMALIZED, TEST SECTION, POROUS STRIP SENSOR, WIND-ON SOUND PRESSURE LEVELS , SOFTWALL TEST SECTION

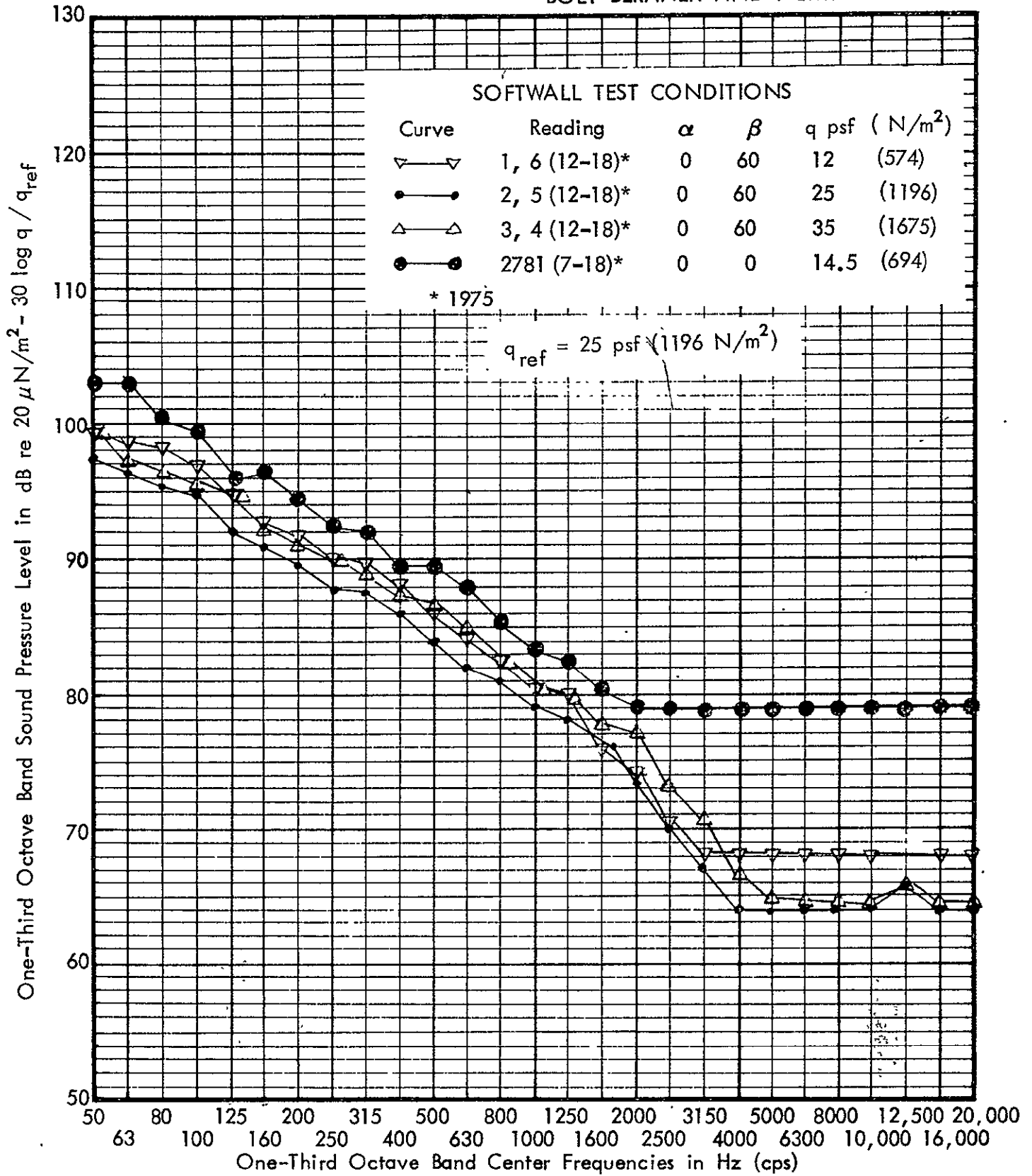


FIGURE 35. NORMALIZED, DIFFUSER, WIND-ON SOUND PRESSURE LEVELS, SOFTWALL TEST SECTION

APPENDIX A

Directivity Measurements of Finite Sized Sources

APPENDIX A

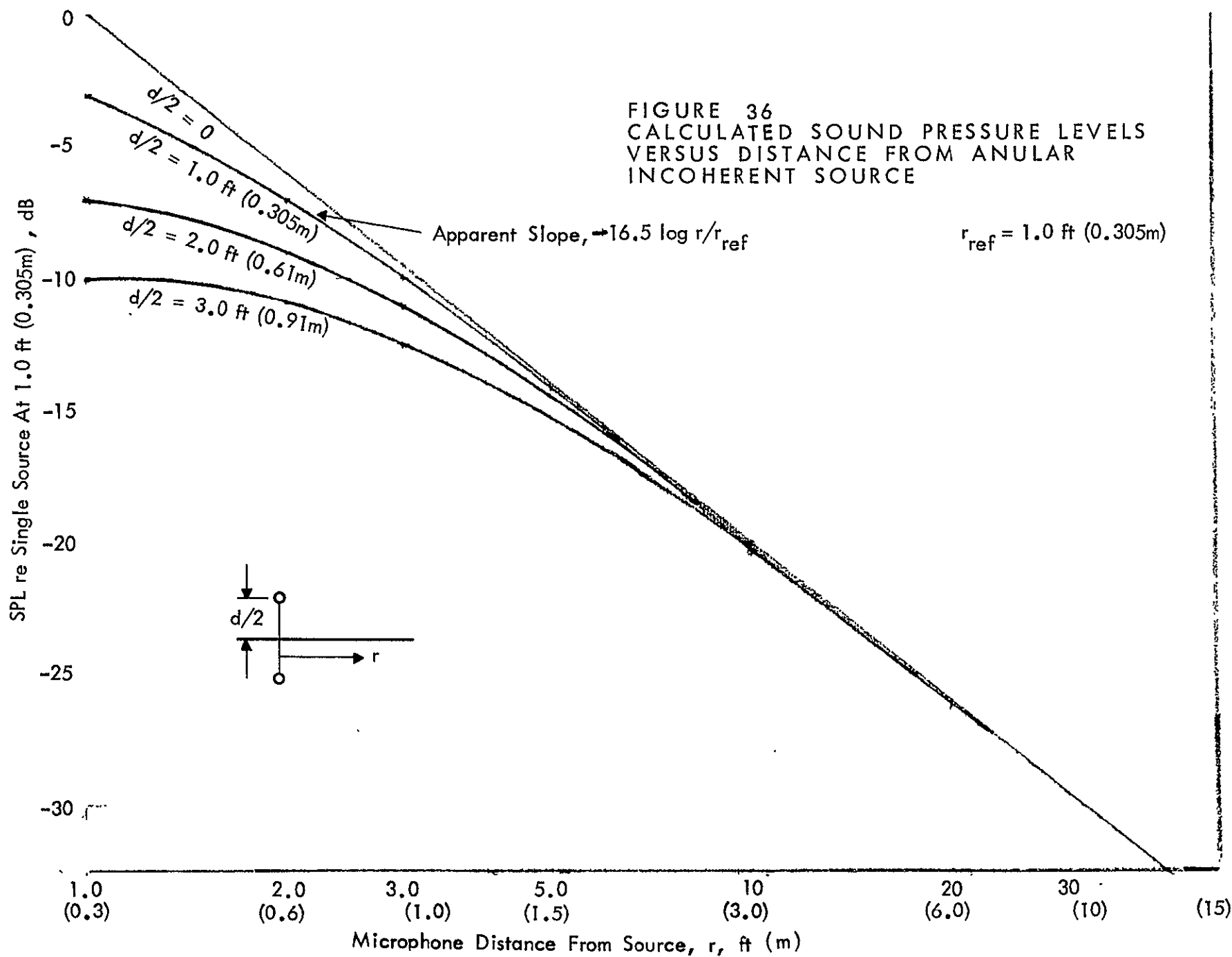
Directivity Measurements of Finite Sized Sources

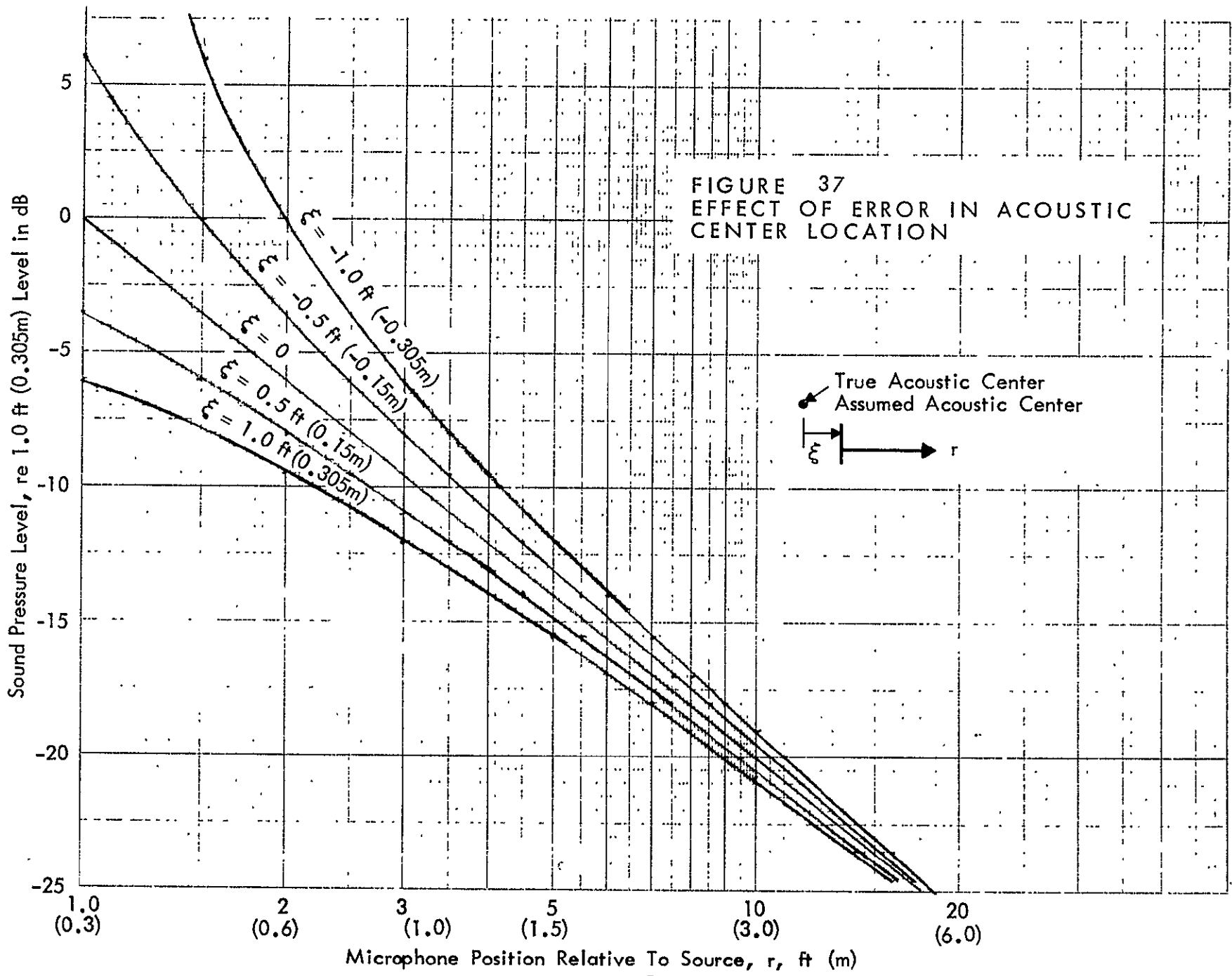
The determination of the far field acoustic characteristics of sources from near field measurements has been of practical concern to acousticians. Procedures for evaluating source sound power using many microphone locations have been formalized (8). A more difficult problem is the mapping of the far field directionality patterns. This problem is of particular interest in wind tunnel measurements because of inherent distance limitations. A study of this specific problem investigated a computational scheme for overcoming this distance limitation.

In order to identify the seriousness of the potential measurement problem, knowledge of the behavior of finite sized sources and the result of measurement geometry errors are helpful. Figure 36 shows the calculated attenuation with distance from incoherent sources separated vertically. Note that the average slope from 1 to 10 feet for sources separated by 2.0 feet is the same as observed with the ILG source.

Errors in measurement of the acoustic center of an ideal source are presented as Figure 37. These types of curves with inflections up or down were observed during radial traverses from the speaker source. The measurement error diminishes rapidly as the microphone is moved from the source

FIGURE 36
 CALCULATED SOUND PRESSURE LEVELS
 VERSUS DISTANCE FROM ANULAR
 INCOHERENT SOURCE





APPENDIX B

Theoretical Response of Continuous and Discrete
Line Sensors in the Presence of Flow

APPENDIX B

Theoretical Response of Continuous and Discrete
Line Sensors in the Presence of Flow

The directivity function of a line sensor of length L , in flow, is developed in Reference 21 as follows:

$$H(k) = \frac{\sin \left[k_s \left(\frac{\cos \alpha'}{1 + M \cos \theta'} - 1 \right) L/2 \right]}{k_s \left(\frac{\cos \alpha'}{1 + M \cos \theta'} - 1 \right) L/2} \quad (1)$$

Where α' is the angle of the axis of the line sensor with the direction of propagation of the plane wave in the flow and θ' is the angle of the flow velocity U and the direction of propagation of the plane wave in the flow. Also,

$$k_s = \frac{\omega_s}{c_0} \quad (2)$$

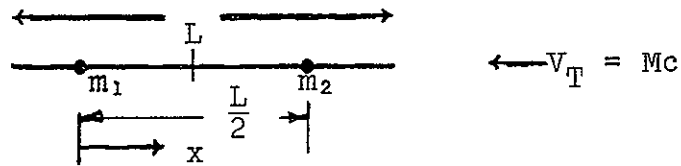
This equation is correct for no flow and for directly upstream and downstream of the source. However, the form is inappropriate for intermediate angles because of difficulty in defining α' and θ' . (The angles have superscripts to differentiate from LeRC common usage.)

In order to develop useful expressions for the response of a line sensor, a number of aspects of sound propagation and line sensor response should be understood.

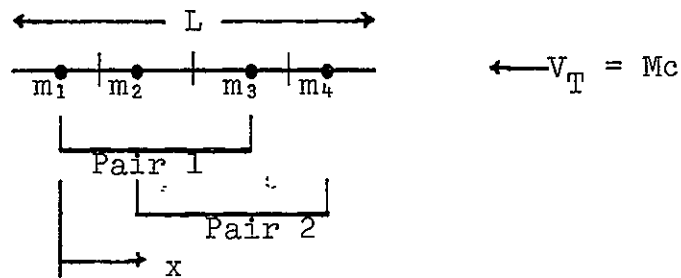
1. For a point source in a moving stream the sound wave radiates in a spherical fashion, just as in stationary fluid. However, each wave has a point of origin which moves along with the flow. In two dimensions, the result is a series of non-concentric rings. Only the special cases with the sensor upstream or downstream of the true source are have normal plane wave propagation, Figure 38.
2. The apparent wavelength or trace wavelength is unchanged along any radius from the true source (for a given frequency).
3. If the source and receiver are fixed in space, the frequency of arrival of wavefronts is equal to the source frequency. This is true even if the fluid is moving (at a constant velocity).
4. Maximum cancellation occurs when the external wave goes a distance $\frac{L}{2} + \frac{\lambda_T}{2}$ at a velocity V_T while the sampling or internal wave goes a distance $\frac{L}{2}$ at a velocity c .

The last point, relating to how a line array works, should be amplified.

The directivity evidenced by the porous strip sensor and the reduction in sensitivity with forward velocity are basically the same phenomena, the mismatching of the external and internal wave fields. To visualize the effect, consider the porous strip sensor as a line array of microphones.



or



Consider the outputs of the microphones to be delayed by a time $\tau_i = x_i/c$ relative to microphone 1 and then summed.

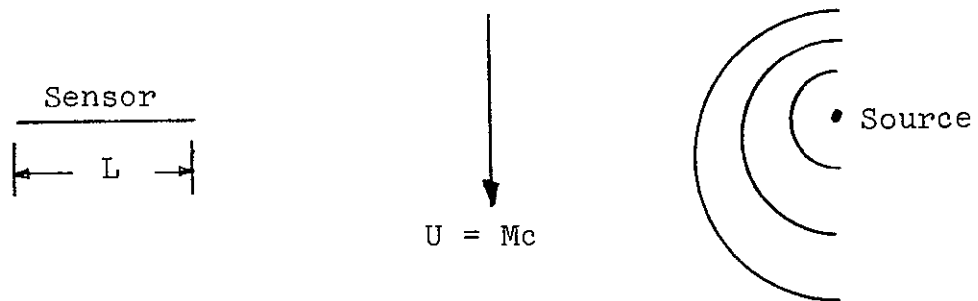
For an acoustic wave traveling with the speed of sound along the axis of the microphone array, the time delayed signals will be identical, no cancellation will occur and the maximum output will occur. A minimum output will occur if the external wave is shifted in speed such that each microphone signal is summed with an equal and opposite microphone signal. This is possible if the external or trace wave goes a distance $\frac{L}{2} \pm \frac{n\lambda_T}{2}$ in a time $\frac{L}{2c}$. To transition to a continuous array, note that equal and opposite signals can be paired at distances of $L/2$ no matter how much discretizing is performed.

This apparent phase shift can occur in a number of ways:

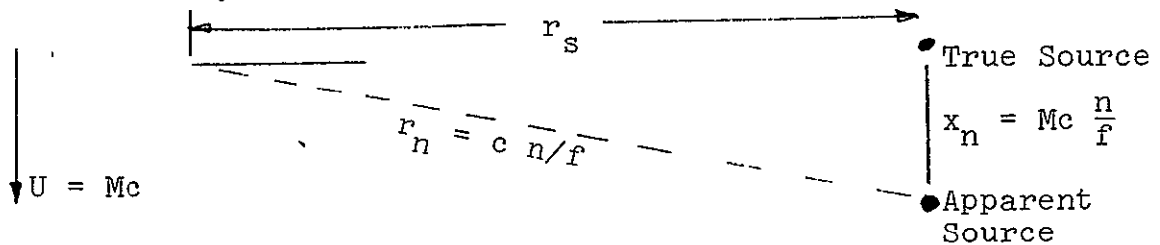
1. The speed of the wave going along the sensor can increase. For example, the sensor can be pointed upstream towards a source.
2. The speed of the wave going along the sensor can decrease. For example, the sensor can be pointed downstream towards a source.
3. The wave front can make an angle with the sensor increasing the trace wavespeed. For example, a far field source can be located off of the axis of the sensor.
4. Combinations of 1 or 2 and 3.

The crosswind situation is directly applicable to measurement in the 9 x 15 foot wind tunnel. The development, which follows, assumes a $\frac{\sin X}{X}$ form.

Case IV Cross wind, pointing at the source



The geometry, noting that the apparent source moves downstream with a velocity $U = Mc$



where n is the n^{th} wave starting at the true source

$$r_n^2 = r_s^2 + x_n^2 \quad (3)$$

$$\left(c \frac{n}{f}\right)^2 = r_s^2 + \left(Mc \frac{n}{f}\right)^2$$

$$\left(\frac{n}{f}\right)^2 = \frac{r_s^2}{c^2 (1-M^2)}$$

Yielding $\lambda_T = \frac{r_s}{n} = \frac{c\sqrt{1-M^2}}{f}$ and $V_T = \lambda_T f = c\sqrt{1-M^2}$ (4)

The first cancellation occurs when a wave front goes $\frac{L-\lambda}{2}$ at V_T

while the sensor delays $\tau = \frac{L}{2c}$. Equating transmission times

$$\frac{L}{2c} = \frac{L-\lambda_T}{2c\sqrt{1-M^2}} = \frac{L-c\sqrt{1-M^2}}{2c\sqrt{1-M^2} f} \quad (5)$$

solving

$f = \frac{c\sqrt{1-M^2}}{L [1 - \sqrt{1-M^2}]}$	$\frac{c}{fL} = \frac{1-\sqrt{1-M^2}}{\sqrt{1-M^2}}$
--	--

Example:

$M = 0.1$

$L = 1.0 \text{ ft}$

$f = 223,113 \text{ Hz}$ (frequency for first null for crosswind case)

Since this equation prescribes the 1st nul, which occurs at $\frac{\sin \pi}{\pi}$, assuming a $\frac{\sin X}{X}$ form and an argument $\pi fL/c$ [Mach effect]

$$H(k, M) = \frac{\sin \left[\frac{\pi fL}{c} \left[\frac{1 - \sqrt{1 - M^2}}{\sqrt{1 - M^2}} \right] \right]}{\frac{\pi fL}{c} \left[\frac{1 - \sqrt{1 - M^2}}{\sqrt{1 - M^2}} \right]} \quad (6)$$

Example: M = 0.15
 f = 9600 Hz
 H(k, M) = 0.98
 20 log (0.98) = -0.17 dB
 c = 1124 ft/sec

Using a similar procedure, solutions for specific and general cases have been developed and are as follows:

Case I Source upstream of sensor, pointing at source

$$H(k, M) = \frac{\sin \left[\frac{\pi fL}{c} \left[\frac{M}{1 + M} \right] \right]}{\frac{\pi fL}{c} \left[\frac{M}{1 + M} \right]} \quad (7)$$

Case II Source downstream of sensor, pointing at source

$$H(k, M) = \frac{\sin \left[\frac{\pi fL}{c} \left[\frac{M}{1 - M} \right] \right]}{\frac{\pi fL}{c} \left[\frac{M}{1 - M} \right]} \quad (8)$$

Case III Directivity

$$H(k, \alpha) = \frac{\sin \left[\frac{\pi f L}{c} [1 - \cos \alpha] \right]}{\frac{\pi f L}{c} [1 - \cos \alpha]} \quad (9)$$

Case IV Cross wind, pointing at source

$$H(k, M) = \frac{\sin \left[\frac{\pi f L}{c} \left[\frac{1 - \sqrt{1 - M^2}}{\sqrt{1 - M^2}} \right] \right]}{\frac{\pi f L}{c} \left[\frac{1 - \sqrt{1 - M^2}}{\sqrt{1 - M^2}} \right]} \quad (10)$$

Case V All angles, sensor pointing at source

$$H(k, M, \phi) = \frac{\sin \left[\frac{\pi f L}{c} \left[\frac{1 + M \cos \phi - \sqrt{1 - M^2} (1 - \cos^2 \phi)}{-M \cos \phi + \sqrt{1 - M^2} (1 - \cos^2 \phi)} \right] \right]}{\frac{\pi f L}{c} \left[\frac{1 + M \cos \phi - \sqrt{1 - M^2} (1 - \cos^2 \phi)}{-M \cos \phi + \sqrt{1 - M^2} (1 - \cos^2 \phi)} \right]} \quad (11)$$

Where ϕ is the angle between the direction of flow and center-line of sensor, Figure 38.

Note that Case V produces the results of the upstream, downstream, and crosswind cases by setting $\phi = 180^\circ$, 0° , and 90° respectively.

An interesting aspect of the relation for the general case, Equation 11, is that there is an angle ϕ for which the response function, $H(k, M, \phi)$ is unity.

Getting the argument of Equation (11) equal to zero

$$\frac{\Pi f L}{c} \left[\frac{1 + M \cos \phi - \sqrt{1 - M^2 (1 - \cos^2 \phi)}}{-M \cos \phi + \sqrt{1 - M^2 \cos^2 \phi}} \right] = 0$$

$$1 + M \cos \phi - \sqrt{1 - M^2 (1 - \cos^2 \phi)} = 0$$

Squaring and rearranging yields

$$\cos \phi = \frac{-M}{2} \quad (12)$$

For example, at $M = 0.15$, the output of the ideal sensor will be unaffected by the flow if $\phi = 94.3^\circ$.

The general relation, Equ. 11, is plotted in Figure 39 for frequencies of 1000, 2000, 4000, 5000, 6300, 8000 and 9600 Hz with Mach Number $M = 0.15$ and $L = 14$ inch (36 cm). This figure shows that the line array or porous strip sensor's output is significantly modified by flow with nulls occurring above 5000 Hz. However, note that in the crosswind region, $\phi = 90^\circ$, effect of flow is greatly diminished.

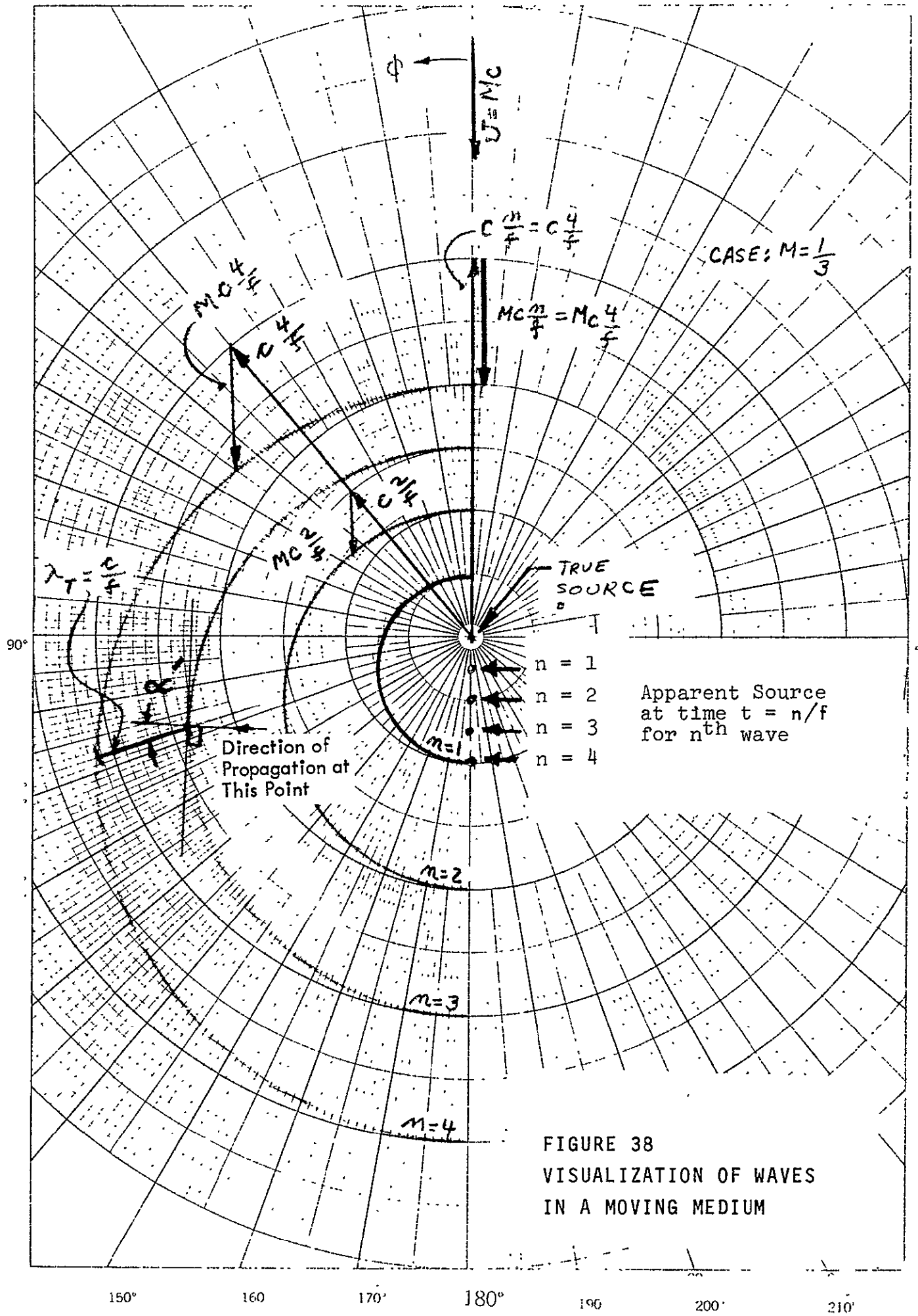


FIGURE 38
 VISUALIZATION OF WAVES
 IN A MOVING MEDIUM

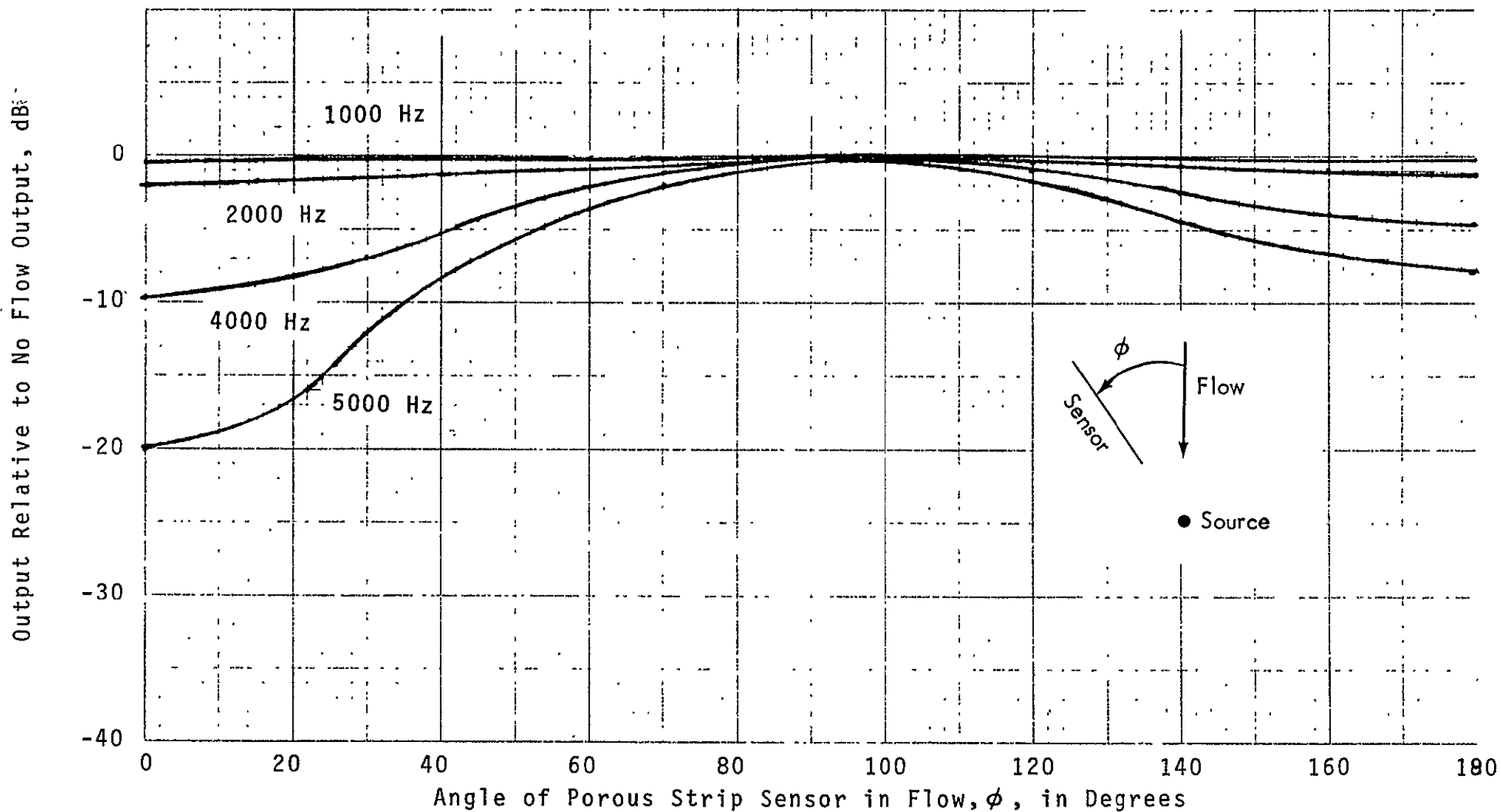


FIGURE 39. VARIATION OF THE THEORETICAL OUTPUT OF A 14 INCH (36 cm) POROUS STRIP SENSOR, IN THE PRESENCE OF FLOW, (MACH NUMBER $M = 0.15$)

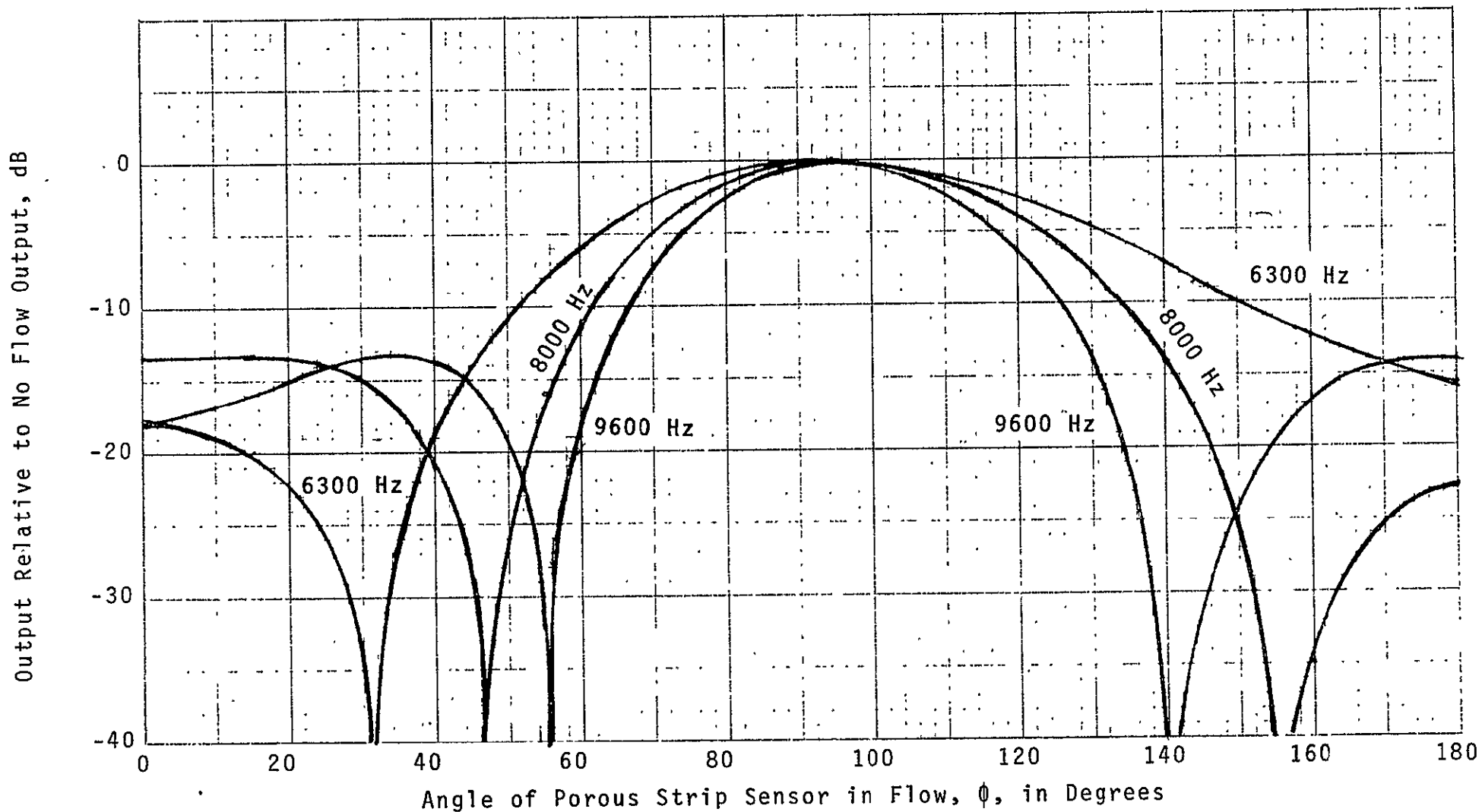


FIGURE 39 (CONT'D). VARIATION OF THE THEORETICAL OUTPUT OF A 14 INCH (36 cm) POROUS STRIP SENSOR, IN THE PRESENCE OF FLOW (MACH NUMBER $M = 0.15$)